HYDRODYNAMIC AND ECONOMIC MODELLING OF TIDAL CURRENT ENERGY CONVERSION SYSTEMS

by

Guy T Melville

A thesis submitted in partial fulfilment of

the requirements for the degree of

Doctor of Philosophy

The Robert Gordon University, Aberdeen

November 2008

DECLARATION

I hereby declare that the work or any portion of it, referred to in this thesis has not been submitted in support of an appreciation for another degree or qualification of this, or any other university or institute of technology. This is an original piece of work undertaken by myself. All results and work other than my own are clearly cited and acknowledged.

HYDRODYNAMIC AND ECONOMIC OF TIDAL ENERGY CONVERSION SYSTEMS

This thesis examines the contribution of computational modelling to the development of the tidal current energy industry, against the background of increasing commercial, government, academic and public interest. It does this through the practical application of a number of computational techniques in the areas of:

1. Tidal current analysis and prediction

2. Hydrodynamic flow modelling

3. Tidal resource analysis

4. Optimised economic modelling

Appropriate survey set-up is essential in gathering data. Given this, processing the data using velocity profiles; statistical techniques; and harmonic analysis can produce valuable data for site development, device design and grid management. This work developed the application of a directional and time-dependent power coefficient and demonstrates its importance in resource evaluation from tidal flow data.

It further concludes that hydrodynamic flow modelling of sites prior to development is important in determining suitable sites, given the scarcity of tidal information in the areas suitable for tidal developments. The same scarcity of data, in terms of boundary conditions, interior validation points and depth does limit the accuracy of such models.

The work demonstrates that using differing resource analyses can obtain dramatically different results; and develops a correlation relating energy extraction to developed energy extraction using a one dimensional channel model. In doing so it concludes that energy resource estimates may be reduced from contemporary estimates.

Overall, computational modelling of tidal current energy conversion systems can have a significant contribution to their design and site development. The most significant capital costs arise from installation, decommissioning and the turbine itself, however significant reduction in the cost of energy production can result from correct placement, array size and component selection.

This work contributes to knowledge in a number of areas, namely:

1. It is the first published work on survey data analysis prior to deployment of a large-scale prototype tidal current energy conversion system;

2. At the time that the work was carried out, it was the first published work considering the use of the least-squared harmonic method for prediction of energy output from a tidal current energy device;

3. It is the first work to propose a directional power coefficient in the process of resource analysis for a tidal current energy conversion system;

4. The work on economic modelling was the first to produce an optimised economic model for tidal current energy conversion systems (TCECS);

5. It is the first work to use an optimised economic model for TCECSs to demonstrate the effect of device placement on the cost of energy produced;

6. It is the first work to use an optimised economic model for TCECSs to demonstrate that the cost of energy for TCECSs is minimised by maximising the rated power, given no topographical impedence;

7. It proposes a method to determine the energy resource available including energy extraction.

ACKNOWLEDGMENTS

TABLE OF CONTENTS

CHAPTER 1 INTRODUCTION

CHAPTER 2   SITE MONITORING AND DATA ANALYSIS

CHAPTER 3   HYDRODYNAMIC MODELLING FOR TIDAL ENERGY CONVERSION SYSTEMS

CHAPTER 4   ENERGY RESOURCE ANALYSIS

CHAPTER 5   ECONOMIC MODELLING OF TIDAL ENERGY CONVERSION SYSTEMS

LIST OF FIGURES

LIST OF TABLES

GLOSSARY

ADCP	Acoustic Doppler Current Profiler
Amphidrome	A point with no tidal range
Bathymetry	measured sea bed depth
CFD	Computational Fluid Dynamics
Coriollis force	Horizontal rotational force caused by the earth's rotation
DBERR	Dept of Business, Enterprise and Regulatory Reform
DLL	Dynamic Link Library
DTI	Department of Trade and Industry
EC	European Commission
EPSRC	Engineering and Physical Sciences Research Council
ESRI	Environmental Systems Research Institute
GIS	Geographical Information System
GPS	Global Positioning System
GUI	Graphical User Interface
Gradicule	Longitude and latitude lines on a navigational chart
HMRC	Hydraulic and Maritime Research Centre
HW	High Water
LAT	Lowest Astronimical Tide
LW	Low Water
MCT	Marine Current Turbines Ltd
OPTCurrenT	Optimising the Performance (Electrical & Economic) of Tidal Current Turbines
OSGB	Ordnance Survey Great Britain
Perigree	The point in orbit nearest the earth
POL	Proudman Oceanographic Laboratory
RCE	Relative Cost of Energy
rpd	revolutions per day
SI	System Internationale unit of measure
SUPERGEN	EPSRC Research Initiative for future energy
TCECS	Tidal Current Energy Conversion System
Tide Rose	Graphical representation of the proportion of flow coming from different directions
UK	United Kingdom
UKHO	United Kingdom Hydrograhic Office
UTM	Universal Transverse Mercator
VB	Visual Basic
Yaw	rotational movement about the vertical axis

NOMENCLATURE

a	the axial spacing factor
A	constant defining the range of the tide
A	the swept area
A	the cross sectional area
A	the swept area of the blades
A	the total amplitude
A	Coefficient in Equations 2.22 to 2.25
A	the flow area
A_C	the cost per metre for the cable
A_C	the cost of cable per unit length
A_i	the amplitude of the component
A_j	the amplitude for each constituent
A_{device}	the swept area of the device
α	the radial spacing of the devices
B	constant defining the range of the tide
B	Coefficient in Equations 2.22 to 2.25
C	constant defining the range of the tide
C	Coefficient in Equations 2.22 to 2.25
CAPEX	the total capital investment
C	the Chezy coefficient
C_b	the safety factor for buckling
C_o	the intercept given by the mean of the data
Cp	the power coefficient of the blades
C_{Trust}	the trust coefficient
C_s	the safety factor defining the maximum allowable stress in the pile
D	Coefficient in Equations 2.22 to 2.25
D	the pile diameter
D	the diameter of the rotor
DV	the support vessel cost per day
E	the modulus of elasticity
E_S	the exceedence for a given magnitude
f	the Corollas coefficient
f	the fraction of the kinetic flux being extracted
F	the gravitational force exerted on the Earth
F_1	the comparison pair to F_o

F_1	the comparison pair to F_o
f_2	the phase delay for the M_2 tidal harmonic
f_f	the phase delay for the M_f tidal harmonic
F_o	the frequency being considered for inclusion
F_o	frequency being considered for inclusion
F_{Thrust}	the thrust
g	the acceleration due to gravity
h	the water depth
I	the total number of days for array installation
i	the harmonic component
i	the number of the speed bin
i	the value for an individual constituent
i	the index of the zone
k	a friction coefficient
k	the Von Kármán constant
K_C	the cost constant for cable manufacture start up
K_c	the fixed cost
K_p	the Rankine passive load coefficient
KSDU	the cost of the subsea distribution unit
l	the length of the hydrofoils (2 x 7.05 m)
L_F	the free standing length of the pile
L_I	the approximate imbedded pile length
L_1	the length of array to shore cable
L_{array}	the length of cable in the array
L_{row}	the length of the cable in the row
MD	the mobilisation/demobilisation days
M_2	the principal lunar semi-diurnal harmonic
M_f	the lunar fortnightly harmonic
N	the number of measurements
N	the total number of values in the data
N	the number of cells in the zone
NH	Neap High
NH	the value at the neap maximum
NL	the value at the neap minimum
NL	Neap Low p is barometric pressure
Nr	the number of rows required for the number of turbines
N_m	the number of devices in the row
N_m	the number of devices in the array
N_m	the number of devices being installed

n	the Manning Friction coefficient
p	phase lag from a reference time
P	the power produced by the rotor
P_C	the pile cost
$P_{device}(u)$	the power produced by the device at current speed
$P_{area}(u)$	derived from Equation 4.1
P_{er}	the wetted perimeter
p_i	the phase advance of the component at the start of the period being analysed
Q	volumetric flow rate
r	the discount rate
r	the radius or arm length (11m)
r	the turbine radius
r	the raw value
R	the Rayleigh comparison coefficient
R	the hydraulic radius given by Equation 3.23
S	the incident flow speed
s	the tidal current magnitude
s	values within the dataset
SH	the value at the spring maximum
SH	Spring High
SL	the value at the spring minimum
SL	Spring Low
T	the lifetime of the project
T	the longevity of the survey
T	the wall thickness of the pile
T_1	the spring-neap tide period
T_2	the ebb-flood tide period
t	the time in hours along the original data set
t	the time in hours along the original data set
t	time
T_S	the surface termination unit cost
T_S	the cost of the cable termination
T	the longevity of the survey
T_2	the period of the M_2 tidal harmonic
T_U	the underwater termination unit cost
T_U	the cost of array termination units
$u*$	the friction velocity determined by Equation 3.21
U	reference velocity

U	the water flow velocity
U_{cmc}	the cube-root mean cube speed given by Equation 4.4
u	the current speed
u^*	the friction velocity
u	the west-east velocity component
$u(z)$	the velocity magnitude as function of the height above the sea-bed
u'	the rotated west-east velocity component
u_{max}	the maximum velocity component normal to the swept area
U_C	the unit cost per unit weight of steel
V	the installation vessel cost per day
v	the south-north velocity component
v'	the rotated south-north velocity component
WOWD	the number of waiting on weather days
$W_{x,y}$	wind velocity 10 m above the sea level
x	the position of the discretisation zone boundary in the x or y direction
X	the real part of the complex variable Z
X_j	the real part of the amplitude of the consituent
X_o	the real part of data's mean
Y_j	the imaginary part of the amplitude of the consituent
Y_o	the imaginary part of the data's mean
y	the height above the sea-bed
Y	the imaginary part of the complex variable Z
y'	the predicted value of velocity magnitude
y'	predicted value of velocity magnitude
Z	complex variable describing tidal magnitude
z_o	a characteristic length related to the roughness of the seabed
z_0	the hub height
z0	the mean level
z_{max}	the height of the water column

γ	the local kinematic turbulent viscosity
ΔP	the difference in power between raw value and that after power extraction
Θ	the angle of the major axis from the x direction
Δu	the difference in velocity between raw value and that after power extraction
Φ	the horizontal velocity component or tidal amplitude
τ_0	the bed friction shear stress term
ρ_b	the seabed sediment specific weight

Φ_{nf} the horizontal velocity components or tidal amplitude at mean neap-flood tides

Φ_{se} the horizontal velocity components or tidal amplitude at mean spring-ebb tides

Φ_{sf}, the horizontal velocity components or tidal amplitude at mean spring-flood tides

Δx	the length over which the energy is being extracted
β	the axial spacing of the devices.
Δ_S	the sample band width
Δt	time interval between measurements
Δx	the resolution of cells in the zone
θ_j	the imaginary part of the phase difference
μ	the product of the efficiencies of gearbox
ρ	the water density
σ_{lim}	the elastic limit stress
Φ	the internal friction angle of the seabed sediment
Φ_j	phase difference for each tidal constituent
Φ_j	the real part of the phase difference
ω	the arm arc (71°)
ω	the frequency of the component
Ω_S	the occurrence for a value band
Φ	the parameter being analysed (depth or velocity)

CHAPTER 1 INTRODUCTION

1.1 Aim

This thesis examines the contribution of computational modelling in the development of the emerging tidal current energy industry. It does this through the examination of four key areas of mathematical modelling applied to the field:

1. Tidal current analysis and prediction

2. Hydrodynamic flow modelling

3. Tidal resource analysis

4. Optimised economic modelling

The work examines these areas through the application of techniques to case studies and sensitivity analysis. The aim is to demonstrate the benefits of mathematical modelling in the development of an area for exploiting tidal currents for electrical energy generation.

1.2 Background

1.2.1 Tidal Currents

Tidal currents are a natural phenomenon caused by the effects of gravitational forces acting on the Earth's seas and oceans. The theoretical basis for this is covered in more detail in Chapter 2, however it will be summarised here based on the theory provided by Doodson & Warburg (1941) and Pugh (Pugh 1987).

The gravitational attraction of the moon is the main force acting on the Earth's ocean. This force pulls the Earth and the surface of the ocean towards the Moon causing two tidal bulges either side of the Earth – one on the side of the

Earth facing the moon and the other on the opposite side. The Earth rotates at approximately 1/24 revolutions/day (rpd) and the moon revolves around the Earth at a rate of approximately one revolution every 28 days or 1/672 rpd. The combination of these rates of progression causes the tidal bulges to progress across the Earth's surface as long tidal waves with a period of approximately 12 hours and 25 minutes. The progression of this wave is observed as a flood tide as the peak of the wave moves towards an arbitrary point and an ebb tide as the peak passes and the trough of the wave progresses towards the same point. High water (HW) is observed at the peak of the wave and low water (LW) is observed at the trough of the wave. In addition, the Sun exerts a gravitational pull on the Earth and its oceans. The strength of this attraction is approximately half that of the Moon and a bulge in the ocean is generated in a similar fashion to that of the Moon's gravitational attraction. The Moon falls in and out of alignment with the Sun and Earth as it progresses around the Earth. This has the effect of enhancing the tide as the magnitudes of the gravitational attractions are additive at New and Full Moon, when the Moon is between the Sun and Earth and when the Earth is between the Sun and Moon, respectively. These enhanced tides are known as spring tides and occur fortnightly. The tidal range, which is the difference between HW and LW, is greater at spring tides. By contrast, the effect of the joint forces of the Sun and Moon is least when they are in opposition or at right angles to one another around the Earth. This causes a neap tide when the tidal range is at a minimum. The increased tidal range at spring tide also causes the tidal currents to be faster as the water has a greater potential head driving it from HW to LW in the same period. In antithesis, tidal currents are slower at neap tides. The tidal range and tidal current speeds are general low in the open ocean. However, the sea bed and topologies restrict flow causing retardation of the tidal wave and acceleration of the flow. These accelerated flows can reach considerable speeds in some inter-island channels and in areas between two large bodies of water. It is these tidal flows that are considered for exploitation for the production of energy from tidal currents.

1.2.2 Tidal Current Energy

The exploitation of the ocean's tides for energy production is not a new concept. Potential energy stored by holding back the tide with a barrage has been used for mechanical energy generation since medieval times. Indeed there is evidence of such tide mills around the North Sea coastline (Langdon 2004). For example, the Eling Tide Mill (Totton & Eling, Southampton, UK) is referenced in the Domesday Book and is still operated today (Eling Tide Mill Trust Ltd 2008). There have been more recent developments of this technology for electrical energy generation. The most famous of these is the La Rance tidal barrage that was commissioned in 1966 (Frau 1993). The technology behind such tidal energy conversion systems is wholly different from those being considered here and therefore will not be elaborated upon.

The contemporary developments in tidal current energy began in the early 1990's. In the European arena, IT Power Ltd trialled a 1.5 m turbine suspended from a boat. This proof of concept proved that power could be produced from tidal flows. However, it also demonstrated the design problems with such devices as it was fouled by one of its tethers. The CENIX study funded by the European Commission (EC), which reported in 1995, developed mechanisms for calculating tidal resources and identified the key European sites that would hold potential for tidal current energy exploitation. At that time there were a minimal number of propositions for tidal energy devices. The Seaflow project was developed by Marine Current Turbines Ltd (MCT) funded by the European Commission (EC), The United Kingdom (UK), and private investment. The project commenced in 1998 and the device was deployed in the Severn Estuary off Lynmouth, Devon, UK in 2002. The Seaflow device was a horizontal axis turbine mounted upon a single pile drilled in to the sea bed. The ENERMAR project was developed around the same period by Ponte Di Archemedes SpA. This was a vertical axis turbine mounted an anchored, floating generator.

Tidal energy research developed in parallel with these concepts. The "Optimising the Performance (Electrical and Economic) of Tidal Current Turbines" (OPTCurrenT) commenced in 1998. The author was one of the contributing researchers on this project, and some of the work presented here is based on the applied research carried out during the programme.

Research and device development has proliferated during this first decade of the 21st century. Dacre & Bullen (2001) presented a study on the social and economic effects of tidal current energy developments in the Pentland Firth, UK; the EC funded the Coordinated Action on Ocean Energy, of which tidal current energy was a key part of the programme; and the UK Engineering and Physical Sciences Research Council (EPSRC) funded the SUPERGEN – Marine consortium. The goal of this programme was to investigate and determine solutions to the technical problems faced by ocean energy development.

1.3 Basis for Work

It is clear from Section 1.2.2 that the amount of research and number of publications in the field of tidal current stream energy is growing. However, the basis for this thesis' contribution to the field is prior to many of the publications presented more recently. The work covers research carried out by the author from 2001 up to 2005.

1.3.1 Tidal currents

Section 1.2.1 covers the theory of tidal flows and their production. However, a new arena of research is stepped into when tidal currents are considered for tidal current energy exploitation – that of the behaviour and measurement of extreme current flows. The author defines extreme currents as greater than 1 ms^{-1}. Howarth (Howarth 1981), comments on the lack of work in the field citing only one further reference (Booth 1978). Howarth (Howarth 1981) compared current meters moored in fast tidal currents. The maximum amplitude of the semi-diurnal principal lunar harmonic M$_2$, current measured was 0.81 ms^{-1}.

Some work has been done using acoustic current measurement in fast currents. For example Lu & Lueck (1989) used Acoustic Doppler Current Profilers (ADCP) to measure turbulence in a tidal channel. However, there are no references to the use of ADCP for measurement of extreme tidal currents prior to the OPTCurrenT study (Lewis & Holmes, 2000, Bryden, Delure, DeNat et al. 2001). This work is considered in greater detail in Chapter 2. Further, there is no public reference to the use of ADCPs for measuring extreme currents to assess

tidal energy resources prior to installation of a large scale tidal current energy converter.

1.3.2 Tidal Current Energy

Interest in tidal current energy, and more generally, flow in extreme tidal regimes was in its early stages at the time of the start of the work. In many ways this provided the justification for the work. The European Commission (Commission of the European Community 1995) raised the issue of tidal stream energy at a European level. The resulting project's aim was to identify locations in Europe that may have an exploitable tidal resource using available published data. In the process it developed concepts from wind energy, such as the power curve, and applied them to the identified areas. The analysis produced an early estimate for the European tidal current energy resource as 12.5 GW over 106 locations in the European Community (Bryden, Naik, Fraenkel, P. et al., 1998). Other studies estimated the total European resource at 53.8 GW with a UK contribution of 47.7% (Bryden and MacFarlane, 2000 reporting from Charlier 1999). The DTI reported (Energy Technology Support Unit 1993) that tidal currents could provide a major proportion of the UK's electricity requirements. The development of interest in tidal energy is not surprising given such favourable estimates. These studies were wide scoping, covered many sites and utilised many general assumptions. For example, channels were assumed to have a rectangular profile and flow was assumed to be uniform across narrow channels. This was partly due to the information available. Many channels do not have detailed atlases of tidal currents, especially those where maritime navigation was not expected. For example, the Admiralty chart (Morris 1986) has tidal diamonds covering the shipping channel to Sullom Voe oil terminal, but not in other areas of fast currents. Also, the Admiralty chart for the Stretto di Messina (Morris 1987) contains no tidal current information.

Bryden, Naik, Fraenkel et al. (1998) developed a method of matching the performance or power curve (see Chapter 2) to the peak spring flow and discussed the restrictions such as depth and marine navigation that would be placed on choice of size and location of tidal current horizontal axis turbines. The paper was written in conjunction with IT Power Ltd, and identified costs for tidal current turbines. The study was done on a theoretical basis and lacks the

practical application of the optimisation of the method to actual sites. The current work investigates the application of such techniques to the real environment.

1.3.3 Hydrodynamic modelling for tidal energy

Hydrodynamic modelling of tidal flows is used widely in flow analysis for environmental purposes such as climate modelling, pollution monitoring, coastal protection, sediment transport and nutrient transfer.

However, there are no references to its use in the field of tidal current energy prior to the work carried out by the author. The OPTCurrenT project (Bryden, Delure, DeNat et al. 2001, Melville, Rados and Bryden, 2001), which forms part of this work was the first published work in the field. The work carried out by the author on the Engineering Business' Stingray project was the first hydrodynamic model produced prior to the deployment of a large-scale tidal current energy conversion system.

1.3.4 Economic modelling of tidal currents

Bryden, INaik, Fraenkel et al. (1998) considered the use of device economics in tidal current energy. However, the technique had not been applied to a real world topology. Dimla, Bryden & Rados (2000) developed a methodology for the process at the start of the OPTCurrenT project. The work carried out by the author extends the theoretical economic model and optimisation methodology to a parametric optimisation to determine the best position for a tidal farm within a tidal channel. It achieves this by considering the effects of the topography of a real channel on the economic return for the tidal flow.

1.3.5 Energy extraction

There is no published work on the effects of energy extraction prior to the author's work. It is, however, envisaged that extracting tidal energy from a channel would have an effect on the flow in the channel.

CHAPTER 2 SITE MONITORING AND DATA ANALYSIS

2.1 Introduction

This chapter considers the use and methodologies for current surveys in regard to tidal current energy. It discusses the logistics of installation, the methods of processing the data and how they may be best processed for the purposes of the tidal energy developer. It does this through analysis of the site survey data produced from several surveys carried out for the purposes of tidal energy research or site development. The approach taken is one of historical review of the methods of site survey and the associated analysis with discussion on the outcome of the surveys and how the survey method influences the decision of tidal developers. Some of the work presented here has been previously presented by the author (Melville 2000, Bryden 2001, The Engineering Business 2003, Melville, Couch & Bryden, 2007).

Site surveys have two purposes in the tidal energy arena. Firstly, there is the need to determine whether the site has sufficient current to generate cost effective energy. Secondly, once the device has been installed, there is the important task of monitoring device performance. In pre-deployment monitoring, a tidal current survey data is analysed for a number of purposes:

1.   Raw current data to validate the hydrodynamic tidal model;

2.   Harmonic analysis to predict future tides;

3.   Statistical analysis to determine the energy resource.

As will be discussed in Section 4, hydrodynamic models are considered important to indicate potential sites for energy extraction. Without validation from data taken in-situ, the models cannot be considered to be a good representation of the flow. Usually, only one position is surveyed, however it is preferable, but more expensive, to survey at a number of locations. Survey points should be positioned at the interior and the boundaries of the model area.

The data used for the analysis presented here comes from 3 surveys:

1. Arklow Bank, Republic of Ireland (1999) (Lewis & Holmes, 2000, Bryden 2001);

2. Yell Sound, Shetland, UK (2001) (Melville, Bryden & Lomax 2002);

3. Fall of Warness, Orkney Islands, UK (2005) (Melville, Couch & Bryden, 2007).

2.2 Arklow Bank

Surveys of Arklow Bank were carried out as part of the Optimising the Performance (Electrical and Economic) of Tidal Current Turbines (OPTCurrenT) project (Bryden 2001, Lewis & Holmes, 2000, Gravilli 2001) funded in-part by the European Commission as part of the Framework III Non-Nuclear Programme (contract no. JOR3-CT1998-0205). The surveys were carried out as part of Work Package (WP) 3 by the Hydraulic and Maritime Research Centre (HMRC) at the University College Cork. Lewis & Holmes (2000) (Bryden, Delure, DeNat et al., 2001) performed the original survey and data processing. The author carried out further analysis for WP4 and WP5 of the OPTCurrenT project. The purpose of this was to provide validation data for the hydrodynamic models developed by the author during WP4 of the project.

Arklow Bank is a low lying sand spit located in the St. George's channel off the Wicklow coast in the Republic of Ireland, extending from 50°40′, to 52°54′ 'N. The location of the site is show in Figure 2.1.

The predominant feature is a narrow bank rising from 30 metres to less than a metre below the sea surface. The bank runs for approximately 21,000 m from Ardmore Point, south of Wicklow to Courtown, lying 9,000 m off the Wicklow shore. The bank runs at an angle of approx. 10° relative to true north. The Irish coastline in this area is a series of bays bounded by cliffs with small beach areas. The coast runs at an angle approx. 15° to true north. To the east of the bank, the seabed ramps off to 70 m depth. At the north of the bank, a shallow shelf extends to 50 m depth several kilometres east of the bank (Haslam 1978, Haslam 1978a). These features can be seen in Figure 2.2.
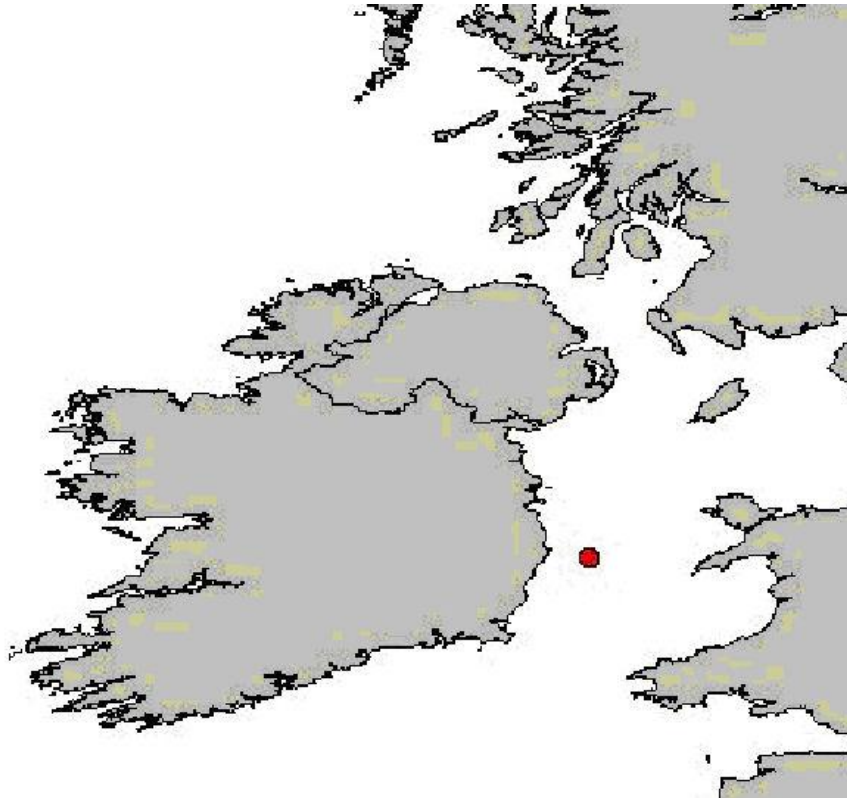
Figure 2.1 The location of Arklow Bank (Bryden 2001)

The flood tide flows in from the Atlantic Ocean, through the St. George's Channel, to the Irish Sea. The phase differences between the two bodies of water create a virtual amphidromic point located near Wicklow (Hall 1971, Pugh 1987). This can be seen in Figure 2.3.
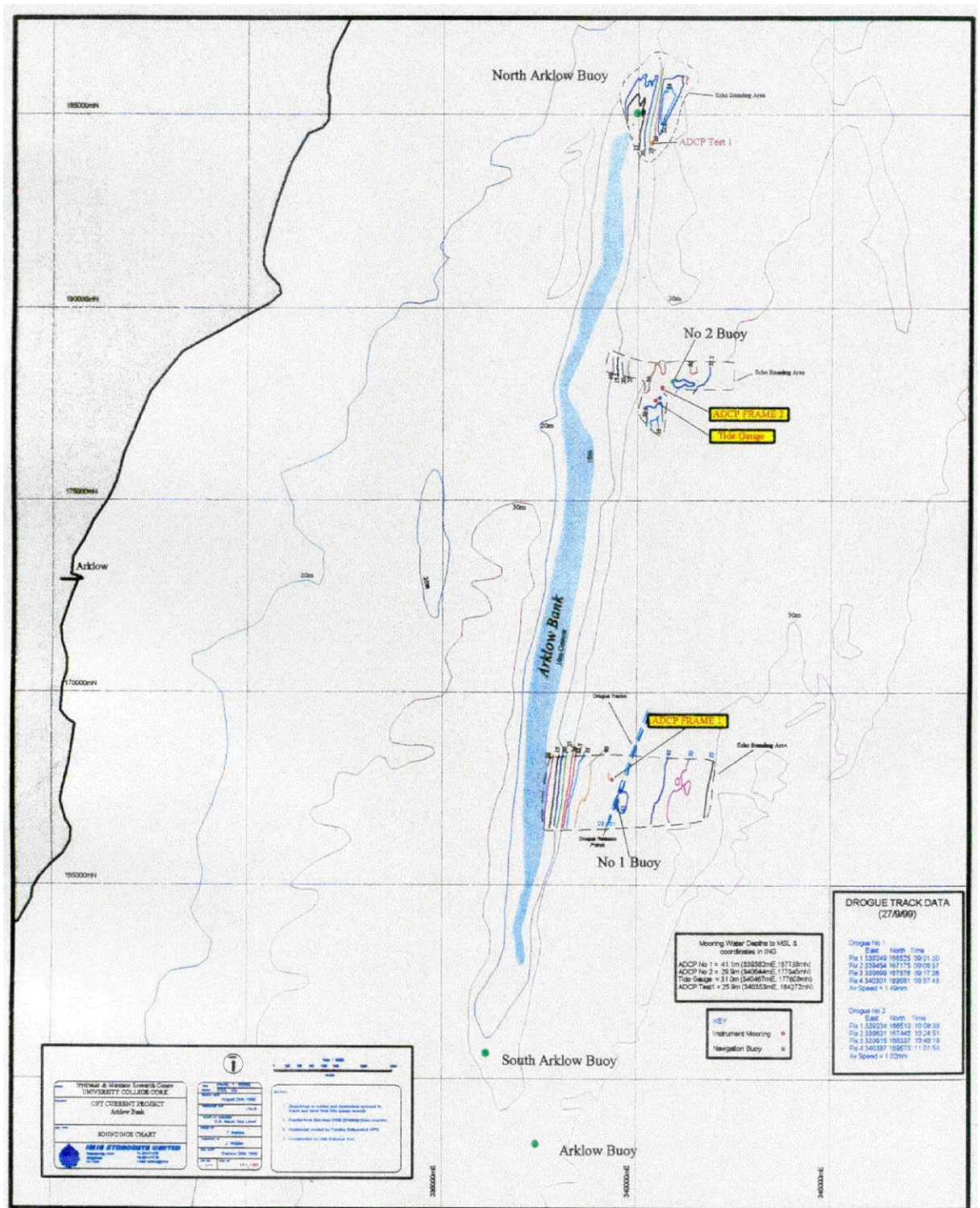
Figure 2.2 The Arklow Bank site showing positions of ADCP surveys (Bryden 2001, Lewis & Holmes, 2000).
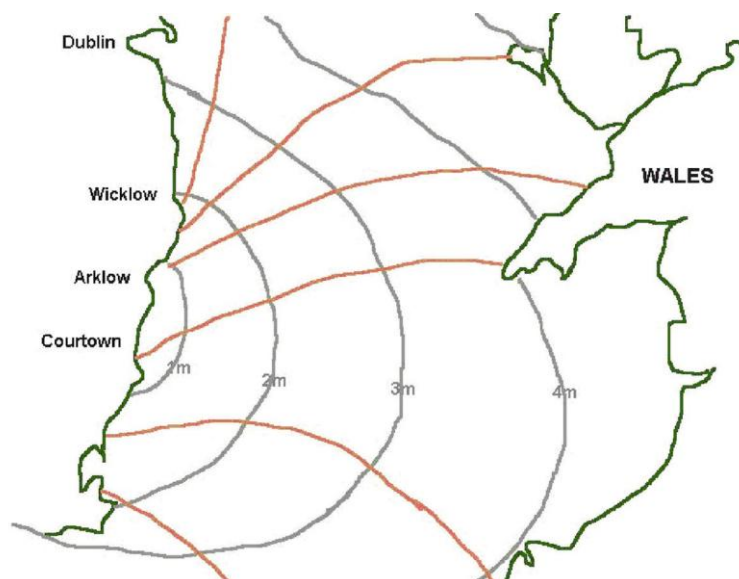
Figure 2.3 The co-tidal chart for the St Georges Channel (adapted from Hall 1971)

2.2.1 Method

The Arklow Bank project took place during the months of August and September in 1999. Two ADCP units deployed at the northern and southern end of the bank at positions 52.8355°N, 5.90916°W and 52.737°N, 5.93166°W (see Figure 2.2). The original concept was to provide boundary data for the hydrodynamic model which was to be produced in WP4 of the project (Bryden 2001). At the time, there was limited experience in deployment and use of ADCP in fast tidal currents. The HMRC experimented at a test site in Gascane Sound, near Cork before the Arklow deployment in order to optimise the ADCP support frame and determine a deployment operating procedure. The ADCP devices at Arklow Bank were operated according the settings in Table 2.1.

Table 2.1 Settings for ADCP meters for Arklow Surveys

Survey	North	South
Depth	29	41
First Ensemble Date	28/08/99	28/08/99
First Ensemble Time	17:07:44	12:00:16
Last Ensemble Date	26/09/99	28/09/99
Last Ensemble Time	11:36:44	13:41:16
Ensemble Interval (s)	20	30
No. of bins	10	12

2.2.2 Data Processing

The original data analysis was carried out by the HMRC (Bryden 2001).

The ADCP records current magnitude and direction readings at each bin through the water column. Time-series of these readings can be plotted to reveal the variation of the current magnitude through the ebb-flood and spring-neap tidal cycles, and how the direction changes between flood and ebb of the tide. The velocity vector components of the current can be produced as a combination of magnitude and direction:

Northerly component:

$$v = U \sin(\Theta) \hspace{8cm} 2.1$$

Easterly component:

$$u = U \cos(\Theta) \hspace{8cm} 2.2$$

Where U is the current magnitude, θ is the current direction in degrees clockwise from the vertical axis, and v and u are the north and east velocity components, respectively.

Plotting this data produces a graph, commonly known as a tidal ellipse. The tidal ellipse gives a visual representation of how the direction varies through the tidal cycle, which is more intuitive than the time series. Many of the tidal current energy systems being designed do not yaw like wind turbines. Rather, they reciprocate power extraction from one direction or its reverse. The tidal ellipse can clearly show whether the current is bi-direction (rectilinear), i.e. flips from one direction in the flood tide to the opposite direction in the ebb tide, or follows a more variable pattern. A further representation of the direction is the tide rose. This is analogous to the wind rose and plots the proportions of measurements recorded in a direction band. The tidal rose can be used to determine the directions in which the majority of the tide flows. In this aspect it is different from a wind rose, where the direction from which the wind comes is plotted.

The ADCP flow measurement instruments record the flow in vertical bins through the water column. It is therefore possible to get a velocity versus depth profile.

2.2.3 Results and Discussion

The variation in magnitude and direction for the northern survey can clearly be seen in Figure 2.5. The variation in magnitude between spring and neap tides can be seen, with the peak currents reaching maxima over 1.8 m/s in the spring tide and reducing to around 1.2 m/s in the neap tide. The three spring tides encountered during the surveys were approximately equal in strength, whilst the second neap tide, which occurred on 19th September was weaker than that of the 5th September. It is not possible to see the ebb to flood variation in magnitude in these figures plotting the entire survey. However, the ebb flood variation can be seen in Figure A.1 and Figure A.4, plotting the reduced data set from the first week of survey. This covers the first spring tide of the survey. It can be seen in these figures that the velocity in one tide was greater than in the other. Comparison with the direction time-series reveals that the ebbing tide (southerly flowing) was the stronger of the two. Though the difference is not great – in the order of 0.1 m/s – this may have implications for any tidal device that converts the energy with greater efficiency from one direction.

It can be seen in the direction time-series (Figure 2.6 and Figure A.3) that the flow direction steps between approximately 020° and 210° for both the northern and southern surveys. This direction change between the flood and ebb tides is consistent throughout the spring to neap cycle.

The direction of flow is in line with the Irish coastline and the Arklow bank at this location. That is the bank forces the tide to run along its length and permits only a small variation in flow normal to its orientation. In this sense, the Arklow Bank is a good site for tidal energy conversion systems.
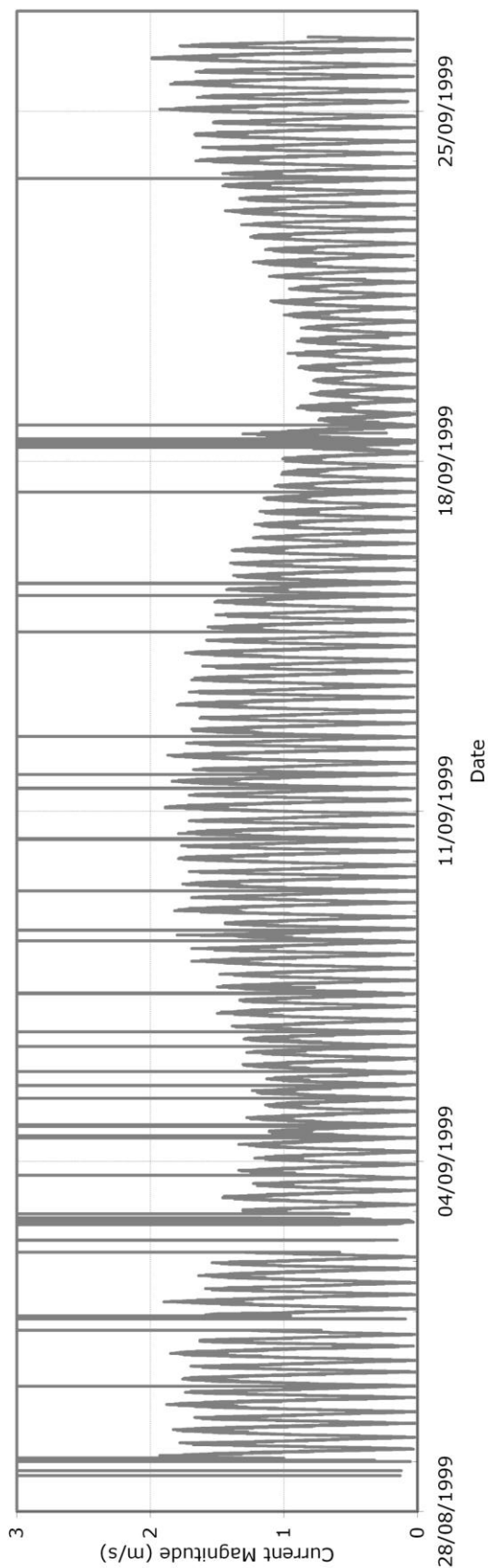
Figure 2.4 Magnitude time-series for the Arklow Bank North Survey (Bryden 2001, Lewis & Holmes, 2000)
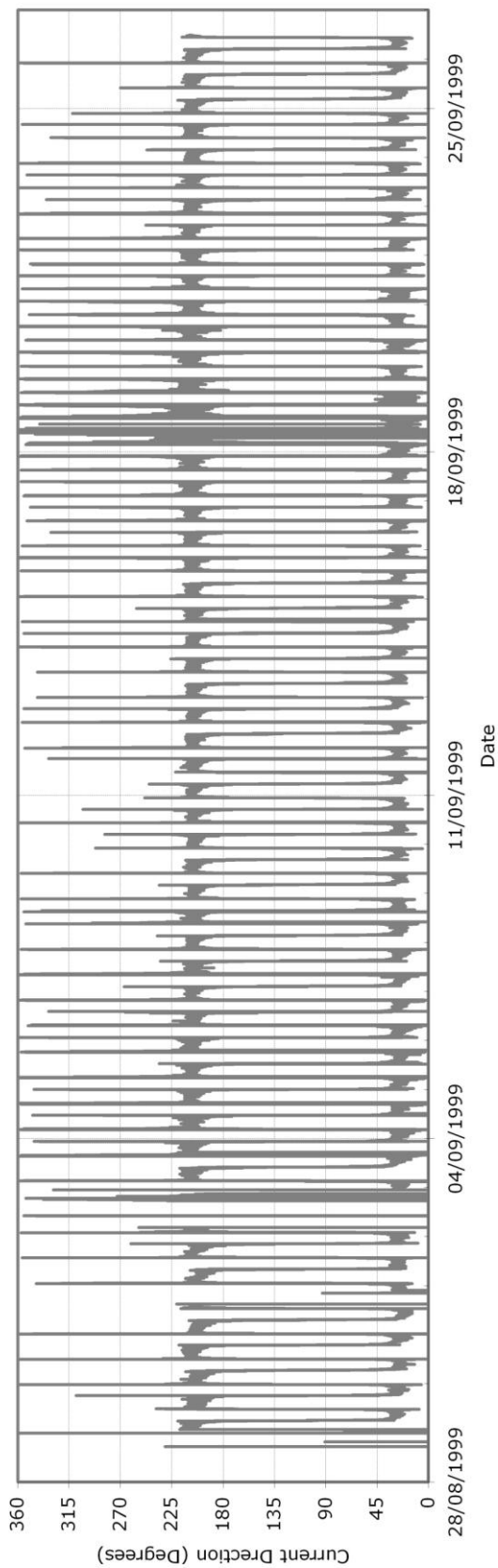
Figure 2.5 Magnitude time-series for the Arklow Bank North Survey (Bryden 2001, Lewis & Holmes, 2000)
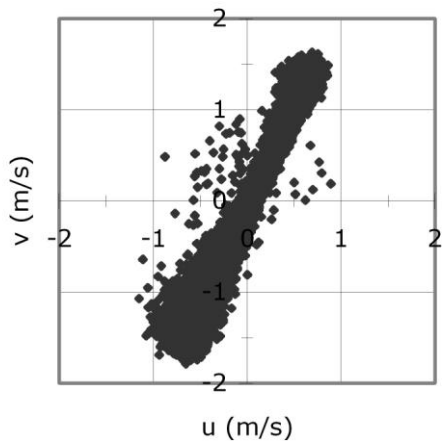
Figure 2.6 The tidal ellipse for 28/8/99 to 5/9/99, Arklow Bank North
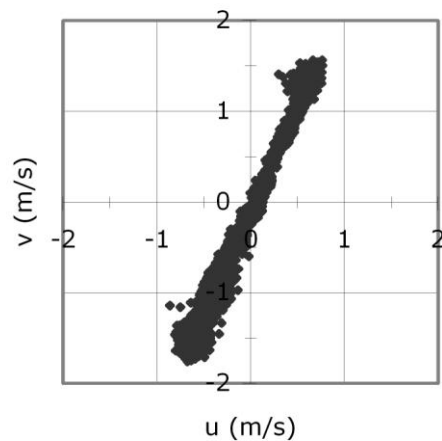
Figure 2.7 The tidal ellipse for 30/8/99 00:00:00 to 30/8/99 12:20:00, Arklow Bank North
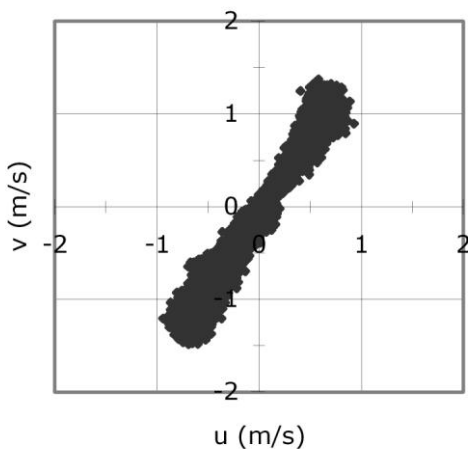
Figure 2.8 The tidal ellipse for 28/8/99 to 5/9/99, Arklow Bank South
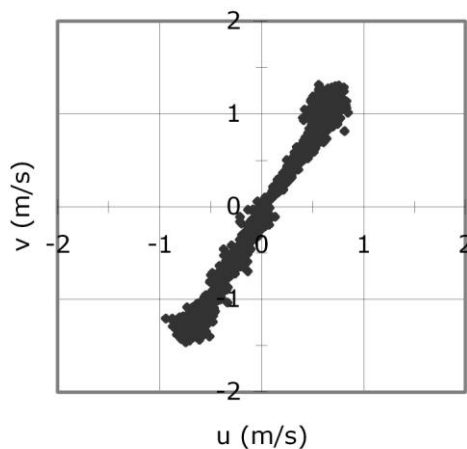
Figure 2.9 The tidal ellipse for 30/8/99 00:00:00 to 30/8/99 12:20:00, Arklow Bank South
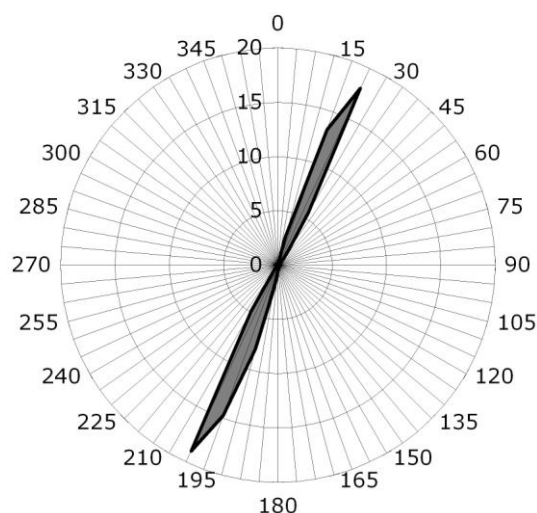
Figure 2.10 The tide rose for the North survey
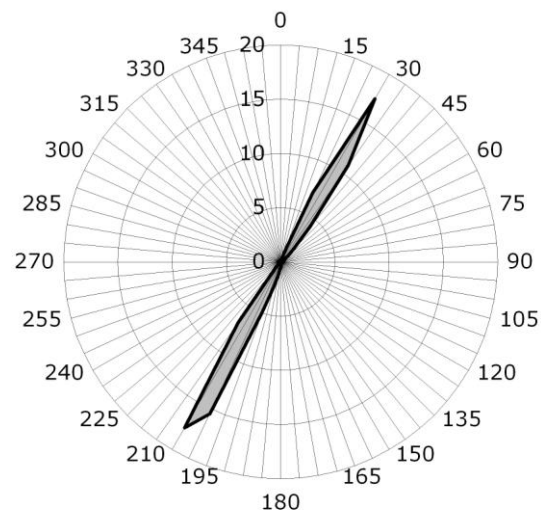
Figure 2.11 The tide rose for the South survey

The magnitude time-series for both deployments produced very noisy results, although the level of noise was greater in the northern survey with results going off-scale and therefore being recorded with a value of 99. These anomalous data can be seen on the plots of current magnitude () and occur frequently throughout the data sets. The anomalous data can be attributed to when the instruments were recovered to download the recorded data. However, this is not the only cause as they occur more frequently than the number of recoveries. Lewis (Lewis 200) commented on the variability of the flow and considered the causes were:

1. Turbulence;

2. Sensor movement;

3. "Numerically introduced (but at the specified pulse rate and bin depth SD < lcm/s. whilst 10% fd ~ 15cm/s)";

4. Instrument set-up including time varying error after calibration;

5. Influence of the mooring buoy on the support structure.

The last of these possible causes was dismissed as the marker buoys were lost during the survey period whilst the variability persisted throughout the survey. The readings were taken with short time-averaging. The ensemble interval on the North survey was 20s, whilst that on the South survey was 30 s. Such short time-scales could have captured the length scales of flow turbulence. It can be seen in Figure 2.7 and Figure 2.9 that there is erratic movement in the current direction and magnitude. This was not useful for the purposes of this study where a smoother current profile is preferred to reveal minima and maxima that can be used effectively as comparison data and boundary conditions for the tidal model. If indeed the noise is due to turbulence then this survey revealed a level of turbulence that had not previously been considered in the development of tidal current energy conversion systems. Turbulence is considered in greater detail later in this work.

The velocity profiles for the Northern and Southern surveys are presented in Figure 2.12 and Figure 2.13. The profiles cover number of time interval measurements over a spring tide. A number of features can be seen. Generally, the velocity profile curves from slower flow near the bottom of the water column. The velocity increases in strength to near the surface. This variation is discussed in greater detail below.

Near the surface – over the top two surface bins – the flow drops off. This is not what would be expected. The fast flow should continue to the water surface. This aberration appears to be a feature of ADCP measurement. It can also be observed in the Yell data (Figure 2.14). It is suspected by the author that this feature is caused by the interaction of the sonar pulse with the water surface – wave action and signal scatter.
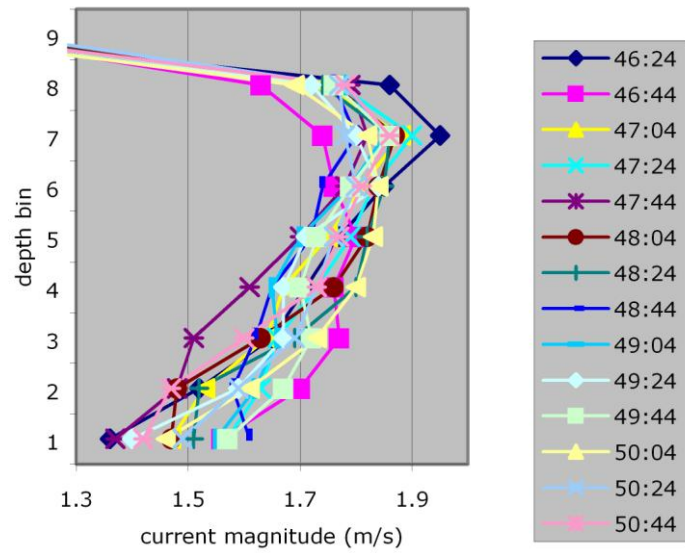
Figure 2.12 Current magnitude depth profile for North Survey at peak tide on 30 August
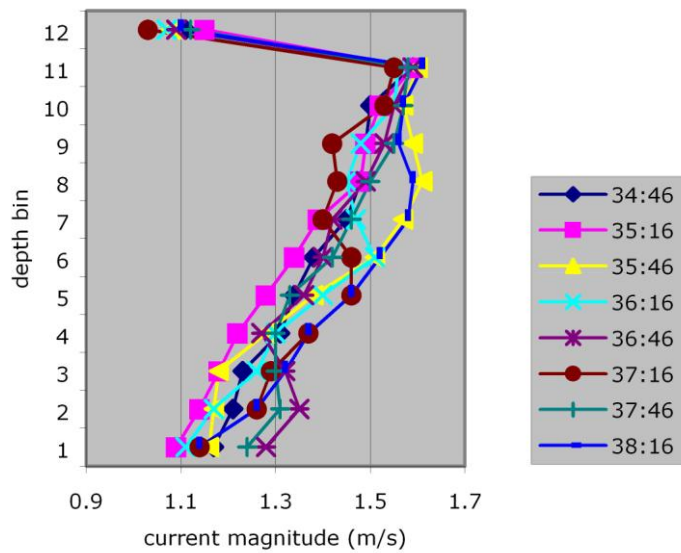
Figure 2.13 Current magnitude depth profile for South Survey at peak tide on 30 August
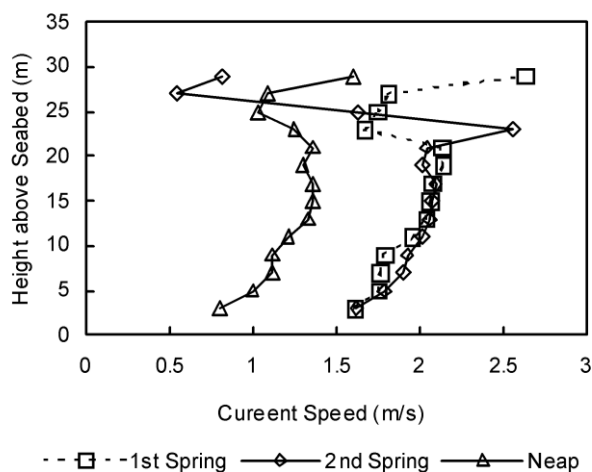
Figure 2.14 Variation of speed with depth over spring and neap tides at Yell Sound

The velocity-depth profile is usually considered to be a $^1/_7{}^{th}$ power law relationship, i.e.

$$u(z) = U \cdot \left(\frac{z}{z_{maz}} \right)^{\frac{1}{7}}$$ 2.1

Where $u(z)$ is the velocity magnitude as function of the height above the sea-bed (z); U is a reference velocity, which is usually considered to be the maximum bulk flow velocity and z_{max} is the height of the water column.

The velocity profile relative to depth alongside the power law relationship can be seen in Figure 2.15 and Figure 2.16. The northern site profile from that time is close to the power-law curve with deviation at the surface and near the sea-bed. That for the southern site has a steeper flow profile, with flow being faster near the sea-bed than is predicted by the power-law. The original study (Lewis 2002) demonstrated a near-uniform profile for the southern site. The difference between the two studies is likely due to the selection of time of profile being analysed.
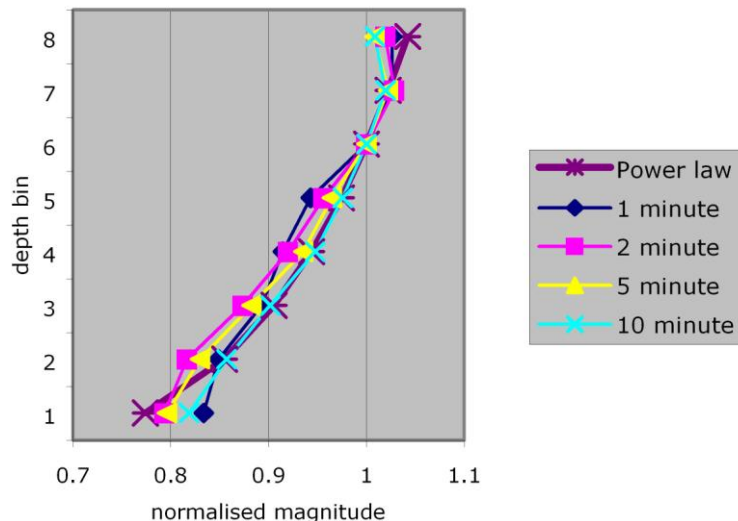
Figure 2.15 Time averaged velocity profile for Arklow Bank north survey alongside power law relationship
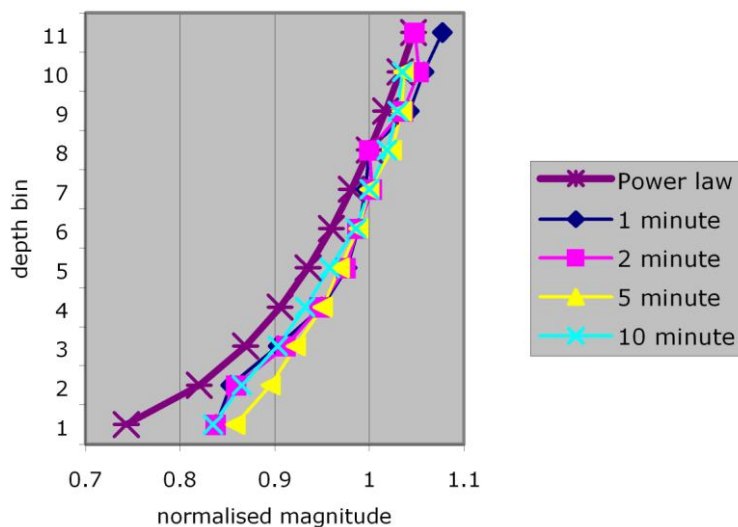
Figure 2.16 Time averaged velocity profile for Arklow Bank South survey alongside power law relationship

Another feature of the velocity depth profiles (Figure 2.12 and Figure 2.13) was that the velocity did not vary smoothly over the depth for any particular time interval and varied by 0.1 m/s to 0.2 m/s over an approximately 5 minute time period. This is further evidence of the flow variation discussed previously that may be due to turbulence.

For both the northern and southern sites, the effect of increasing the time-averaging period smoothes the velocity profile. At the southern site (Figure 2.16), the profile varies little between the 10 minute and 5 minute averaging period.

2.3 Yell Sound, Shetland

This section considers the survey work and analysis carried out for the Engineering Business' Stingray project. The survey work was carried out by the Engineering Business as part of their pre-deployment survey. The data was analysed by this author to provide them with information as to the expected currents and the suitability of the site for a tidal energy development. Yell Sound is located between the islands of Unst and Yell in the Shetland Islands. The complete channel is approximately 30 m long. The fastest currents are found in the narrowest section at 60.504^ON, 1.196^OW. The wider sections to the North and South East drop to over 100 m depth, whilst the maximum depth in the shallowest section is approximately 38 m on the chart (Haslam 1980, Morris 1986) as can be seen in Figure 2.17. The Stingray device can be seen in Figure 2.18, and was a reciprocating hydrofoil design. The 15.5m horizontal hydrofoil was controlled by hydraulics to vary its angle of attack in to the oncoming current stream. The resultant lift forces moved the hydrofoil up and down on an 11 m arm through at $71^°$ arc. The reciprocating motion drove a hydraulic motor which, in turn drove an electrical generator. The device had a rated power output of 150 kW at 1.5 m/s (The Engineering Business Ltd 2003). The hydrofoil had an asymmetric profile such that the device could only extract energy from one flow direction.
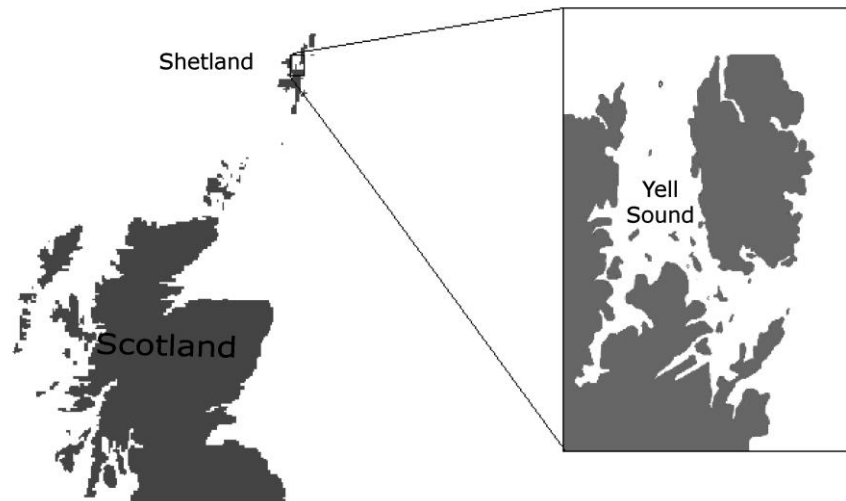
Figure 2.17 Yell Sound

Figure 2.18 The Stingray tidal energy converter (courtesy of Engineering Business Ltd)

Three survey deployments were carried out. The first two were to validated the tidal current simulation (Chapter 3) and confirm the strength of the tidal currents in the site being considered for deployment of the Stingray device.

The third survey was carried out during the deployment of Stingray to monitor the input current to the device.

2.3.1 Method

Seabed mounted ADCP units were used for all three surveys, similar to that used at Arklow Bank in Section 2.2.1, although those deployed here operated at a higher sound frequency of 615 kHz. The sensor unit was mounted on gimbals in a pyramidal support frame (Figure 2.19). The purpose of the gimbals was to ensure that the device pointed vertically upwards when located on sloping seabeds. The settings for the ADCP unit are given in Table 2.2. The sensor recorded depth, pitch, roll and heading, in addition to the magnitude and direction of the current at each bin.

Table 2.2 Settings for ADCP meters for Yell Sound Survey

Broadband (kHz)	614.4
First Ensemble Date	01/03/2001
First Ensemble Time	12:15:00
Ensemble Interval (s)	900.00
1st Bin Range (m)	1.00
Bin Size (m)	2.00
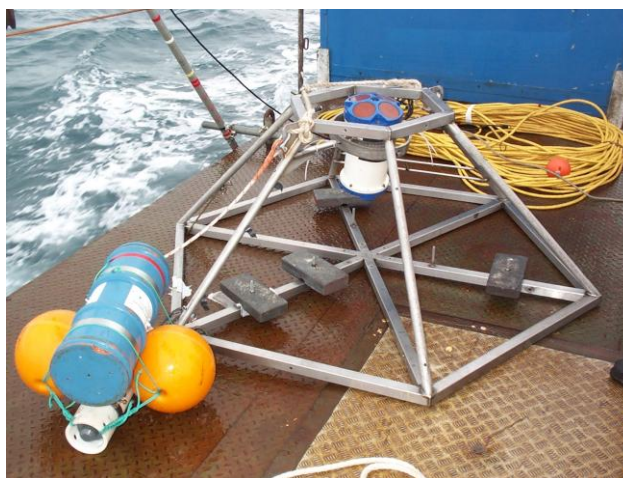
Figure 2.19 The ADCP used in Yell Sound (courtesy of Engineering Business Ltd)

2.3.2 Data processing

The data processing in the Arklow Bank survey was aimed at a generic tidal turbine. Although flow direction was considered in the tidal ellipse and tide rose analysis, the analysis of the flow strength considered the scalar magnitude. As far as Stingray was concerned, the analysis was device-specific. The Stingray was only able to extract energy from one direction. As such, the analysis had to consider the most suitable orientation of the device from which the greatest power could be extracted and how much power could be extracted in that orientation. In the Arklow Bank study, the data was examined at a position 60% up the water column. This corresponds to the mean flow speed for a $1/7^{th}$ power-law flow profile. The original analysis of the Yell Sound data (Melville, Rados & Bryden 2001) considered analysing the flow characteristics at all bins through the water-column in order to maximise the information available to Stingray's designers. However, the information at 13 m above the sea-bed was considered in special detail as this was the height of the pivot point of the device and mid-sweep of the hydrofoil.

2.3.2.a   Analysis of measured data

It was necessary to plot normalised data for the purposes of this thesis due to the commercial sensitivity of the data. The velocities were normalised against the mean of the magnitude.

$$s_{norm} = \frac{s}{\dfrac{\sum\limits_{I=1}^{N} s_i}{N}}$$ 2.2

Where s is the tidal current magnitude, N is the number of measurements.

Time-series of the current magnitude and direction were plotted to obtain a visual appreciation of the variability and quality of the data over the survey period with the Arklow study, as were the tidal ellipses and the tide rose during the spring and neap tides. The prevailing flow direction was used to determine the most suitable orientation of the device. This set the angle of the velocity

vector upon which the other analyses were performed since the hydrofoil only gets lift from the velocity component normal to the leading edge. The hydrofoil is asymmetrical, and consequently only gets lift in one direction. As such, calculations of the power output potential of the site based on flow magnitude would over-estimate that actually available to Stingray. It was therefore necessary to determine the power based on the normal incident flow using the flow in the principal axis of the tidal ellipse.

Having obtained the velocity vectors *u(x)* and *v(y)* using equations 2.2 and 2.1, it was necessary to rotate the tidal vectors from the angle of the major axis of the tidal ellipse to align with the *u(x)* axis.

$$\begin{bmatrix} \cos(-\varTheta) & \sin(-\varTheta) \\ -\sin(-\varTheta) & \cos(-\varTheta) \end{bmatrix} \begin{bmatrix} u \\ v \end{bmatrix} = \begin{bmatrix} u' \\ v' \end{bmatrix} \qquad\qquad 2.3$$

Where *u* and *v* are the vector components of the original tidal current data, *Θ* is the angle of the major axis from the x direction and *u′* and *v′* are the vector components of rotated flow. Now calculations can be performed solely on the value *u′*.

The exceedence is the number of values in a data set that are greater than a particular value. This statistic is used to plot the load curve as it is called in the wind power industry. It is usually normalised to be a fraction of the total data set for the purposes of comparison.

$$\mathrm{E}_S = \frac{\mathrm{N}(s > S)}{N} \qquad\qquad 2.4$$

Where E_S is the exceedence for a given magnitude, S; *N* is the total number of values in the data and *s* are values within the dataset.

The occurrence is of greater use in determining the energy potential of a site. It is taken as the fraction of readings at a particular value within the data set. It is usual to take a band of values rather than individual values with the occurrence being assumed to apply to the mid-point value of the band.

$$\Omega_S = \frac{N(s > S + \frac{\Delta s}{2}) - N(s > S - \frac{3\Delta s}{2})}{N}$$

2.5

Where Ω_S is the occurrence for a value band, the mid-point of which is S, N is the total number of values within the sample; s are the values in the data set and Δs is the sample band width. If exceedence is calculated for a data set at intervals of Δs, the occurrence calculation simplifies to

$$\Omega_S = E_{S - \frac{\Delta s}{2}} - E_{S - \frac{3\Delta s}{2}}$$

2.6

i.e. the subtraction of sequential values of exceedence.

The probability density can be derived from the occurrence using

$$P(S) = \frac{\Omega_S}{\Delta S}$$

2.7

The occurrence is an important statistic as the average power from a device can be derived from it. The instantaneous power from a tidal turbine is given by

$$P(S) = \tfrac{1}{2}\rho \cdot Cp \cdot A \cdot U^3$$

2.8

Where P is the power produced by the rotor, ρ is the water density, Cp is the power coefficient of the blades, A is the swept area of the blades and S is the incident flow speed (Boyle 2004).

The average power output is then

$$\overline{P} = \int_0^{S_{max}} P(S) \cdot P(S) dS$$

2.9

Or in discrete form

$$\overline{P} = \sum_{i=1}^{i_{max}} P(S_i) \cdot P(S_i) \Delta S_i \qquad\qquad 2.10$$

Where i is the number of the speed bin.

It is simpler to use the occurrence in this calculation for processing purposes. Substituting the definition of the probability density in equation 2.7, the above equation becomes:

$$\overline{P} = \sum_{i=1}^{i_{max}} \Omega(S_i) \cdot P(S_i) \qquad\qquad 2.11$$

Equation 2.10 is the form generally quoted for tide and wind power (Bryden 2007, Bryden 2001), whereby the current magnitude is used. As described previously, the Stingray extracts power from a narrower flow window. It was therefore necessary in this work to use the magnitude of the current vector lying along the line of the principal axis of the tidal ellipse and to split it in to its positive and negative directions.

It is then possible to determine the potential power output from the Stingray device placed at the survey location in Yell Sound. The Engineering Business (The Engineering Business Ltd 2003) noted that the power output varied throughout the reciprocating cycle of the hydrofoil. This is because the control system has to shed energy in order to slow the arm down and reverse direction at the top and bottom of the cycle. The peak power produced by Stingray during the trials was 250 kW at 1.5 m/s, although on average it produced 40 to 50 kW in a 1.75 m/s current. It is possible to determine a power coefficient, *Cp*, for Stingray from these figures by re-arranging Equation 2.8. By considering the water density to be the 1025 kg/m^3; and the swept area for Stingray as:

$$A = \frac{\omega}{180} \pi r l \qquad\qquad 2.12$$

where *A* is the swept area; ω is the arm arc (71°); *l* is the length of the hydrofoils (2 x 7.05 m) and r is the radius or arm length (11m).

A power-curve may then be produced assuming the standard format of cut-in speed, rated speed and cut-out speed (Boyle 2004) with Equation 2.8 being used to determine the power output between the cut-in and rated speeds. It is important to note that insufficient information could be gained from the published report on the Stingray project (The Engineering Business Ltd 2003) to determine the working power-curve from Stingray. For the purposes of this analysis, a hypothetical power curve was assumed, having a cut-in speed of 0.75 m/s, along with the published rated power and rated speed of 150 kW at 1.5 m/s and power coefficient of 0.451.

2.3.2.b Analysis of predicted data

Following on from the analysis of the measured data, it is necessary to consider how the data may be modelled. The predictability of tidal flow is one of the key advantages of tidal power energy over wind and wave power. This feature can be used to predict tidal flows and therefore energy output into the future away from the time of the survey. It also may be used to fill in anomalous data areas of the measured data set, as considered in the observations of the measured data in section 2.3.2.a.

Two methods of predictive analysis were used on the Yell Data.

The concept of harmonic analysis is based upon the Newtonian theory of the equilibrium tide and described by Doodson (Doodson 1941). The theory that follows is taken from Doodson (Doodson 1941) and Pugh (Pugh 1987). The theory proposes that for an elliptical earth with no continental land mass, the tides are caused purely by the gravitational forces exerted on the earth's ocean by the moon and sun. The Moon rotates around the Earth, the Earth around the Sun and the Earth rotates on its axis with periods of 28 days, 365 days and 24 hours respectively. In addition, the lunar orbit is elliptical so that the Moon is closer to the earth on approach to perigee, whilst the Earth's orbit around the Sun is also elliptical, with the Earth closest to the Sun at the time of perihelion. The Earth's axis of rotation tilts at 23.5° relative to its orbital plane such that the Sun and Moon follow a sinusoidal ecliptic over the Earth's surface. The Moon and Sun thus exert forces on the Earth's surface that vary as a summation of the influences of these sinusoidal varying effects. Harmonic

analysis breaks this summation down in to a number of identifiable frequencies such that

$$F = a\cos(\omega t + p)$$ 2.13

Where F is the gravitational force exerted on the Earth, ω is the frequency of the component, or constituent, t is time and p is a phase lag from a reference time.

Thus the total force exerted is

$$F = \sum_i a_i \cos(\omega_i t + p_i)$$ 2.14

Where the suffix i denotes the value for an individual constituent. The resultant effect on the amplitude of the tidal wave can then be described by:

$$A = z0 + \sum_i A_i \cos\left(\frac{2\pi \cdot t}{T_i} + p_i\right)$$ 2.15

Where A is the total amplitude; $z0$ is the mean level; i is the harmonic component; A_i is the amplitude of the component; t is the time; T_i is the period of the component; p_i is the phase advance of the component at the start of the period being analysed.

The constituents are divided into 4 major groups – semi-diurnal, diurnal, long-term and nodal. Semi-diurnal tides are those constituents that have a period in the order of half a day. In nomenclature, they are denoted by a suffix of 2. The principal of these is the M_2, which is the principal lunar constituent. The principal solar semi-diurnal tide, S_2, has the next strongest influence. Diurnal components are those with a period in the order of a mean solar day and are denoted with the suffix 1. The constituents O_1 and K_1 are the strongest of these defined as (Doodson 1941): a lunar declinational diurnal constituent, with speed $= 13°.943$ per mean solar hour and a lunar declinational diurnal constituent, with speed $= 15°.041$ per mean solar hour, respectively.

The long-term constituents refer to those with periods longer than a day up to approximately a mean solar year (365.25 mean solar days). These constituents are not predictable from surveys less than 6 months owing to their small amplitudes and long period. The principal constituents of this type are S_a, the solar annual; S_{sa}, the solar semi-annual; M_m, the lunar month; and M_f the lunar fortnight.

The Nodal variations are due to very long term astronomical variations in the earth's orbit. The variation has a period of 18.7 years. In this case, there are no constituents. Instead, variations in amplitude and phase are applied to the semi-diurnal, diurnal and long term constituents.

The aforementioned constituents are derived from the equilibrium theory of tides where the Earth is assumed to have no land mass. This is obviously not the case. Land mass and seabed topography affect the tides in several ways - amplifying the tidal wave, retarding or accelerating its phase and causing additional secondary maxima and minima in the tidal cycle. These shallow water effects can also be accounted for by tidal constituents. Dodson and Warburg (1941) advocate that since these shallow water effects are caused by resonance, enhancement and attenuation of the equilibrium tide, then the shallow water constituents occur at periods that are integer parts of the equilibrium tide. Thus, we have M_4, M_6 and M_{10}, which are the quarter, sixth and tenth diurnal lunar tides with frequencies of ¼, $1/6^{th}$ and $1/10^{th}$ of the lunar diurnal tide. Similarly, we also have S_4, and S_8 are the quarter and eighth diurnal tides with periods of ¼ and $1/8^{th}$ of the solar diurnal tide. There are also combinations of frequencies derived from shorter period interaction between the solar and lunar tides such as MSN_2.

The equilibrium theory and shallow water theory of tides refers to prediction of tidal height. However, tidal currents are driven by the flow within the tidal wave in the open ocean, and local differences in tidal amplitude in shallow water. Forman (1978) proposes that tidal currents may also be predicted using tidal constituents.

The issue then is how the amplitude and phase differences for each constituent that make up the tidal variation and hence predict the tidal flow.

Fourier analysis is a useful technique for identifying the amplitude of each tidal harmonic and its phase lag in Equation 2.15. Fourier analysis assumes that a signal is the summation of a number of different frequencies with differing amplitudes and phase lags. Since this is the assumption behind tidal harmonic analysis, the technique is clearly one suited to the harmonic analysis of tides. It can be shown that Equation 2.15 can be re-written as:

$$A(t) = z_o + \sum_{n=1}^{\infty}\left[a_n \cos\frac{2n\pi}{T}t + b_n \sin\frac{2n\pi}{T}t \right]$$

2.16

Where

$$z_o = \frac{1}{T}\int_{-T/2}^{T/2} A(t)dt$$

2.17

$$a_n = \frac{2}{T}\int_{-T/2}^{T/2} A(t)\cos\frac{2n\pi t}{T}dt \; ;$$

2.18

and

$$b_n = \frac{2}{T}\int_{-T/2}^{T/2} f(t)\sin\frac{2n\pi t}{T}dt$$

2.19

Thus, values for z0, a_n and b_n can be derived for each constituent of the harmonic series. The predicted values can then be compared with the measured values. This form of Fourier series analysis doesn't allow for 'holes' in the data. Thus the analysis was performed on a data set that started after the first set of recorded anomalous data and the data exceeding the pitch/roll criterion towards the end of the data set.

An alternative model of the tidal sequence is to use the value of one tidal frequency to contribute to the amplitude of another. The simplest version of this sort of equation uses the M_f and M_2 harmonics.

$$\Phi = A + B\cos\left(\frac{2\pi \cdot t}{T_f}\right)\cos\left(\frac{2\pi \cdot t}{T_2}\right)$$ 2.20

where Φ is the parameter being analysed (depth or velocity); A, B are constants defined by the amplitude at M_f and M_2 maxima and minima; T_f is the period of the M_f tidal harmonic; T_2 is the period of the M_2 tidal harmonic.

In order to take account of variations in the semi-diurnal tide, a more complex form was used to analyse the Yell data. This model employed four constants: A, B, C and D.

$$\Phi = A + \left[B + C\cos\left(\frac{2\pi \cdot (t + f_f)}{T_f}\right)\right]\left[\cos\left(\frac{2\pi \cdot (t + f_2)}{T_2}\right)\right]$$ 2.21

where A, B, and C are constants defined by the amplitude at M_f and M_2 maxima and minima; f_f and f_2 are the phase delays for the M_f tidal harmonic and the M_2 tidal harmonic, respectively.

A set of linear simultaneous equations (Equation 2.22) can be generated from Equation 2.21 by assuming values of 1 or 0 for the cosine terms at the spring and neap, high and low tides.

$$A + (B + C) \cdot (D + 1) = SH$$ 2.22

$$A + (B + C).(D - 1) = SL$$ 2.23

$$A + (B - C).(D - 1) = NL$$ 2.24

$$A + (B + C).(D + 1) = NH$$ 2.25

Where SH is the value at the spring maximum; SL is the value at the spring minimum; NL is the value at the neap minimum and NH is the value at the neap maximum.

The p_1 phase delay is estimated so that the time of maxima of the M_f tide matches that of the measured data. The p_2 delay is similarly set. When calculating velocity components, it sets the delay between components to give the correct current direction.

2.3.3 Results and Discussion

2.3.3.a Quality of measured data

The expected ebb-flood and spring-neap flow variations can be seen in the normalised magnitude time-series (Figure 2.20). The survey covered three spring tides and two neap tides in its 30 day duration. However, there was a high noise level on this data set. The noise was greatest during the spring tides, and one third of these spring tides was especially affected by the noise. Anomalous data, as recorded by the instrument, was given a value of 99 and it can be seen on the time-series as off-scale. There were less of these anomalous data points in comparison to the Arklow time-series (and Figure A.2). This may be due to the longer time-averaging ensembles on this survey, which were 15 minutes compared to 20 or 30 seconds in the Irish data. The noise made it difficult to visually distinguish a value for the spring peak tide. From a careful look at the first spring tide it is possible to get a value of approximately 2 for the normalised magnitude. The third spring tide has values in excess of 2.5, but the signal is noisier and assumed less trustworthy.
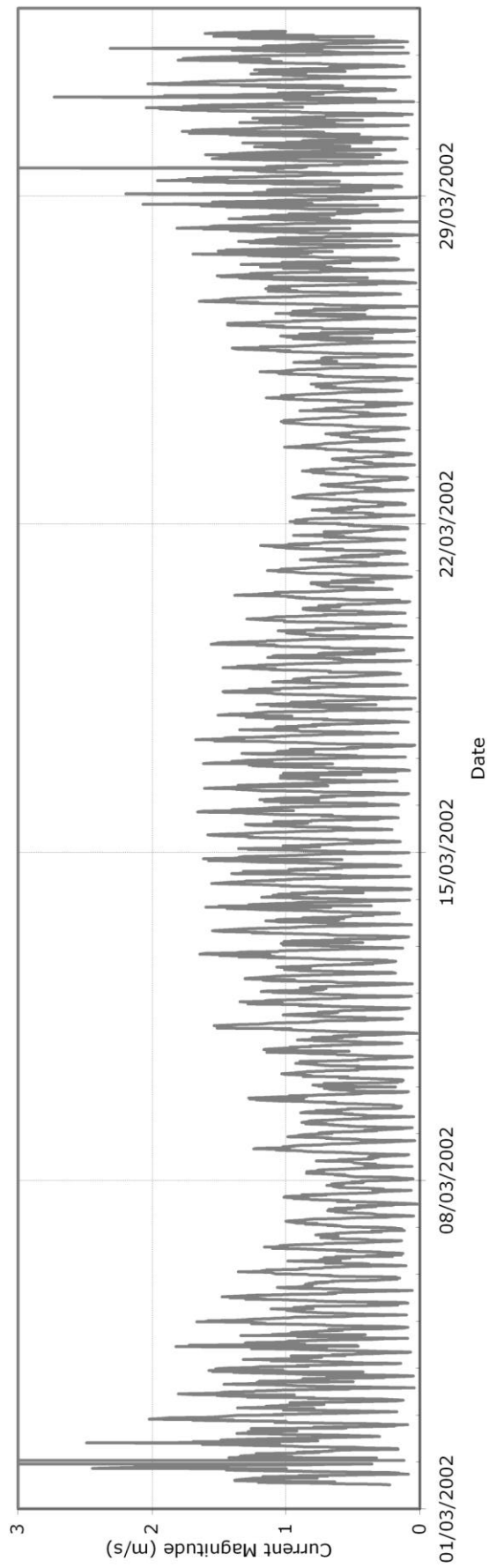
Figure 2.20 Normalised magnitude time-series at 13 m above sea-bed

It was felt that the noise level could not be attributed to turbulence. The time-averaging investigation in the Arklow study determined that most turbulent noise was averaged out with an averaging period of 5 minutes. Any effects from turbulence would have be averaged out by the 15 minute ensemble time averaging. The weather log reported bad weather in the latter part of the survey period. Lewis (Lewis 2000) noted some effect of bad weather in their results. However, the noise was notably greater than that in the Arklow study. It was noticed that there was a significant variation in the pitch and roll measurements. This can be seen in Figure 2.21 and Figure 2.22. It can be seen that the pitch varies in a sinusoidal fashion analogous to the tidal flow. The variation in pitch appeared proportional to the tidal flow. During the spring tide, when the data noise was greatest, the ADCP unit pitched by 28° up to its end-stop, and vibrated against it.
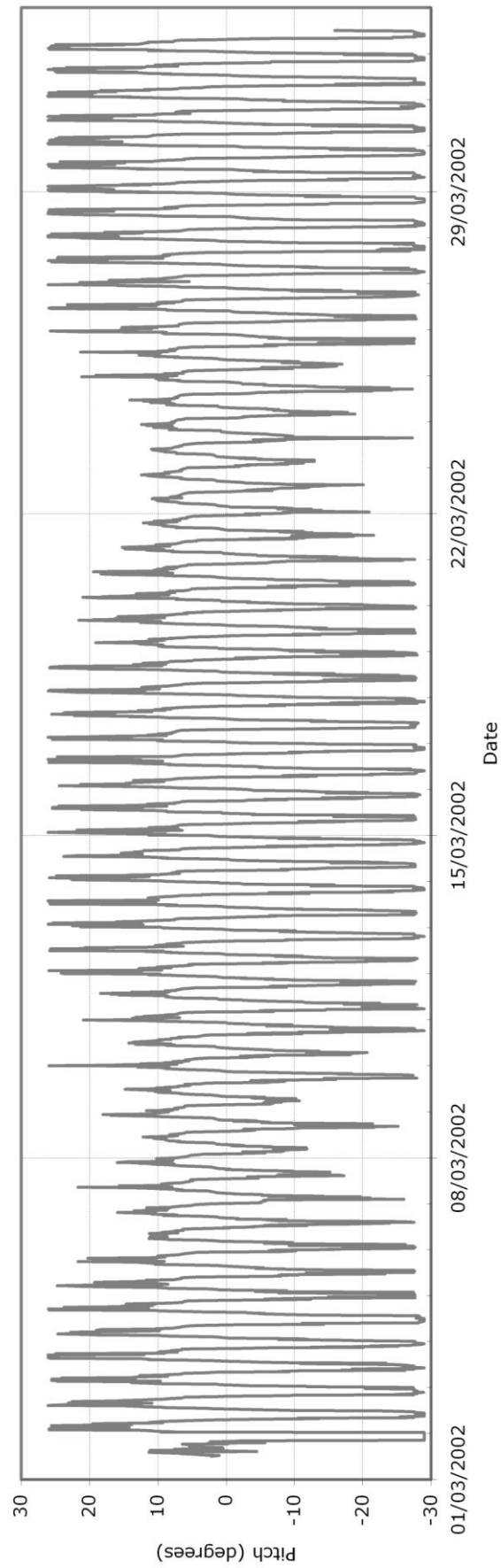
Figure 2.21 Time-series of sensor pitch at Yell
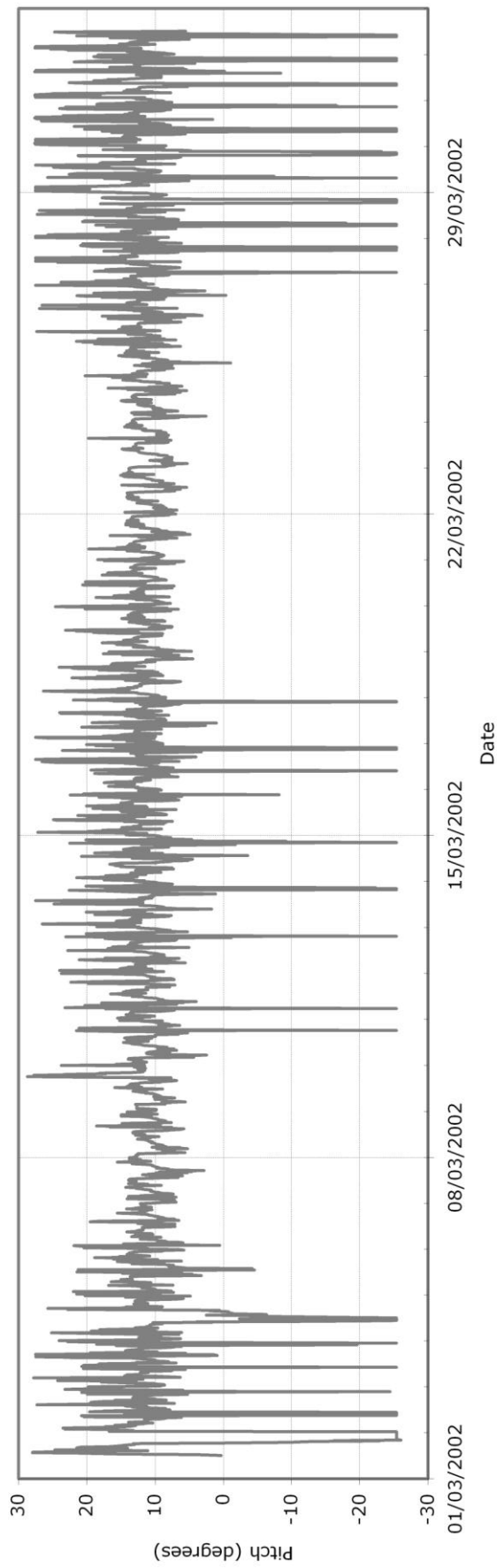
Figure 2.22 Time-series of sensor roll at Yell

Gimbals are designed to allow the ADCP unit to be placed on sloping and uneven seabed. In such circumstances the ADCP pivots to point directly upwards, vertically, through the water column. The measurement software within the ADCP unit that processes the signals has been designed to deal with a pitch or roll up to 26° (RDI Instruments Ltd). It is believed however that the angle compensation software is designed to process a stationary pitch or roll angle rather than a moving sensor whether or not it is within the angular correction limits. It was, therefore, concluded that the movement of the ADCP unit within its gimbals was the source of the extreme noise on the signal. A plot of the data set where the pitch or roll exceeded 26°is given in Figure 2.23. It can be noted that values are mid-range values and not high values as might be expected from a current that pushed the sensor to its pitch limit. It was found that 16.1% of the data exceeding the 26° limit, with 12.3% of these measurements occurring during the flood tide. This is further evidence that the sensor movement had affected the results. It can be seen in Figure 2.19 that the support frame for the ADCP is open and there is no guard protecting the instrument from the force of the tidal flow.
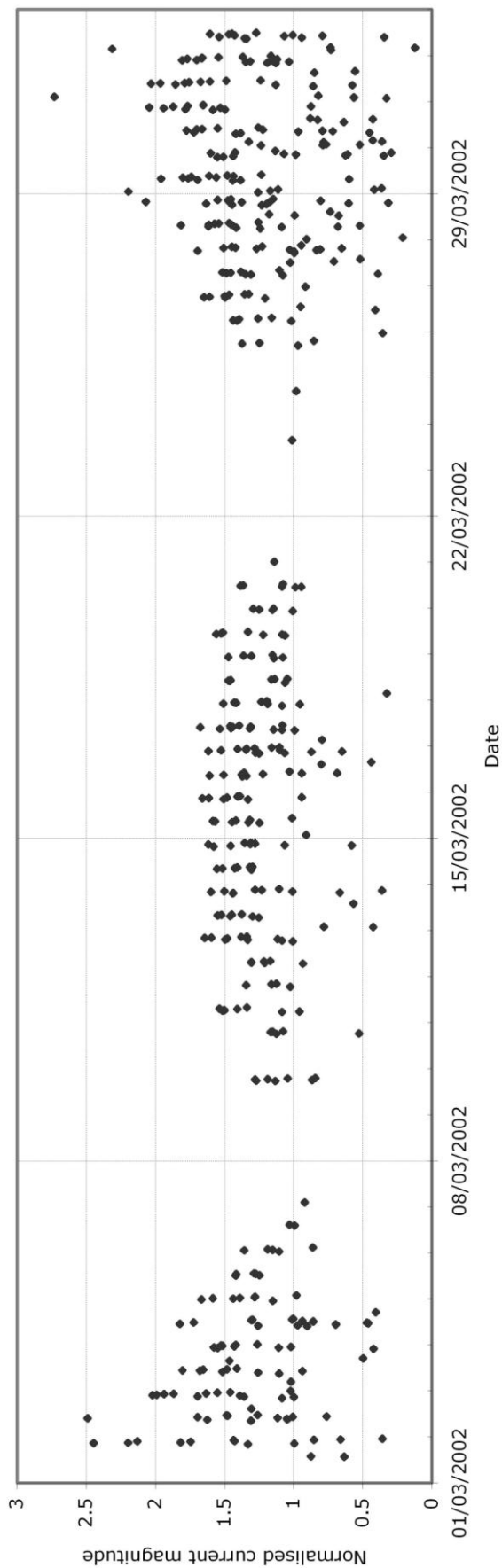
Figure 2.23 Data where the pitch or roll exceeded maximum allowable value
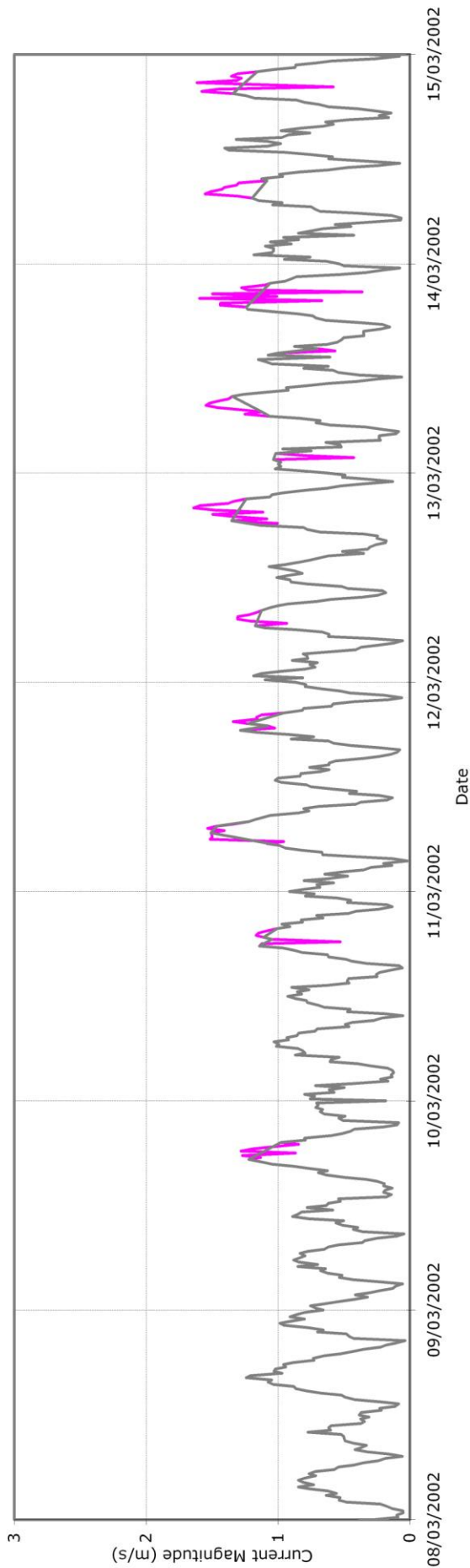
Figure 2.24 Normalised magnitude from 8 March to 15 March. The 'bad' data is emphasised in pink.

As a result, it is recommended that gimbals should remain fixed, or the sensor be well protected from the force of the flow for surveys in such extreme tidal areas. An ADCP instrument at an attitude of 26° would permit the ADCP to be deployed with its gimbals locked on sloping or uneven seabed conditions.

2.3.3.b   Suitability for tidal power exploitation

It is still possible to process the data for the purposes of assessing the site for its suitability for the Stingray tidal energy device despite the poor data quality at spring tide

From the normalised magnitude the values of 2 for the first spring peak may be taken as a typical spring peak value and a neap peak of 1 from the first neap tide. The mean value was in excess of 1 m/s. This indicated a significant tidal flow at the survey site.
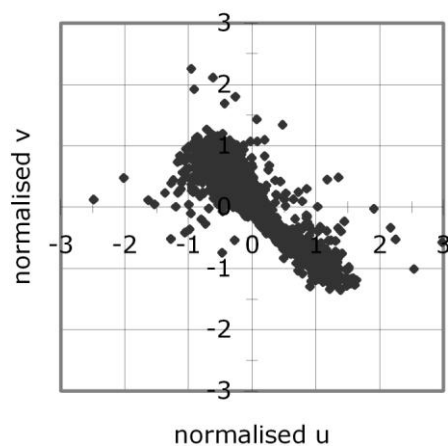
Figure 2.25 Tidal ellipse from entire survey data set   **Figure 2.26 Tidal ellipse from the good data**
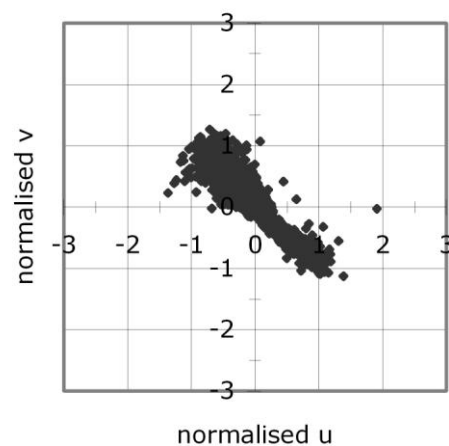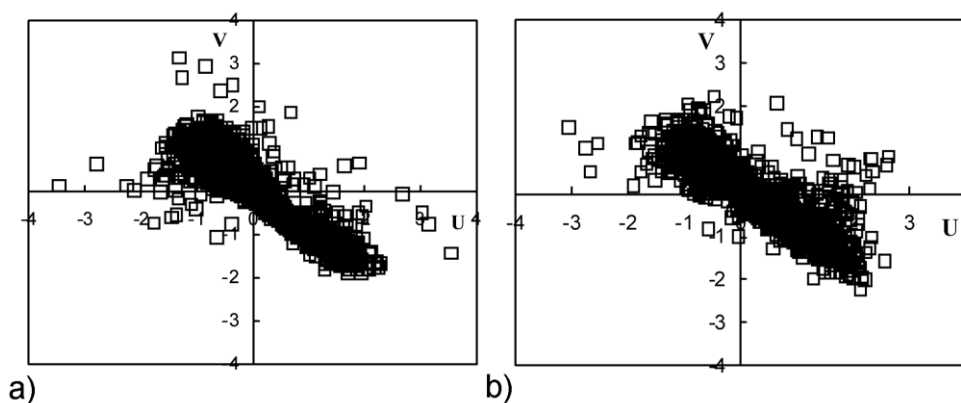
Figure 2.27 Measured tidal magnitude and direction at 13 m (a) and 21 m (b) above the seabed

□ Spring ◇ Neap
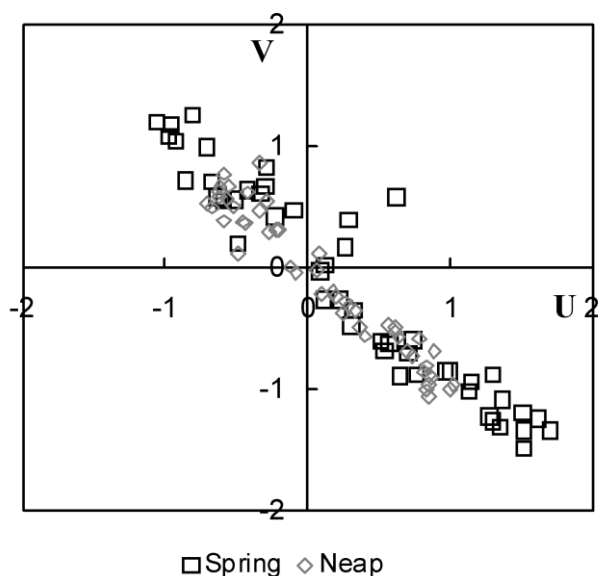
Figure 2.28 Measured tidal magnitude and direction at 13 m above sea-bed for a spring and a neap tide.

The flow was rectilinear, as can be seen in the tidal ellipses (Figure 2.25 and Figure 2.26) and the tide rose (Figure 2.29). Also the majority of the data points fall on a NW-SE diagonal. However, many of the highest values fall outside this region. In addition, the data in Figure 2.27 also demonstrates that the flow at the axis point of Stingray and at the top of the sweep have the same orientation. The spring and neap tides during the survey period (Figure 2.28)

also follow the same flow pattern. This important for a device that cannot change its direction.

The tide rose agrees with the ellipse in that the vast majority of the data is either going NW or SE. It can also be seen that the tide is skewed such that the tide runs in the SE direction for the majority of the survey period. The indication from the tide rose would be for the Stingray to face SE, whilst the indication from the ellipse would be to orientate the device to the stronger currents, i.e. NW to NNW.
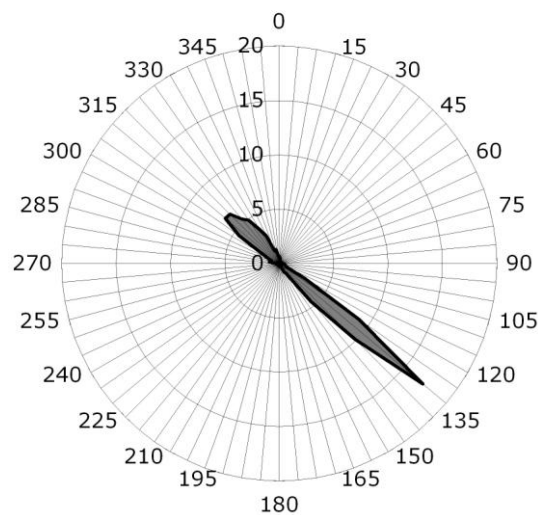
Figure 2.29 Tide rose from entire survey data set

There are a number of issues that can be seen in this data set. The data raises a number of issues which are considered in the foregoing paragraphs:

There is only 83.8% of the measured data accounted for. The remainder of the data was excluded as it was outside the allowable range of pitch or roll.

There is an apparent disagreement between the tide rose and this data set. The impression from the tide rose is that the majority of the flow is in the south easterly direction. However these data indicated that the majority of the flow is in a north westerly direction. In fact, there was agreement. The flow in the south easterly direction was mostly concentrated between 130˚ and 135˚ (over

25%). However, the same proportion is spread over 20° in the north-westerly direction.

2.3.3.c   Analysis of predictive data

The amplitudes resulting from the Fourier analysis are given in Table 2.3.

Table 2.3 Amplitudes for the harmonic constituents resulting from Fourier analysis of the normalised U_{135} magnitude.

Constituent	phase lag	Amplitude
Z0		0.125235
S6	151.6355	0.010362
M6	37.48527	0.094814
S4	42.42925	0.010646
M4	77.4021	0.064502
K2	128.9487	0.371686
S2	124.9048	0.340172
L2	119.3137	0.063579
M2	169.7735	0.920359
nu2	11.77451	0.10155
N2	4.436957	0.245315
K1	80.94758	0.020775
O1	26.34974	0.010692
P1	61.33721	0.009056
Mf	14.37703	0.011473
Mm	-20.8729	0.005057

This Fourier method of harmonic analysis did not produce good results with this data set (Figure 2.30). The residuals were large on occasion with the first and second spring tides, and the residuals were almost equal to the actual value of prediction during the third spring tide (**Figure 2.31**). This in itself was not bad, as this was the part of the data which contained the majority of the anomalous data. The biggest relative error was during the neap tides. In both neap tides the residual was as great as the actual measured value.

The technique assumes that the data set contains many cycles of each constituent frequency. It is likely that there is insufficient data to perform a good Fourier analysis.
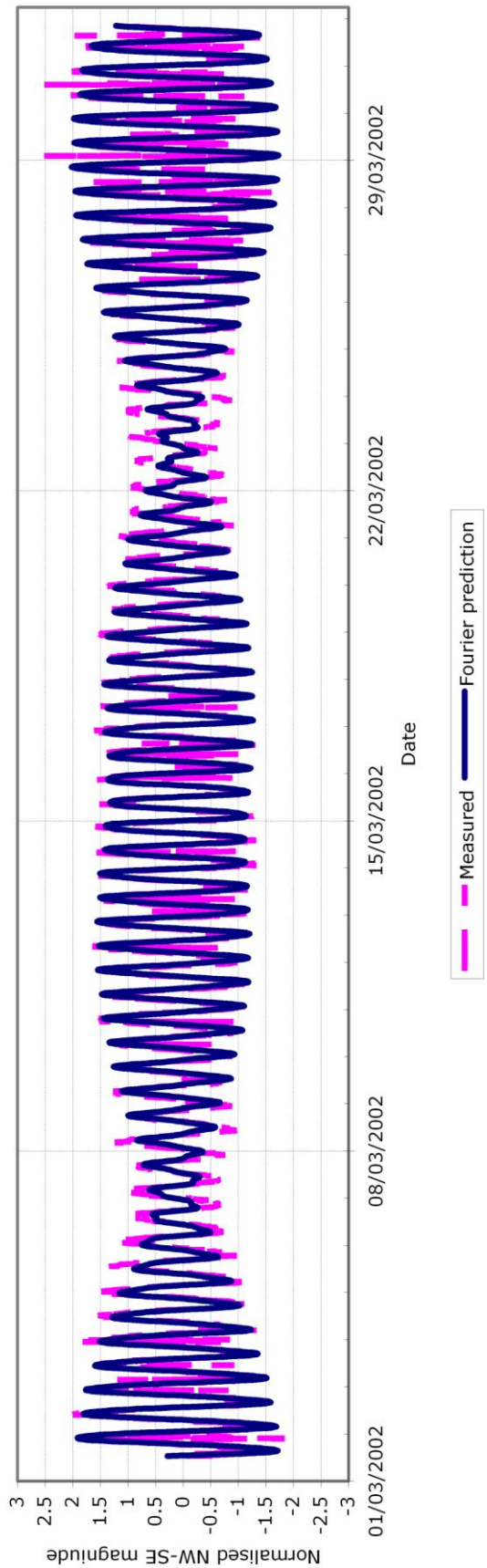
Figure 2.30 Comparison of fourier prediction and unfiltered normalised current measurements€
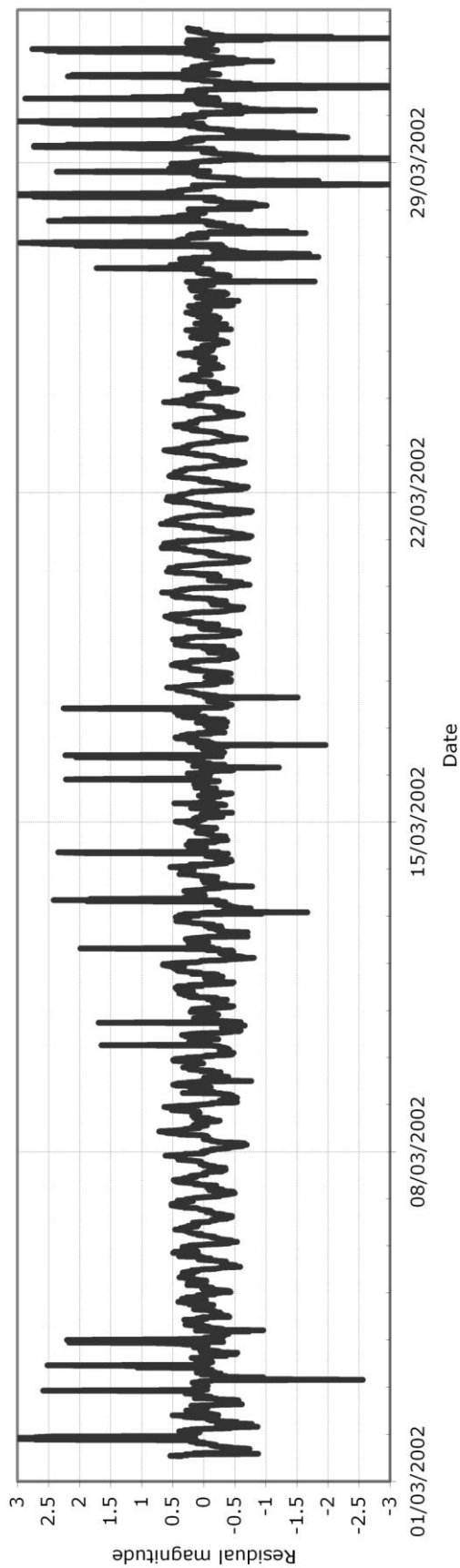
Figure 2.31 Residual between normalised measured magniutde and fourier prediction
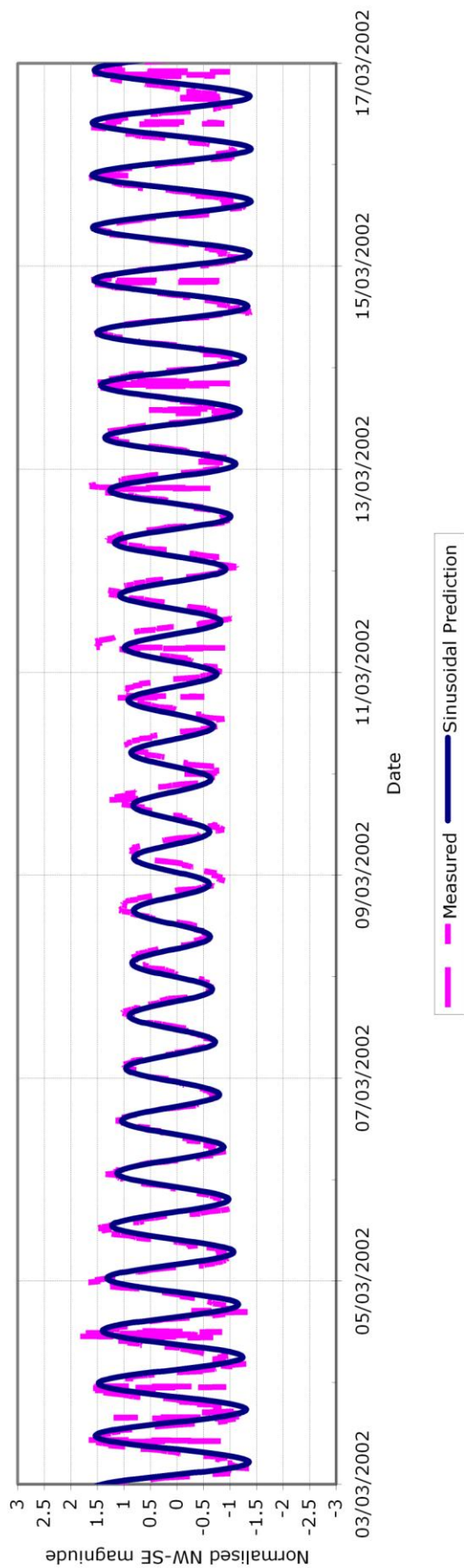
Figure 2.32 Comparison between measured data and sinusoidal prediction

One purpose of predictive analysis is to fill in the missing data and so provide a more complete data.   The Fourier analysis presented above does not do that with accuracy. For this reason the simplified alternative method as describer in Equations 2.22 to 2.25 as applied to the Yell sound velocity data.

Table 2.4 Velocity parameterisation at 13m above the seabed

Value	Nw-SE velocity
NH	0.79
NL	-0.61
SL	-1.4
SH	1.6
A	0.1
B	1.105
C	0.395
M2 delay (hours)	0
Mf delay (hours)	100

The results for this alternative analysis can be seen in Table 2.6. This method obtained better predictions with a lower residual than the Fourier method.

2.3.3.d   Measured power production from Yell using Stingray

Instantaneous and average power outputs were measured during the deployment of Stingray at Yell (Engineering Business 2003). The values of power coefficient, *Cp*, for the rated output and measured values are given in Table 2.5. It is noticeable that the maximum power produced exceeds the rated power. It is usual that the power curve flattens off above the rated power and rated speed (Bryden 1998, Boyle 2004).

Table 2.5 Predicted and measured performance for Stingray

	Rated	Maximum measured	Lower average	Upper average
Current speed (m/s)	1.5	1.5		
Power output (kW)	150	250	40	50
Power coefficient (*Cp*)	0.451	0.752		

The Stingray generator was of reciprocating design. As such, the definitions of rated power and power coefficient are slightly different from that of a rotating device. A rotating device should produce the same power for a given water speed whatever the position of the blades. Thus the average and instantaneous power coefficients are the same and the rated power is the maximum that the generator can produce. The speed of the blade on a reciprocating device varies with its position with it being stationary at the top and bottom and having maximum seed passing the central position.   The instantaneous power produced for a given water speed is thus dependent on the position of the blade. Hence, an average power coefficient for the entire blade cycle should be taken. In the same way, the generator produces its maximum power output while passing through the central position and the rated power should be taken as the average power output at the rated speed.

The measured values for average power were lower than expected by the Engineering Business (2003). However, there was insufficient time during the deployment to fully optimise the control system (The Engineering Business Ltd 2003). A fully optimised control system may have reached the modelled performance.

2.3.3.e Estimate of power production for a uni-directional TCECS using measured flow at Yell

There is insufficient information in the published Stingray project report (The Engineering Business Ltd 2003), and it would be inappropriate to assume a likely time-varying power profile for the device. However, a demonstration power curve was considered using the Stingray's published (The Engineering Business 2003) design power coefficient of 0.451. Optimum control of a variable pitch device would mean that this power coefficient would apply over the operational current speed range up to the rated speed. The example results for a number of directional configurations are given in Table 2.6.

There was a difference of 1.41 kW between the omni-directional power extraction (using the overall magnitude of the flow) and that of purely bi-directional flow. That is a 3.4% power production increase would be gained from having a device that could capture energy from all directions in this site.

There was a difference of 7.7% between the power extraction between the north-westerly and south-easterly orientations.

Only three velocity bands are calculated using Equation 2.10 with the 0.75 m/s cut-in speed and 1.5 m/s rated speed. It is probable that more accurate power output could be calculated using a higher resolution of velocity bands. This was investigated later during the analysis for Fall of Warrness.

It is significant to note that a device that is rated at 150kW, and has a generator capable of producing 250kW, if this was its power curve, is only generating, on average, approximately 19kW. This is a load factor of 7.6%.

The latter observations had to be tempered by the first in that it was not possible to determine from this analysis how much power was lost through the missing data. It cannot be assumed that the missing data would agree with the good data. Otherwise the occurrence data could simply be normalised. However it is known that the missing data occurred when the instrument was over-pitched and thus probably occurred at the higher velocity bands.

Table 2.6 Results of power calculations using measured flow at Yell

Velocity	Exceedence Speed	Exceedence Ux-45	Mid-point	Occurrence Speed	Occurrence Ux-45	Power curve	Omni	bi	facing NW	facing SE
<-3	0.000	0.000								
<-2.75	0.000	0.000	-2.875	0.000	0.000	150.000	0.000	0.000	0.000	0.000
<-2.5	0.000	0.000	-2.625	0.000	0.000	150.000	0.000	0.000	0.000	0.000
<-2.25	0.000	0.000	-2.375	0.000	0.000	150.000	0.000	0.000	0.000	0.000
<-2	0.000	0.000	-2.125	0.000	0.000	150.000	0.000	0.000	0.000	0.000
<-1.75	0.000	0.009	-1.875	0.000	0.009	150.000	0.000	1.310	0.000	1.310
<-1.5	0.000	0.034	-1.625	0.000	0.026	150.000	0.000	3.829	0.000	3.829
<-1.25	0.000	0.094	-1.375	0.000	0.059	115.485	0.000	6.866	0.000	6.866
<-1	0.000	0.172	-1.125	0.000	0.078	63.252	0.000	4.929	0.000	4.929
<-0.75	0.000	0.263	-0.875	0.000	0.091	29.761	0.000	2.719	0.000	2.719
<-0.5	0.000	0.340	-0.625	0.000	0.077	0.000	0.000	0.000	0.000	0.000
<-0.25	0.000	0.395	-0.375	0.000	0.056	0.000	0.000	0.000	0.000	0.000
<0	0.000	0.444	-0.125	0.000	0.049	0.000	0.000	0.000	0.000	0.000
>0	0.838	0.394	0.125	0.078	0.049	0.000	0.000	0.000	0.000	0.000
>0.25	0.760	0.345	0.375	0.116	0.050	0.000	0.000	0.000	0.000	0.000
>0.5	0.645	0.294	0.625	0.125	0.047	0.000	0.000	0.000	0.000	0.000
>0.75	0.520	0.247	0.875	0.153	0.063	29.761	4.549	1.869	1.869	0.000

Table 2.6 (cont) Results of power calculations using measured flow at Yell

Velocity	Exceedence	Mid-point		Occurrence	power curve	Omni	bi	facing NW		facing SE
	Speed	Ux-45		Speed	Ux-45					
>1	0.367	0.184	**1.125**	0.151	0.072	63.252	9.582	4.547	4.547	0.000
>1.25	0.216	0.113	**1.375**	0.121	0.058	115.485	13.965	6.711	6.711	0.000
>1.5	0.095	0.054	**1.625**	0.067	0.038	150.000	9.976	5.694	5.694	0.000
>1.75	0.029	0.016	**1.875**	0.024	0.013	150.000	3.628	1.915	1.915	0.000
>2	0.004	0.004	**2.125**	0.004	0.003	150.000	0.554	0.504	0.504	0.000
>2.25	0.001	0.000	**2.375**	0.000	0.000	150.000	0.050	0.050	0.050	0.000
>2.5	0.000	0.000	**2.625**	0.000	0.000	150.000	0.050	0.000	0.000	0.000
>2.75	0.000	0.000	**2.875**	0.000	0.000	150.000	0.000	0.000	0.000	0.000
>3	0.000	0.000				150.000	0.000	0.000	0.000	0.000
Average Power (kW)						42.356	40.944	21.290		19.654

2.3.3.f   Estimating power output using predicted flows

The avove power estimates were performed using the measured data. However, as has been discussed, much of the data during the faster flowing tides is anomalous and it is suggested that better power predictions may be obtained using the predicted flow data.

Table 2.7 Power output from predicted tidal flows

Method	Bi-directional (kW)	facing NW (kW)	facing SE (kW)
Measured	40.944	21.290	19.654
Parametric	61.61	36.15	25.46
Fourier	63.44	37.16	26.28

Both sets of predicted data produce higher power outputs than the measured data. The total output power for the bi-directional case is up by approximately 48%. It can be seen in Table 2.7 that approximately 15% of the data was considered as bad during the pitch and roll criteria, and it was commented above that much of this data would have occurred during the faster tides. Thus the missing data has contributed to nearly 30% of the energy potentially available from the site. The value of the correct orientation of a mono-directional device, such as Stingray was also more defined. The measured results suggested that comparatively little power would be 'lost' by placing the device in the incorrect orientation. The predicted results suggest, however, that 28% of the possible power could be lost through incorrect device placement.

This example demonstrates the importance of predictive analysis in determining the energy potential of a tidal site. However, this conclusion has to be guarded considering the level of error seen in the comparison of the measured and predicted results at lower flow rates. Other methods of flow prediction will be considered later in this chapter that produce better matches and that allow for anomalous data.

2.3.3.g   Discussion on directional nature of power coefficient

The Stingray device illustrates an extreme situation in which the device takes no power from one direction of current flow. If Equation 2.10 is considered then effectively the Stingray has a Cp of zero when the flow comes from the non-operational direction, as used in the calculations in Table 2.6. However, this directional, flow-splitting approach can be used more widely for power calculations for other tidal energy converters. Most proposed designs for tidal current turbines, unlike wind turbines, do not have a yaw mechanism, and many, like those being developed by Marine Current Turbines Ltd (MCT) rely on blade rotation (Marine Current Turbines Ltd 2005). In addition, the structural support for the device can block or interfere with the flow to the turbine. The MCT Seaflow project's turbine could only operate on the flooding tide due to eddy shedding from the support pile (Marine Current Turbines Ltd 2005) despite being designed with variable pitch blades. Again, this is an extreme case caused by an unforeseen design flaw. MCT's next generation design, Seagen, has a twin rotor design such that the turbines are held away from the flow behind the pile and the support arms are streamlined to reduce flow disturbance (www.marineturbines.com 2007). Despite this, it is unlikely that the flow on the blades will be even from flood and ebb directions. Effectively the value of *Cp* is directionally dependent for many designs of current energy converter. The power extracted is therefore directionally dependent. It is suggested here, therefore, that average power should be calculated using the directional flow-splitting method with direction dependent *Cp* should be calculated as standard for resource assessment. Currently tidal energy conversion developers base their power calculations on a single value of power coefficient for ebb and flood directions. They therefore over-estimate the average power output from their design.

2.4 Fall of Warness, Eday, Orkney

The Fall of Warness is located 19km NNE of Kirkwall in the Orkney Islands at approximately 59° 8.192'N, 2° 48.406 (WGS84). The 4km long stretch of water is between the islands of Muckle Greenholm and Eday, and lies in a NNW to SSW direction.

2.4.1 Method

A number of ADCP units were deployed in over-lapping or consecutive surveys. The data sets considered in this report came from three locations denoted as Survey 6 (S6), Survey 7 (S7) and Survey 8 (S8). All three sites are located within the stretch of water known as the Falls of Warness in Orkney. The location and duration of each survey are given in Table 2.8.

Table 2.8 Locations and dates of Fall of Warness surveys

Survey	Latitude	Longitude	Start	End
6	59° 8.040'N	2° 48.440'W	17/03/2005	02/04/2005
7	59° 8.449'N	2° 49.750'W	19/03/2005	21/04/2005
8	59° 7.909'N	2° 47.996'W	20/04/2005	04/05/2005

The settings, time and date of the surveys being discussed here are given in Table 2.8 and Table 2.9.

It was noted that survey 7 (S7) is of a different longevity and sampling frequency than the other surveys. The consequence of this will be discussed more fully in Section 2.4.3.

Table 2.9 Settings for ADCP meters for Fall of Warness Surveys

Survey Reference No.	7	6a	9
Broadband (kHz)	614.4	614.4	614.4
Pings/Ensemble	50	50	50
Time/Ping	00:12.00	00:24.00	00:24.00
First Ensemble Date	05/03/19	05/03/17	05/07/20
First Ensemble Time	10:47:37.06	10:55:18.77	09:23:29.85
Ensemble Interval (s)	600.00	1200	1200
1st Bin Range (m)	2.10	1.86	1.86
Bin Size (m)	1.00	0.75	0.75

2.4.2 Data processing

The data was analysed in a similar method to that of Yell Sound in section 2.3.2. That is, time series of magnitude and direction were plotted, along with tidal ellipses and depth profiles. Again the data is normalised to the mean magnitude of the bin at 60% of the water column, which corresponds to the depth-average velocity assuming a $1/7^{th}$ power-law profile. For concise reporting for this work the detail of these results will not be reported here, but can be found in the report on the study (Melville 2007).

Harmonic analysis was used to carry out future tidal predictions and determine the exceedence, occurrence and probability density based annual and longer term predictions.

Two methods are considered in this analysis – the least squares regression method (LSRM) and Fourier analysis.

2.4.2.a Tidal flow prediction - The Least-Squares Regression Method

This method involves sequential application of least square regression for each of the constituents against the measured data, and is a common method for determining tidal harmonics.

The particular version of this method used in the current work was that described by Foreman (2004). The method was originally developed for tidal height analysis by Godin (1972), Godin and Taylor (1973) and Foreman (1977).

The method analyses hourly tidal current data for 69 tidal constituents. It may be argued that the use of hourly data does not capture enough information on the tide. However, the method was developed during the 1970's and was designed to process long term data sets of a year's duration or more, and hourly data was probably at the limit of the computational power available at that time. Additionally, the shallow water constituents, which are the shortest period constituents being analysed for are in the range 3.105 hours/cycle to 8.494 hours/cycle. It is therefore unnecessary to use a higher resolution.

The LSR is performed in a series of comparison pairs, which combine together to give the predicted frequency spectrum. The method according to Foreman (1996) employs a Rayleigh comparison, whereby a constituent will be included in an analysis if

$$|F_0 - F_1| \cdot T \geq R \qquad\qquad 2.26$$

Where F_o and F_1 are the frequency being considered for inclusion and its comparison pair respectively; T is the longevity of the survey and R is the Rayleigh comparison coefficient. This coefficient is normally assumed to have a value of 1 and thus the value used in this analysis. Within each constituent grouping, formulation of the pairs is important so as to include the important tidal frequencies and to take proper account of the contributions of similar frequencies. This is applied by consideration of three further criteria:

Constituents should be included in order of decreasing tidal potential

Constituents should be compared with one of nearest neighbouring frequency that is already included in the analysis

In the case of two neighbouring constituents with approximately equal tidal potential amplitude, comparison pairings should be chosen such that both constituents can be included in the shortest survey length. This criterion maximises the number of constituents that may be included to analyse survey data.

Shallow water constituents do not have potential amplitude and, therefore, the order of inclusion cannot be determined by these rules. Foreman (1996) reports that the inclusion order used in this LSR method has been derived from the experience of Godin.

The LSRM for tidal height obtains the best fit between the data set and equation 2.11, finding the values of amplitude for each constituent, A_j, and its phase difference Φ_j.

$$y' = Co + \sum_{j=1}^{M} A_j \cos\left[2\pi\left(o_j \cdot t_i - \Phi_j\right)\right] \qquad\qquad 2.27$$

Where y' is the predicted value of velocity magnitude; C_o is the intercept, which is given by the mean of the data; and t is the time in hours along the original data set.

This expression may be linearised by substitution to give:

$$y' = C_o + \sum_{j=1}^{M} \left[C_j \cos\left(2\pi o_j \cdot t_i\right) + S_j \sin\left(2\pi o_j \cdot t_i\right)\right] \qquad\qquad 2.28$$

Where $C_j = \cos\left(2\pi\Phi_j \cdot t_i\right)$, $S_j = \sin\left(2\pi\Phi_j \cdot t_i\right)$ and A_j are given by $\sqrt{S_j^2 + C_j^2}$ and Φ_j are given by $\tan^{-1}\left(S_j/C_j\right)$. The task is therefore to minimise $\sum_{i=1}^{N} \left(y_i - y_i'\right)^2$, or in expanded form

$$\sum_{i=1}^{M} \left[y_i - C_o - \sum_{j=1}^{N} \left[C_j \cos\left(2\pi o_j \cdot t_i\right) + S_j \sin\left(2\pi o_j \cdot t_i\right)\right]\right]^2 \qquad\qquad 2.29$$

for *Co, C_j* and *S_j* for all constituents, j = 1,M.

This is done by solving 2*M*+1 simultaneous equations of the partial differentials with respect to *Co, C_j* and *S_j* (Equation 2.31 to 2.32)

$$-2\sum_{i=1}^{M} \left[y_i - C_o - \sum_{j=1}^{M} \left[C_j \cos\left(2\pi o_j \cdot t_i\right) + S_j \sin\left(2\pi o_j \cdot t_i\right)\right]\right] = 0 \qquad\qquad 2.30$$

$$-2\sum_{i=1}^{M} \left[y_i - C_o - \sum_{j=1}^{M} \left[C_j \cos\left(2\pi o_j \cdot t_i\right) + S_j \sin\left(2\pi o_j \cdot t_i\right)\right]\right] \cos\left(2\pi o_j \cdot t_i\right) = 0 \qquad 2.31$$

$$-2\sum_{i=1}^{M}\left[y_i - C_o - \sum_{j=1}^{M}\left[C_j \cos(2\pi o_j \cdot t_i) + S_j \sin(2\pi o_j \cdot t_i) \right] \right] \sin(2\pi o_j \cdot t_i) = 0 \quad 2.32$$

The solution matrix of this problem is given in Forman (1996). For tidal currents, the method is more complex since the solution must deal with solution of a vector problem rather than the scalar problem of tidal height. The tidal current velocity can be resolved to a vector v acting in the south-north direction (y) and a companion component u acting in the west-east direction (x).

The approach of Foreman (2004) is to consider the problem as a complex domain such that

$$Z = u + iv \qquad\qquad 2.33$$

such that

$$Z = Xo + \sum_{j=1}^{M} X_j \cos[2\pi(o_j \cdot t_i - \Phi_j)] + Yo + \sum_{j=1}^{M} Y_j \cos[2\pi(o_j \cdot t_i - \Theta_j)] \qquad 2.34$$

Where the X and Y are the real and imaginary parts of the complex variable Z; and Xo, X_j, Φ_j, Yo, Y_j, θ_j are analogous to C_o, A_j, and Φ_j in equation 2.28. A similar linearization can also be made such that $CX_j = \cos(2\pi\Phi_j \cdot t_i), CY_j = \cos(2\pi\Theta_j \cdot t_i)$, $SX_j = \sin(2\pi\Phi_j \cdot t_i)$ and $SY_j = \sin(2\pi\Theta_j \cdot t_i)$. Equation 2.34 then becomes

$$Z = X_o + \sum_{j=1}^{M}\left[CX_j \cos(2\pi o_j \cdot t_i) + SX_j \sin(2\pi o_j \cdot t_i) \right]$$
$$+ i\left[Y_o + \sum_{j=1}^{M}\left[CY_j \cos(2\pi o_j \cdot t_i) + SY_j \sin(2\pi o_j \cdot t_i) \right] \right] \qquad 2.35$$

Substituting for the complex definitions of sine and cosine, this becomes

$$Z(t) = X0(t) + iY0(t) + \tfrac{1}{2}\sum_{j=1}^{M}\left\{\begin{array}{l}[(CX_j + SY_j) + i(CY_j \text{ - } SX_j)]\exp(2\pi i o_j t)\\ + i[(CX_j \text{ - } SY_j) + i(CY_j + SX_j)]\exp(\text{-}2\pi i o_j t)\end{array}\right\} 2.36$$

Having produced equation 2.36 based on stationary normal vector components, it is also possible to resolve Z in to counter-rotating vectors Z^{+} and Z^{-}, such that $Z=Z^{+} + Z^{-}$ for any constituent.

The effect of this is to assume that flow follows a symmetrical ellipse with major axis $a^{+} + a^{-}$ when the two rotating vectors are in conjunction and $a^{+} - a^{-}$ when the vectors are in opposition. The ellipse is inclined to the west-east axis by $\dfrac{(\varepsilon^{+} + \varepsilon^{-})}{2}$.   On the face of it, this assumption may cause problems in the prediction of some tidal flows, particularly those flows around headlands, where the flow is not rectilinear. However, the contribution of all the constituents in the analysis will compensate for this.

The constituents input in to the analysis were as follows:

Offset: Z0

Nodal: SA, SSA, MSM, MM, MSF, MF

Diurnal: α1, 2Q1, σ1, Q1, ρ1, O1, τ1, β1, NO1, CHI1, PI1, P1, S1, K1, ψ1, φ1, τ1, J1, SO1, OO1, υ1

Semi-diurnal: OQ2, ε2, 2N2, μ2, N2, ν2, γ2, H1, M2, H2, MKS2, λ2, L2, T2, S2, R2, K2, MSN2, η 2

Shallow water: MO3, M3, NK3, SO3, MK3, SK3, MN4, M4, SN4, MS4, MK4, S4, SK4, 2MK5, 2SK5, 2MN6, M6, 2MS6, 2MK6, 2SM6, MSK6, 3MK7, M8 and M10.

The primary output from this analysis is a list of the tidal constituents used in the analysis along with the magnitude and direction of the major axis of its tidal ellipse and its Greenwich phase difference

2.4.3 Results and Discussion

The constituents used in the analysis as filtered by the Rayleigh critera are presented in Table 2.10 for surveys S7 and S6.

Table 2.10 Constituents selected by Rayleigh criteria for analyses

Survey	Constituents selected for analysis
S7	Z0 MM MSF α1 2Q1 Q1 O1 NO1 P1 K1 J1 OO1 υ1 ε2 η2 N2 M2 L2 S2 K2 η2 MO3 M3 MK3 SK3 MN4 M4 SN4 MS4 S4 2MK5 2SK5 MN6 M6 2MS6 2SM6 3MK7 M8 M10
S6	Z0 MSF O1 P1 K1 M2 S2 K2 M3 M4 M6 M10

The difference in number of selected constituents lay in the duration of the surveys. Survey 7 was twice as long at 30 days. However, this permitted the use of more than 3 times as many constituents. This in turn influences the accuracy of the two predictions.

The values of ellipse major axis, minor axis, inclination of the major axis and the Greenwich phase for S7 are presented in Table 2.12.

From these results, it is possible make an analogy to common tidal amplitude terms using the definitions given in Doodson (Doodson 1941). The terms are produced by the summation or subtraction of the elevation magnitudes for the Z0, M2 and S2 constituents. However, vector arithmetic has been used in dealing with velocities rather than the scalar terms used for tidal amplitude used by Doodson (Doodson 1941). The results are presented in Table 2.11. These may be used in the parametric prediction presented for the Yell study in section 2.3.2.b.

Table 2.11 Summary of non-harmonic terms

Survey	S7		S6	
Term	magnitude	direction	magnitude	direction
Mean High Water Spring (MHWS)	3.50	347.5	3.5	348.6
Mean High Water Neap (MHWN)	1.70	347.1	1.4	354.2
Mean High Water (MHW)	2.60	347.4	2.4	350.2
Mean Low Water (MLW)	2.26	158.6	2.3	169.7
Mean Low Water Neap (MLWN)	1.38	152.6	1.2	173.9
Mean Low Water Spring (MLWS)	3.15	161.2	3.2	168.25

In this analogy, High Water (HW) is taken as the positive direction of the major axis or the tidal ellipse. In this case, HW is the ebbing tide and Low Water (LW) is the flooding tide.

Table 2.12 Results of harmonic analysis of survey 7 ADCP data

Name	Speed (Cycles/ Hour)	Major Axis	Minor Axis	Inclination of Major axis	Greenwich Phase	Anti-clockwise Rotational Phase	Clockwise Rotational Phase
Z0	0	0.25	0	31.1	360	328.9	31.1
MM	0.001512	0.021	0.019	22.3	303	280.7	325.3
MSF	0.002822	0.056	-0.015	37	45.2	8.1	82.2
α1	0.034397	0.018	0.003	162.7	40.7	238	203.4
2Q1	0.035706	0.006	0.002	157.6	359.9	202.3	157.5
Q1	0.037219	0.041	-0.006	165.8	254.9	89.1	60.8
O1	0.038731	0.089	0	162.7	295	132.3	97.7
NO1	0.040269	0.017	0.001	157.3	304.8	147.5	102.1
P1	0.041553	0.015	0.004	163.2	87.1	284	250.3
K1	0.041781	0.059	0.002	165.3	84.8	279.5	250.1
J1	0.043293	0.006	0.002	123.7	116.4	352.7	240
OO1	0.044831	0.006	-0.001	139.7	354.4	214.7	134.1
υ1	0.046343	0.003	-0.002	129.6	125	355.4	254.6
ε2	0.076177	0.103	0.001	160.4	18.1	217.7	178.4
μ2	0.077689	0.271	0.012	162.8	82.9	280.1	245.7
N2	0.078999	0.423	0.009	162.9	194.3	31.4	357.2
M2	0.080511	2.424	-0.017	163.3	238.2	74.9	41.5
L2	0.082024	0.099	-0.005	158.8	347.1	188.3	145.8
S2	0.083333	0.898	-0.001	167.8	267.6	99.7	75.4
K2	0.083561	0.182	-0.009	146.8	261.4	114.5	48.2
v2	0.085074	0.044	-0.005	168.3	223	54.7	31.3
MO3	0.119242	0.01	0	159.3	351.8	192.5	151.1

Table 2.13 Results of harmonic analysis of survey 7 ADCP data (Cont'd)

Name	Speed (Cycles/ Hour)	Major axis	Minor Axis	Inclination of Major axis	Greenwich Phase	Anti-clockwise Rotational Phase	Clockwise Rotational Phase
M3	0.120767	0.024	0.004	154.5	171.9	17.4	326.4
MK3	0.122292	0.005	0.002	171.6	28.9	217.3	200.5
SK3	0.125114	0.015	0	3	195.5	192.5	198.5
MN4	0.159511	0.015	0.009	33.7	334.8	301.1	8.4
M4	0.161023	0.062	-0.009	30.2	50.3	20.1	80.5
SN4	0.162333	0.017	-0.008	2.2	127.1	124.9	129.2
MS4	0.163845	0.055	-0.026	17.3	107.4	90.1	124.6
S4	0.166667	0.018	-0.001	150.2	70.5	280.3	220.7
2MK5	0.202804	0.012	-0.003	136.7	104.9	328.2	241.7
2SK5	0.208447	0.005	0.001	89.8	82.4	352.7	172.2
2MN6	0.240022	0.049	-0.006	158.2	174.7	16.5	332.9
M6	0.241534	0.085	-0.011	158.7	219	60.3	17.7
2MS6	0.244356	0.142	-0.021	158.7	249.1	90.4	47.9
2SM6	0.247178	0.059	-0.006	161.1	257.3	96.3	58.4
3MK7	0.283315	0.005	-0.002	96.5	206	109.5	302.5
M8	0.322046	0.009	0.003	15.2	289.3	274	304.5
M10	0.402557	0.004	-0.001	72.7	99.6	27	172.3

The comparisons of the current magnitude from original survey data sets with the harmonic analysis predictions for the same periods can be seen in Figure A.5 and Figure A.6. It can be seen that there is a good match in the S7 results. However, the S6 predicted data set does not fit the measured data well with disparity in both magnitude and phase, especially during the neap tide. This is undoubtedly due to the short duration of the survey. The length of survey not only determines how many constituents may be predicted but also there is less data to fit during the analysis. The result in this case is a significant deterioration in the quality of the results. This short survey period is fine if the purpose is to obtain an appreciation of the flow behaviour such as whether the flow is recti-linear and the depth velocity profile. However this analysis demonstrated that a longer 30 day analysis is required for accurate flow prediction.

Previously in this chapter, tidal prediction has been used to generate error-free data for power calculations. Using the LSRM it has been possible to generate an accurate replica of the original data set that can be used also for future predictions. These predictions can be used to determine future energy production and peak tides. With the accuracy of the S7 results it can be presumed that the predictions would have a similar degree of accuracy.

It would be beneficial to have a quantitative indication of the amount of error in these results and thereby confidence in the prediction they produce. The program t_tide (Pawlowicz, Beardsley & Lentz 2002) calculates the harmonic constants by Foreman's LSHM (Foreman 2004). However, it processes the data further to calculate the 95% confidence interval for each for the evaluated constituents. The frequency density spectrum of the residual data is subdivided into analyses widths of size of the principal lunar tide, M2, and its sub-frequencies. The 95% confidence interval is calculated based on the background noise level around the constituent in question.

The resultant constituents from the t_tide analysis were a little different from those of the Foreman program. This was most likely because the t_ tide analysis can take the complete data set whereas the Foreman program takes hourly values averaged from the original data. However, for the most part, the Foreman values fall within the confidence intervals generated from t_tide. The

signal noise ratio (SNR) is the ratio of the 95% confidence error and the actual value. This can be used to eliminate constituents from the analysis whose values are not significantly different to the background noise level.

The fractional errors for the analysed constituents for S7 are presented in Figure A.7. For many of the components the errors are small compared to the value of the major semi-axis. However, the analysis revealed that a further set of constituents could be removed from the predictive analysis due to low confidence in the value of their magnitude. These results give confidence in proceeding with long-term current prediction.

Figure A.8 is a time-series of the high currents predicted for ten years from the date of the original survey. It can be seen that there is a large variation in the peak tides through the each year and further variation year to year. Although the peak current during the survey was in the order of 3.5 m/s, it can be observed that there are tides that exceed 4 m/s, and with a maximum value of 4.3 m/s.

This exemplifies the importance of the tidal prediction and getting good data from a tidal survey to produce the prediction. The device designers would be under-designing their devices if they were to solely consider the flow measured during the survey as their design peak flow rate. The peak flow rate not only influences the generation capacity but the design of blades, support structure and anchorage. Drag force is proportional to the square of the velocity. Using a peak flow of 3.5 m/s would underestimate drag forces by 44% given these predictions.

However, the purpose of this predictive analysis was not solely to predict the value of the tidal flow. The effect on the size of the tidal energy resource was the ultimate aim. There was a difference in the probability density curves for the predicted and measured results for S7 predicted and measured data sets (Figure 2.33). There also differences between the prediction for a year and the measured data (Figure 2.34). This is not unexpected. As was seen in Figure A.8, there was signification variation in the maximum values throughout the year. However, the main differences occur in the low and mid-range velocity bands. The curves virtually match at the higher velocity bands. This was

significant in that the devices extract the majority of the energy in the mid-range velocity bands.
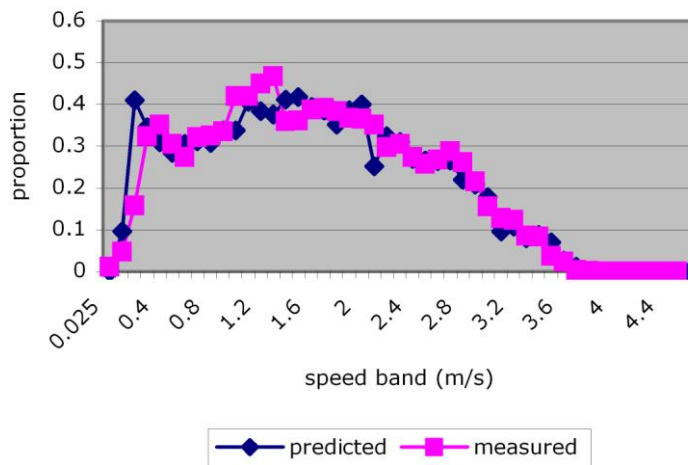
Figure 2.33 Comparison of measured and predicted current magnitude probability density for S7 Warrness
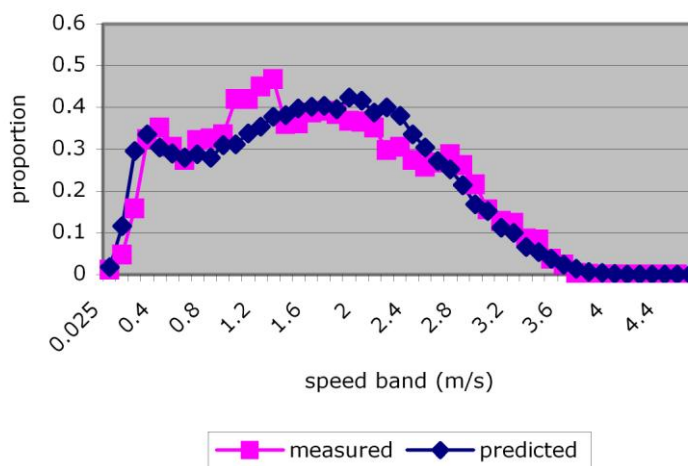
Figure 2.34 Comparison of probability density for measured data and annual prediction of current magnitude for S7 Warrness

In order to consider the effect of this variation in occurrence on energy production it was necessary to assume a power production profile for a tidal energy converter. Unlike Yell Sound, the Fall of Warrness site is a test site for many different types of device. Some of these devices extract from bi-directional flow whilst others have larger windows of extraction. The devices will

also have differing generating capacities and power factor profiles. Power calculations were carried out assuming a 16 m 600kW device with a cut-in speed of 0.75 m/s and a power coefficient of 0.45. The average power produced for the measured data was 256.8 kW whilst that for the year's prediction was 264.5 kW.

The difference in average power output for this selected power profile indicated that calculations based on the measured data, or monthly predictions if there an abundance of anomalous data is sufficient to get a good indication of the average output power of a device given other sources of error in the calculation such as assuming a constant power coefficient.

2.5 Conclusions

This chapter has examined a number of techniques used in the deployment of Acoustic Doppler Current Profilers (ADCJPs) in extreme current areas and methods of the resultant data analysis in order to obtain statistics that are of use to the tidal energy developer and those involved in researching tidal energy.

It has been noted that the method of deployment in these fast currents has a strong influence on the quality of data recovered. These are summarised bellow:

Marker buoys present very little benefit in the process of the survey. Even high buoyancy ones are swept beneath the surface at anytime except absolute slack water. What's more, their rigging can have a detrimental effect on the measurements taken. They can drag the ACDP frame out of position when attached directly to the frame. The buoy will also interfere with the acoustic signal. It is believed that such demarcation had a strong influence on the quality of the Arklow Bank data as commented by the original surveyors (Lewis 2000). The author agrees with this prognosis and concludes that this demarcation is definitely not recommended. Lead marker buoys, where the buoy is connected to a separate anchor and a line leads off to the ADCP, have less influence on the ADCP readings providing that they are placed appropriately such that the buoy does not influence the measurement beams. Although as commented above,

there have been problems encountered in finding them in the slacking tide prior to recovery of the ADCP. The recommended method is that of acoustic release buoys as used in the Yell Sound survey. These are only released by an acoustic ping when the unit is ready for recovery and so do not influence the measurement process. However, there is a risk of failure to deploy on demand. In practice, permanent buoyage is required by the Maritime and Coastguard Agency (MCA) for safe navigation so a permanent high buoyancy buoy is necessary. Taking this into consideration, the recommended course of action would be a lead buoy, appropriately positioned at a vector normal to the ADCP unit with sufficient buoyancy and line to remain on the surface during the majority of the tide and a good anchorage weight and chain as anchorage. An acoustic release marker may be attached to the ADCP frame for security of recovery.

The mounting frame and gimbals are another source of data corruption, as seen in both the Arklow and Yell surveys. The frame should be well weighed to prevent vibration and movement. This was a suggested cause by the original surveyor in the Arklow survey (Lewis 2000) and this author agrees that it is a contributory factor. The Yell survey appeared to be better designed in this respect. However the gimbals were shown in the data analysis to be a larger source of error, with the sensor moving in the current and being moved out of its pitch and roll windows of operation. It is recommended by this author that the gimbals' operation should be locked for operation of ADCP units in extreme currents. The ADCP unit's software can cope with up to 26° of slope on the sea bed terrain and so measurement should not be affected provided that the placement is correct.

After the physical design of the survey placement, the biggest contribution to effective ADCP operation is the sampling and time-averaging period combined with the bin size. A variety of combinations were used on the case studies considered in this chapter. The Arklow survey used a coarse bin size that led to poor resolution of the vertical depth profile. Simultaneous velocity-depth profiling is one of the major benefits of acoustic measurement. Although it was not strictly required for the future data use in the hydrodynamic model, it is felt that an opportunity was lost not to be able characterise the velocity profile at a higher resolution at such an early stage in the development of tidal current

power. It is accepted that concessions had to be made on the memory available for data storage at the time of this survey, and that temporal resolution was more important at the time or survey. The Yell data was collected at higher temporal and spatial resolution. This gave a good picture of these variations in the tidal flow. It is unfortunate that the data during the fastest tides was corrupted by the sensor movement as discussed previously. The Warness surveys used a variety of spatial and temporal resolutions, though it was not clear as to the reasoning for this. The longer of the surveys at station 7 had higher depth resolution (smaller bin size) and higher temporal resolution (shorter time ensembles) than those of the survey at station 6 that had a shorter overall duration. The result was that the S6 survey produced little constructive information aside form an indication of the peak flows at the time of the survey. The harmonic analysis applied to the Yell and Warness data demonstrates the importance of the survey duration. The 30 day survey period proved more reliable in generating tidal harmonics with which to predict future tidal currents and energy production. The author was not involved in the prescription of these surveys. It was believed by those performing the surveys that the short term surveys would yield the required information faster given a short time line to installation of the first devices a the tidal test centre.

The author recommends a minimum duration of 30 days with 10 minute time averaging and 1.0 m bins in order to capture the flow field and yield suitable data for planning a tidal energy development. This is easily achievable given the modern advances in data storage memory and reduction in its cost in recent years.

Surveys with a 10 minute ensemble are not suitable for analysing the degree of turbulence in these extreme tidal currents. Variations can be seen in the data that may be associated with turbulence, but the data is time averaged over the ensemble period and many higher frequency variations that could be directly related to turbulence are averaged out. Determining turbulence will be a key contributor to designing devices for longer survivability and longer maintenance intervals. It is recommended by the author that shorter duration very higher resolution surveys should also be undertaken, as carried out at Yell and subsequent to the analysed surveys at Warrness. It is recognised that there is unpublished work by other authors on the turbulence of high velocity tidal

flows, but more work will need to be carried out and placed in the public domain if designers are to refine their tidal device designs for lower capital and maintenance costs.

This chapter has demonstrated a number of techniques that are of value to the tidal energy developer in assessing the suitability of a site to their design. The tidal rose and tidal ellipse are important in determining the directional nature of the flow. This is important as many designs do not yaw and so are limited to recti-linear flow. It can be seen that the statistical measures of occurrence and exceedence can be used to develop an indication of the raw energy available at a particular site. The author developed the technique for considering only the flow normal to the plane of the device, in effect using a directionally dependant power coefficient (*Cp*). The driver for this was the Stingray device for which the work was done on Yell Sound. However, this work has demonstrated the impact of assuming a non-directionally varying *Cp* can have on over-estimating the potential of a site.

CHAPTER 3 HYDRODYNAMIC MODELLING FOR TIDAL ENERGY CONVERSION SYSTEMS

3.1 Introduction

This chapter considers the role of hydrodynamic modelling in the analyses of a tidal current energy development. Some of the work presented here has been previously reported by the author (Bryden, Delure, DeNat, 2001, Melville 2000, The Engineering Business 2003). It considers methods of creating topological models and computational grids and looks at boundary conditions as applied to a number of practical case studies. The chapter does not explore an in-depth development of tidal models. This topic has been explored and developed by many authors (Forester, Couch & Copeland, 2003, Pugh 1987). Hydrodynamic models are used in a large variety of applications in the tidal energy arena. Large scale models have been used to predict tidal behaviour around large sea basins, for example the North Sea (Davies & Furnes, 1980). Smaller scale models have been used to predict flow in harbours, estuaries and channels for monitoring sediment transport, shipping navigation and coastal development and protection. Couch & Copeland (2003) considered a variety of models and modelling techniques to develop an accurate tidal flow model. In comparison, this work did not set out to develop modelling techniques.   Rather it concentrates on the application of existing models to tidal energy.

3.2 Topology and Grid generation

Generation of a properly representative topology is of key importance to producing a representative flow model of the real environment. When dealing with the discretisation of regular engineering forms or smoothly contoured surfaces without irregular spot depths, the vertical displacement of any point can be done using splines and linear interpolation. The presence of spot depths requires a different approach. In many circumstances the available bathymetry data is limited. In the UK, the seabed is mapped by the United Kingdom Hydrographic Office (UKHO). The UKHO produce a series of charts that represent the seabed bathymetry along with many other features used by

mariners to navigate. The bathymetry in these charts is aimed at navigation of vessels. As such, spot depths are plotted in terms of hazards to shipping, and consider the minimum values within the contour banding of the area where they are located. In shallow waters, or in areas of heavy shipping traffic, there are small contour intervals and many spot depths. However, in deeper waters, the bathymetry is not as detailed. This presents a problem to the modelling of tidal flow for tidal current energy purposes in that developers will be looking to areas where the flows are strong and away from shipping traffic with enough depth to allow effective operation of the tidal device. The developer can, and should, carry out their bathymetric survey of the development site. However, surveys are expensive, and need to be selective. In large areas or areas where the tidal current strength is not obvious from charts, a survey will not be carried out in advance of the tidal model in order that the developer may use this to choose the development site. In such instances the modeller must use UKHO bathymetry.

It is therefore necessary to develop a method of accepting a mixture of relatively sparse spot depths and contours.

Early methods used grid overlays. A transparency with boxes of the desired grid discretisation was laid over the chart. It was then a laborious task of counting boxes in which contours or spot depths occurred. The depths in the unmarked boxes were produced by linear interpolation. This method was limited by the extensive time taken, the propensity for errors and the inflexibility such that the process would have to be repeated for a different grid size.

This author has developed two methods of topology modelling that are more practical and produce a better representation of the sea floor for tidal current models.

3.2.1 Map Digitisation

To produce bathymetric data in digital form, it is necessary first to extract the

bathymetry from the chart of the region to be modelled. A process was devised to digitise them using the facilities of Microsoft ™ Visual Basic™ (VB) and its picture manipulation functions. The digitisation procedure is as follows:

The desired area of chart is scanned using a standard flatbed scanner and the picture saved as a JPEG file.

The chart file is loaded into the VB Picture Object of the map digitisation program.

In its original form, the size or the map section and the scale of the map are entered to achieve the appropriate map scale for digitisation. A simple scale relationship between the size of the image in pixels and the entered map scale provided a chart position for digitisation. A later development allowed for rotation of the chart to better suit the computational domain. In this method, cross-hairs were used to locate and enter the location of known positions on the map grid. Three points were used to set the scale. A point of known latitude and longitude is selected towards the bottom left of the chart. Two further points are selected, one with the same latitude and one having the same longitude. This process set the scale relationship between pixels and the chart gradicule whilst recording the degree of rotation of the chart image.

The data was entered by one of 3 methods:

Depth data read from file

Spot depths - the position of the depth is clicked on using the mouse and the depth is entered through a dialog box.

Contour depths - The spacing of the data points and the depth of the contour are entered through a dialog box. The position data is obtained by clicking the mouse on the contour and dragging along the line of the section to be entered.

The resultant data is in the form of x, y and z co-ordinates ordered by y then x value, which can be saved at any time to file. The UKHO Standard Chart Series is a Mercator projection using the Airy 1850 ellipsoid. The units of measure for this projection are degrees of latitude and longitude. It is possible to perform tidal modelling in these units, and indeed necessary for large area models (Davis 1980). However, it is preferable to work in SI units for small area models where the effects of earth curvature are far less apparent. It is therefore necessary to convert from this angular coordinate system to a grid in SI units of measure. The process for this is described in section 3.2.3 below. The depth points were stored as distances in metres east and north from the origin of the projection used. The depth was stored as metres relative to the chart datum. This is the water level relative to which all depths on the chart are measured. For many charts, the chart datum, including those used in these studies, is the Lowest Astronomical Tide (LAT), which describes the minimum predictable depth for any point on the chart.

This data can then be used in the discretisation of the digitised area. A variety of discretisations (grid size and clustering) can be applied using the same stored depth points.

3.2.2 Digital Charts

Since the late 1990s, the UKHO have been producing electronic raster versions of their charts for maritime navigation integrated with Global Positioning Systems (GPS). Further development has led to the charts in vector format, and in 2002 charts for the UK continental shelf were produced in the Geographical Information System (GIS) Environmental Systems Research Institute, Inc. (ESRI) shapefile and Mapinfo tab file formats. These charts were produced under the name Seazone™. The Seazone digital charts store depth soundings as points or polypoints and depth contours as polylines or areas.

The availability of this data in digital form is a great advance in facilitating tidal modelling. However, the data still requires manipulation to extract the position of individual depth points for a topographical model prior to hydrodynamic

modelling. The shapefile file format is a GIS format developed by ESRI and has become a published industry standard format (Environmental Systems Research Institute, Inc. 1998). A program to read in the depth information from the Seazone shapefiles was developed by the author. The positional data in the Seazone charts are in World Geodetic System 84 (WGS84) projection. Thus the coordinates have also to be transformed to a metric coordinates for flow modelling purposes using the method described in Section 3.2.3.

3.2.3 Co-ordinate Projection Transformation

In the manual gridding method mentioned above, the intensity of the labour required was high and thus modelling areas were minimised and the discretisation relatively coarse. In limiting the size of the area, the grid could be constructed from the scale on the map.

In automating the topology discretisation method, larger areas may be used and finer discretisation may be used. Admiralty Charts, as published by the UKHO, use a Mercator projection on the Airy 1850 ellipsoid with co-ordinates in latitude and longitude. The Mercator projects the near-spherical surface of the Earth on to a cylindrical plane. This projection means that latitudes near the equator are well represented. However, the there is increasing distortion with increasing latitude as converging lines of longitude are held parallel (Figure 3.1). Thus, the scale of these charts does not vary over small areas. In order to produce a grid of set size, it is necessary to convert the longitude, latitude co-ordinates to easting and northing of a universal transverse Mercator (UTM) projection. The transverse Mercator projection, which rotates and elongates the original longitude/latitude grid, is not affected by this distortion at high latitudes. The distortion is transferred to the longitudinal direction. This is not an issue so long as the measurements made are close to the origin, which is the case here. The projection is normally used for local grid systems such as the Ordinance Survey Great Britain (OSGB) or Irish National Grid. For mapping the entire surface of the Earth, the earth is divided in to 6° segments of longitude extending westward from the International Date Line at 180°. Each of these segments provides a new origin for the projection and therefore, the latitude distortion is minimised within each segment. A degree of distortion remains in

the easting. This is compensated for in a scale reduction factor. For UTM this scale reduction factor has a value of 0.996.

The UTM projection system also uses a different ellipsoid from that of the Ordinance Survey Mercator projection. That is the International 1924 ellipsoid. The different ellipsoids are methods of modelling the globe of the Earth, which is not an exact sphere. Various ellipsoids have been suggested by a variety of cartographers as a greater understanding of the earth's geometry has developed. The differences between the two systems are given in Table 3.1.

Table 3.1 Ellipsoids for the OSGB and UTM projections

Ellipsoid	Semi-major axis (m)	Semi-minor axis (m)
Airy 1850	63777563.396	636256.910
International 1924	6378388	6356911.946

It is possible to approximately convert from one system to the other using the techniques described in Ordinance Survey (1999) and programmed in utms.f (U.S. National Geodetic Survey 1993). This code was modified by the author to function as a dynamic link library (DLL) to the tidal code.

Both the positions' digitised points (contours and spot depths) and the grid cell centres are transformed by this technique.

Mercator projection

Transverse Mercator projection
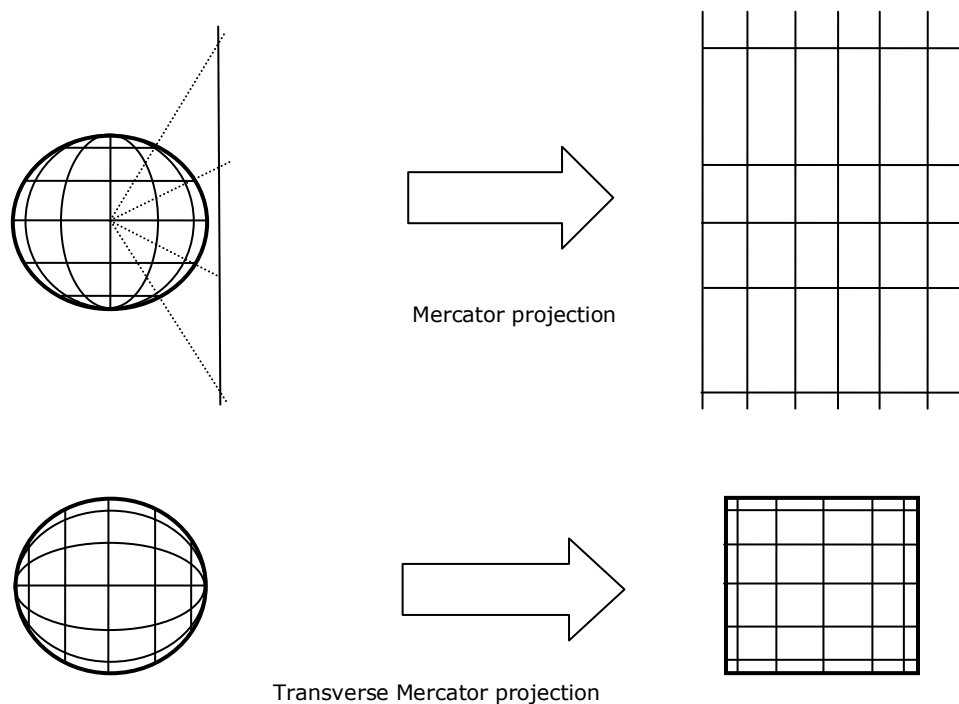
Figure 3.1 Differences between the Mercator and transverse Mercator projection

3.2.4 Map and Coordinate Rotation

In many circumstance, it can beneficial for the domain to be rotated. This is done so that the coast runs parallel to the computational domain boundary. This reduces the discretisation required for the coast, and it facilitates boundary condition settings. In some sites, it can dramatically reduce the size of domain required.

At a purely practical level, it is an easy task in most picture editing packages to rotate the scanned image of the chart being used as the basis of the topology. However, it becomes necessary to perform a co-ordinate rotation on chart positions. This is the case in entering the topology, pulling previously saved position-depth data to a rotated chart, saving position-depth data for use on charts with other rotations and transformation of the grid centre co-ordinates to

transverse Mercator, or latitude and longitude. The transformations in either direction are performed using the same transformation matrix as in Equation 3.1:

$$\begin{bmatrix} \cos(\Theta) & \sin(\Theta) \\ -\sin(\Theta) & \cos(\Theta) \end{bmatrix} \begin{bmatrix} x \\ y \end{bmatrix} = \begin{bmatrix} x' \\ y' \end{bmatrix} \qquad 3.1$$

Where x and y are the coordinates of the original point, Θ is the angle of the major axis from the x direction and x' and y' are the coordinates of rotated point.

3.2.5 Defining the domain

The definition of the computational domain size is another important step. It should be chosen such that boundary values can be easily defined and such that the region of interest is well within the domain. There is a risk of flow at the site of interest being dominated by the boundary conditions if it is not well within the domain.

The manual methods alluded to in Section 3.2.1 do not easily permit variation of domain size to optimize the results. A graphical method was developed using the VB Graphical User Interface (GUI) developed for map digitisation in Section 3.2.1. The positions of the north, south, west and east boundaries were selected directly from the chart in the Picture Box Control with a mouse click. A similar method of domain selection was developed for the GIS data. Here a control produced by ESRI known as MapObject LT™ was used to display the Seazone chart. Again, the position of the mouse pointer when clicked set the coordinates of the north, south, west and east boundaries.

3.2.6 Grid Generation – Method of Planes

It is common practice within the field of computational fluid dynamics (CFD) to increase the resolution of the computational grid in the region of interest to the investigator. This is partly to have good resolution of the flow in that area of the

domain and partly to reduce the resolution and thereby computational effort in the far field of the domain. Considering the large domains being considered with this GUI data entry technique it was seen as advantageous to introduce variable grid resolution.

A 'point and click' method was developed similar to that of defining the extent of the domain. However, in this case the x and y positions determined the start of a new discretisation zone within the domain in either the x or y direction. On setting a zone boundary the user is prompted for an estimated resolution. The actual size of each cell is determined by Equations 3.2 and 3.3.

$$N_i = \mathrm{int}\left(\frac{x_{i+1} - x_i}{estimate\Delta x_i}\right)$$ 3.2

$$\Delta x_i = \frac{x_{i+1} - x_i}{N_i}$$ 3.3

Where x is the position of the discretisation zone boundary in the x or y direction, N is the number of cells in the zone, Δx is the resolution of cells in the zone and the suffix i is the index of the zone.

3.2.7 Method of Planes

The method was developed during the Optimising the Performance (Electrical and Economic) of Tidal Current Turbines (OPTCurrenT) programme, which was funded in part by the European Commission (Bryden, Delure, DeNat, 2002).

The method of planes generates a regular grid of depth centred cells. A plane is constructed around the cell centre position based on the known points (contours and spot depths) that surround it.   An approximation for the vertical displacement can then be calculated analytically from the equation of this plane.

The rules for choosing the plane depend on whether the cell is in the interior of

the domain, and the number of known points that surround it near the boundaries of the area to be discredited.

1. The data is searched for four closest points that surround the desired position (north, south, east & west).

2. Four planes are constructed using the four sets of three points (see Figure 3.2).

3. It is determined whether the resultant triangular plane surrounds the position.

4. The depth of the position is determined to be the average value.
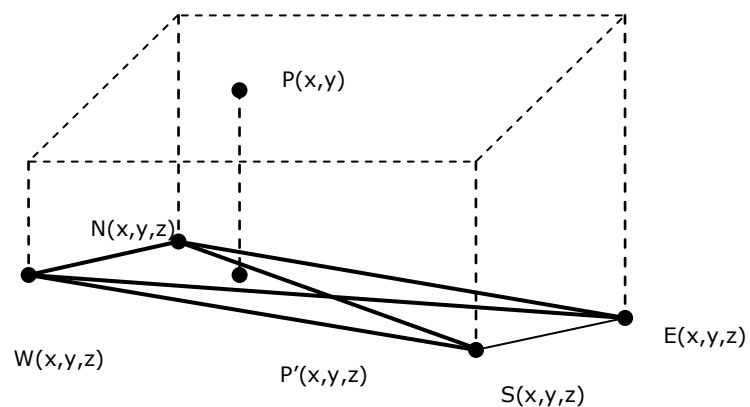
Figure 3.2 The construction of four planes based on four points surrounding a point of interest

For a boundary point (3 surrounding points) (Figure 3.3)

The whole process is similar to the aforementioned except that there is only one plane created so no averaging is required. Only one plane is used given by

those planes, the constructing points of which surround the position.
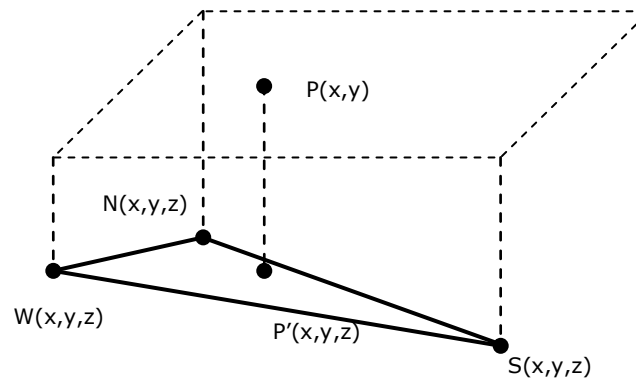
Figure 3.3 Construction of a boundary plane with three points surrounding a point of interest

For a boundary point (where points do not surround the position) (Figure 3.4)

1.   Search data for the three closest points to the position of interest.

2.   If the three closest points are collinear then the next closest point that is not collinear is used.

3.   Calculate the equation of the plane constructed from these points.

4.   Calculate the depth of the position from this plane.
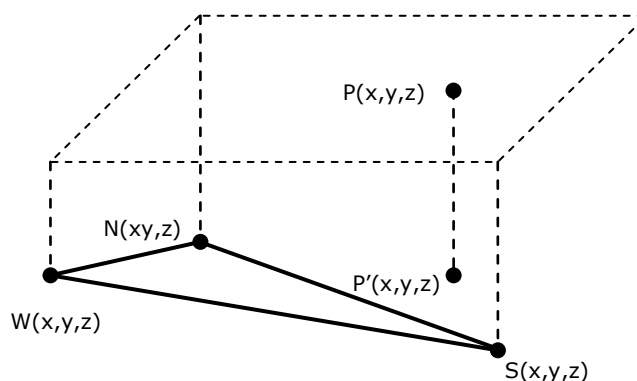
Figure 3.4 Construction of a plane where the point of interest is beyond the boundary

3.2.8 Delaunay Triangulation

The method of planes technique described in Section 3.2.7 above, appeared to work well for the Arklow Bank area used in the first case study. However, the technique is computationally expensive as all the depth points must be searched for the four enclosing values each time a new grid point is defined. These calculations must be performed for any new grid specification. In addition problems were encountered with the 3 point boundaries when applied to the more complex Yell domain. A further evolution of the pre-processing was then to employ Delaunay Triangulation (Press, Teukolsky, Vetterling et al. 1992, Bourke 1989). This is a common method of generating an unstructured triangular tessellation for numerical modelling of flow and structures. The process is designed to produce a triangular mesh with optimal aspect ratio using a series of Vornoi circles. This mesh may be stored as a data file thereby reducing the computational effort on grid design.

Having produced the triangular mesh, the structured grid is produced by searching the triangles for the one containing the proposed grid point and its

depth calculated by planar linear interpolation. The code of Bourke (1989) was modified by the author for inclusion into the tidal model as a DLL.

3.3 Hydrodynamic model

The governing equations for coastal tidal flow are commonly referred to as the shallow water equations. The principal assumption in their development is that in shallow waters the water density can be considered constant throughout the water depth. This assumption holds true in areas of high tidal currents due to the increased level of turbulent mixing. They may be derived from the Navier-Stokes Equations (Drago & Lovenitti, 2000) or more directly derived from first principals of mass and momentum conservation (Pugh 1987). The model used here is developed from that of Bryden (1998). The code approximates the continuity equation together with the *u* and *v* momentum equations.

In the model, the local depth (*H*) is described by a "fixed" depth *h(x,y)* and a time varying perturbation $\xi(x,y,t)$ such that H = *h*+ξ, as shown in Figure 3.5.
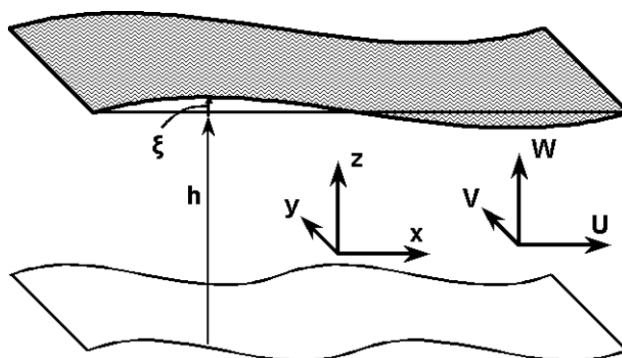
Figure 3.5 Coordinate system for hydrodynamic model (Bryden, 2000)

By assuming a constant density, the mass conservation or continuity is given by equation 3.4:

$$\frac{\partial u}{\partial x} + \frac{\partial v}{\partial y} + \frac{\partial w}{\partial z} = 0 \qquad\qquad 3.4$$

Where *u*, *v* and *w* are velocity components in the *x*, *y* and *z* directions. The horizontal momentum is described in equations 3.5 and 3.6.

$$\frac{\partial u}{\partial t} + u\frac{\partial u}{\partial x} + v\frac{\partial u}{\partial y} + w\frac{\partial u}{\partial z} = fv - g\frac{\partial \xi}{\partial x} + \gamma\frac{\partial^2 u}{\partial z^2}, \qquad\qquad 3.5$$

$$\frac{\partial v}{\partial t} + u\frac{\partial v}{\partial x} + v\frac{\partial v}{\partial y} + w\frac{\partial v}{\partial z} = -fu - g\frac{\partial \xi}{\partial y} + \gamma\frac{\partial^2 v}{\partial z^2}, \qquad\qquad 3.6$$

where γ is the local kinematic turbulent viscosity; *g* is the acceleration due to gravity and *f* is the Coriolis coefficient given by Equation 3.7.

$$f = -2\omega\cos\varphi \qquad\qquad 3.7$$

Where ω is the Earth's angular velocity (radians/sec) and φ is the latitude. For simplicity, the latitude is taken as that at the origin of the model. This is acceptable as long as the modelled area is small, which it is in the cases investigated here.

If the vertical, *w*, velocity is considered negligible in comparison *u* and *v*, the vertical (*w*) momentum equation can be simplified to equation 3.8.

$$g = -\frac{1}{\rho}\frac{\partial p}{\partial z}. \qquad\qquad 3.8$$

Where *p* is barometric pressure and ρ is the water density.

This treatment of the w-velocity component has some validity in areas without strong up-welling flows.

A transformation of the vertical dimension (Drago & Lovenitti, 2000) is used prior to discretisation. This is expressed in equation 3.9.

$$z' = \sigma = \frac{z + h}{\xi + h} = \frac{z + h}{H}$$

3.9

The new vertical coordinate, σ, now varies from 0 to 1 throughout the flow domain. This spatial mapping simplifies calculation. The water column is discretised in to layers. Without it, the number of depth cells would vary with varying depth as a function of position and as a function of time. This would be computationally destabilising. The governing equations of fluid motion can now be rewritten as equations 3.10 to 3.14.

$$\frac{\partial Hu'}{\partial x'} + \frac{\partial Hv'}{\partial y'} + H\frac{\partial w'}{\partial \sigma} + \frac{\partial \xi}{\partial t} = 0$$

3.10

$$\frac{\partial \xi}{\partial t} + \frac{\partial Uh}{\partial x'} + \frac{\partial Vh}{\partial y'} = 0$$

3.11

$$\frac{\partial u}{\partial t} + u'\frac{\partial u'}{\partial x'} + v'\frac{\partial u'}{\partial y'} + w'\frac{\partial u'}{\partial \sigma} = fv' - g\frac{\partial \xi}{\partial x'} + \frac{\gamma}{H^2}\frac{\partial^2 u}{\partial \sigma^2}$$

3.12

$$\frac{\partial v'}{\partial t} + u'\frac{\partial v'}{\partial x'} + v'\frac{\partial v'}{\partial y'} + w'\frac{\partial v'}{\partial \sigma} = -fu' - g\frac{\partial \xi}{\partial y'} + \frac{\gamma}{H^2}\frac{\partial^2 v'}{\partial \sigma^2}$$

3.13

Where u'=u; v'=v; x'=x; y'=y;

$$w = \sigma\frac{\partial \zeta}{\partial t} - Hu'\frac{\partial \zeta}{\partial x} - Hv'\frac{\partial \zeta}{\partial y} + Hw';$$

3.14

u and *v* are the depth-averaged components of local velocity.

3.3.1 Discretisation

A staggered grid is used to discretise these equations in the horizontal dimensions whereby the varying height, ζ, is applied to the cell centres and the velocity components are applied at the cell edges as show in Figure 3.6. Forward differencing is used for the time domain and central differencing is used in the spatial domain.
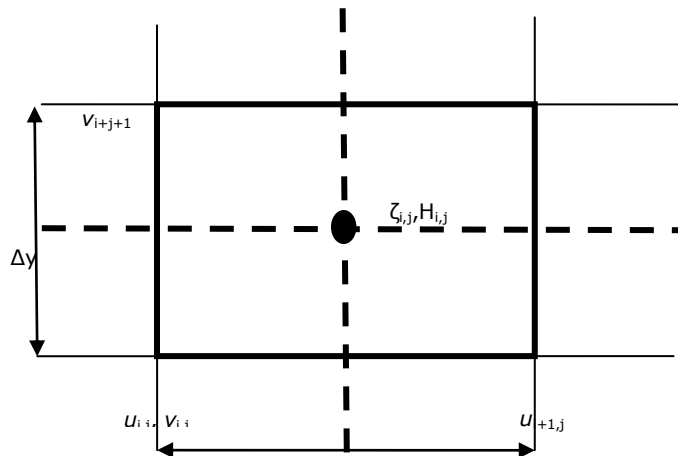
Figure 3.6 Horizontal discretisation system

The depth transformation (Equation 3.8) means that the depth dimension is also discretised to a regular rectangular grid as shown in Figure 3.7. Five layers were used in the analyses performed in this study. This provided a sufficient number of cells to produce a varying depth profile. More layers could have been used, but there is a balance with the period of time that it takes to obtain the model solution.
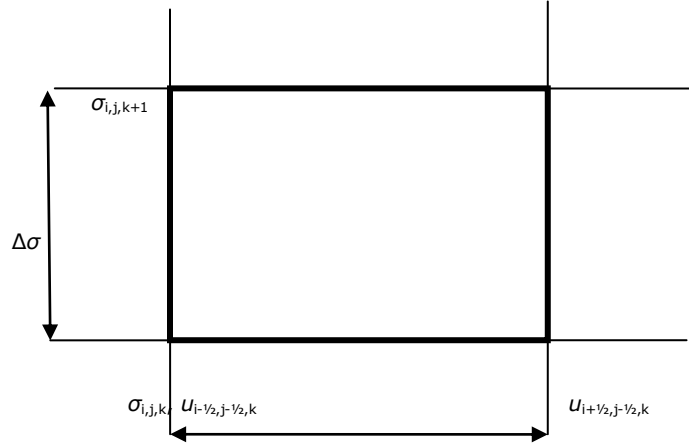
Figure 3.7 Vertical discretisation system

The discretised equations can be seen below in Equations 3.15 to 3.18.

$$\zeta_{i,j}^{t+1} = \zeta_{i,j}^t - dt \left[\frac{U_{i+1,j}^t \left(H_{i+1,j}^t + H_{i,j}^t \right) - U_{i,j}^t \left(H_{i-1,j}^t + H_{i,j}^t \right)}{2dx} + \frac{V_{i,j+1}^t \left(H_{i,j+1}^t + H_{i,j}^t \right) - V_{i,j}^t \left(H_{i,j-1}^t + H_{i,j}^t \right)}{2dy} \right] \qquad 3.15$$

$$w_{i,j,k}^{t+1} = w_{i,j,k-1}^{t+1} - \frac{d\sigma}{H_{i,j}^t} \left[\begin{array}{l} u_{i,j,k}^t \dfrac{H_{i+1,j}^t - H_{i-1,j}^t}{2dx} + H_{i,j}^t \dfrac{u_{i+1,j,k}^t - u_{i-1,j,k}^t}{2dx} \\[2mm] + v_{i,j}^t \dfrac{H_{i,j+1}^t - H_{i,j-1}^t}{2dy} + H_{i,j}^t \dfrac{v_{i,j+1,k}^t - v_{i,j-1,k}^t}{2dy} \\[2mm] + \dfrac{U_{i+1,j}^t \left(H_{i+1,j}^t + H_{i,j}^t \right) - U_{i,j}^t \left(H_{i-1,j}^t + H_{i,j}^t \right)}{2dx} \\[2mm] + \dfrac{V_{i,j+1}^t \left(H_{i,j+1}^t + H_{i,j}^t \right) - V_{i,j}^t \left(H_{i,j-1}^t + H_{i,j}^t \right)}{2dy} \end{array} \right] \qquad 3.16$$

$$u_{i,j,k}^{t+1} = u_{i,j,k}^{t} - dt \left[\begin{array}{c} \dfrac{\left(u_{i,j+1,k}^{t} + u_{i,j,k}^{t}\right)^2 - \left(u_{i,j,k}^{t} + u_{i,j-1,k}^{t}\right)^2}{8dx} + vv\,\dfrac{u_{i+1,j,k}^{t} + u_{i+1,j,k}^{t}}{2dy} \\[2ex] - w_{i,j,k}^{t}\,\dfrac{u_{i,j,k+1}^{t} - u_{i,j,k-1}^{t}}{2d\sigma} \\[2ex] + g\,\dfrac{\zeta_{i,j}^{t} + \zeta_{i,j-1}^{t}}{dx} + \dfrac{\gamma}{H_{i,j}^{t\,2}}\,\dfrac{u_{i,j,k+1}^{t} - 2u_{i,j,k}^{t} + u_{i,j,k-1}^{t}}{d\sigma^2} - fvv \end{array} \right] \qquad 3.17$$

$$v_{i,j,k}^{t+1} = v_{i,j,k}^{t} - dt \left[\begin{array}{c} uu\,\dfrac{v_{i+1,j,k}^{t} + v_{i+1,j,k}^{t}}{2dx} + \dfrac{\left(v_{i,j+1,k}^{t} + v_{i,j,k}^{t}\right)^2 - \left(v_{i,j,k}^{t} + v_{i,j-1,k}^{t}\right)^2}{8dy} \\[2ex] - w_{i,j,k}^{t}\,\dfrac{v_{i,j,k+1}^{t} - v_{i,j,k-1}^{t}}{2d\sigma} \\[2ex] + fuu + g\,\dfrac{\zeta_{i,j}^{t} + \zeta_{i,j-1}^{t}}{dy} + \dfrac{\gamma}{H_{i,j}^{t\,2}}\,\dfrac{v_{i,j,k+1}^{t} - 2v_{i,j,k}^{t} + v_{i,j,k-1}^{t}}{d\sigma^2} \end{array} \right] \qquad 3.18$$

Where the nomenclature is as above with the primes removed for simplicity,

The local kinematic turbulent viscosity, γ, can be estimated using Equation 3.19 (Davies & Furnes 1980):

$$\gamma = \frac{K\,\overline{U^2}}{\rho\sigma} \qquad\qquad\qquad\qquad 3.19$$

where ρ is the water density (kgm^{-3}), σ is 10^{-4} s^{-1}, K is a dimensionless constant which is equal to 2.0×10^{-5}, and $\overline{U^2}$ is the depth-averaged mean square current speed (m^{2}s^{-2}).

3.3.2 The Boundary Conditions

In its present form, the software utilises five types of boundary condition. These are:

The "Law of the Wall" is applied to the seabed (White 1999). This can be

characterised by Equation 3.20. This is an empirical relationship that describes the nature of the current profile in the close vicinity of the seabed:

$$u(z) = \frac{u^*}{k} \ln\left(\frac{z}{z_0}\right),$$

3.20

where u is the current velocity a distance z from the sea bed; u^* is the friction velocity determined by Equation 3.21; k is the Von Kármán constant, given as 0.4, and z_0 is a characteristic length related to the roughness of the seabed.

$$u^* = \sqrt{\frac{\tau_0}{\rho}},$$

3.21

Where ρ is the water density and τ_0 is the bed friction shear stress term (Chanson 2004) given in Equation 3.22.

$$\tau_0 = \rho g \frac{U^2}{C^2}$$

3.22

where C is the Chezy coefficient (Bryden, 1998, Bryden, Couch, Owen et al. 2007) given by $\frac{R^{\frac{1}{6}}}{n}$; n is the Manning Friction coefficient and R is the hydraulic radius given by Equation 3.23.

$$R = \frac{H \cdot b}{b + 2H}$$

3.23

Where b is breadth of the cell, i.e. the horizontal dimension of the cell normal to the velocity component being calculated.

Long term experience of modelling tidal flows (Bryden 1998) has led to the use of 0.5 m for the sea-bed roughness. Work on turbulence length scales in energetic tidal areas, as part of the UK Engineering and Physical Sciences

Research Council (EPSRC) SUPERGEN research programme, should give a further empirical basis for the value of such length scales.

A sea surface slip wall (Koutitas 1988), to which wind shear can be applied, where the wind induced stress can be modelled by Equation 3.24.

$$\begin{bmatrix} \tau_x \\ \tau_y \end{bmatrix} = \rho k \sqrt{W_x^2 + W_y^2} \begin{bmatrix} W_x \\ W_y \end{bmatrix}$$ 3.24

Where ρ is the water density (kgm^{-3}); k is a friction coefficient (0[k]=10^{-6}); and $W_{x,y}$ = wind velocity 10 m above the sea level. Added wind shear has not been applied by the author in the case of tidal modelling for tidal energy resource purposes. This is because the analysis is aimed at average conditions rather than conditions of wind and tide at a specific time.

A coastal slip wall, where the flow is constrained to flow parallel to a coastal boundary. The equations for the north, south, west and east boundaries are given below in Equations 3.25 to 3.28.

West: $u_{i,j} = 0$ 3.25

East: $u_{i+1,j} = 0$ 3.26

North: $v_{i,j+1} = 0$ 3.27

South: $v_{i,j} = 0$ 3.28

Defined time-varying velocity and/or defined tidal amplitude on open boundaries, where the surface elevation and/or the local velocity at the boundary cells are specified for the duration of the simulation. These are the driving boundary conditions for the simulation, and take the form of a summation of sinusoidal equations, having periods of the semi, quarter and

eighth diurnal tides. In most cases, the use of only the semi-diurnal tidal period (12.4 hours) is sufficient.

Gradient Boundaries, in which the local flow is not specified, but it is assumed that the velocity and surface elevation gradients across the boundary are all zero, may be used within the model.

Experience has shown that, to avoid numerical inaccuracies near the open sea boundaries, it is advisable to ensure that the simulation area is sufficiently large that the area under consideration for tidal development is well away from the boundaries.

3.4 Applications of the model

3.4.1 Arklow Bank

The modelling of Arklow Bank was carried out to generate flow data for the OPTCurrenT economic model (Bryden, Delure, DeNat, 2002). The location, and a description of Arklow Bank area can be seen in Section 2.

One of the key features, and arguably the causal feature of the strong tides in the area, is a degenerate amphidromic point inland from the bank (Pugh 1980, Hall 1971). This results in a low tidal range near the coast and a $2^1/_2$ - $3^1/_2$ hour phase difference between Wicklow and Courtown (Hall 1971, Clarke 1999). Overall, there is a $5^1/_2$ hour phase difference between Dublin to the north and Carnsore Point on the Southeast tip of the Irish coast. Tidal diamonds indicate spring currents in excess of 1.5m/s (Hall 1971). The survey carried out as Task 3 of the OPTCurrenT project, referred to in Section 2 of this work, measured the tidal stream magnitude in excess of 1.8m/s during the spring tide.

3.4.1.a   Domain

The domain, initially, only considered the immediate viscidity of Arklow Bank taking in the adjacent coast and extending an approximately equal distance into

the St. George's Channel. A variety of amplitude and velocity boundary conditions was placed on the north and south of the domain, with the eastern boundary being left as a gradient boundary. This small domain, although computationally stable, did not produce results that compared with the field results. The domain was expanded so that data next to the boundary, where the flow conditions were fixed, was not used by the optimisation. This larger grid proved easier to set the boundary conditions. However, the results were still not reliable, especially close to the boundary.

It was decided that the driving force for this tidal system was the very large phase difference between the southern tip of Ireland and the Irish Sea. It was decided that it was not feasible to model the tidal conditions around an amphidromic point by only considering the near field boundary conditions. The domain was expanded to the north and south to a distance where the full tidal phase change around the amphidromic point could be applied.

3.4.1.b Rotation

A model can benefit from grid rotation if there is a course which the current is anticipated to follow. Aligning the grid with this flow makes computation easier. Grid rotation is also advantageous if there is a linear feature; the modelling of which can be improved by localised grid refinement.

With respect to Arklow Bank, there were two obvious features for which grid rotation might benefit the hydrodynamic modelling - the coast and the Arklow Bank. The first models were rotated by 10° such that the Arklow Bank was orientated in line with the grid. This was done so that a refined grid could be applied more easily to the bank.

With the application of the far field grids, it was deemed more important that the grid ran in line with the currents following the coastline. This grid had a 15° rotation.

3.4.1.c   Discretisation

In any computational model there is a balance between accuracy, computational time and memory requirements. Fortunately, as affordable computers have become more powerful, accuracy has benefited. The check for the most efficient grid is grid dependence. A coarse grid is used, which is gradually refined until the solution is deemed grid independent within the desired order of accuracy. The duration of the solution is also taken into account. A highly refined grid has an extended calculation time, not only due to there being more cells to calculate, but also because a shorter time step must be used to keep the solution stable.

The most efficient grid spacing for the area of interest was 250 m to 350 m. The far field does not need the same degree of refinement as it is used to develop the flow and to apply the required tidal phase difference. The routine used to expand the grid uses a factor of $^5/_3$ for the expansion of cells in neighbouring zones. This factor maintains stability whilst still allowing a fast expansion away from the area of refinement. The information in these far field cells is not used in the optimisation model.

3.4.1.d   Time step

The optimum time-step is one that maintains stability whilst still providing an accurate, fast solution. The model appears to be more dependent on the spatial discretisation for accuracy. Therefore, the optimum time step is the largest without losing stability. For spring tides, where the temporal changes are greater, the model was started on a 2-second time-step, this was increased to 3 seconds for the stable phase of calculation. The neap calculations could use larger time steps up to 5s.

3.4.1.e   Results

The area is dominated by a bi-directional current running approximately northeast - Southwest. The fastest currents are located to the east of the

Arklow Bank and to the north of the region. The slowest currents are found between the coast and the western side of the Arklow Bank. The ebb-flood tides are bi-directional as demonstrated by the tidal ellipse (Figure 3.38).
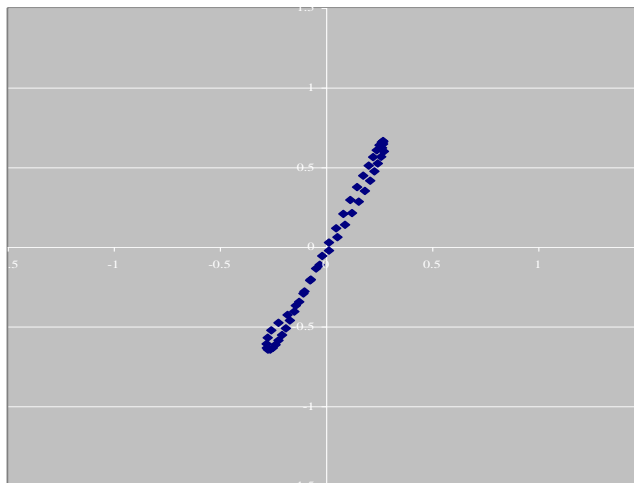
Figure 3.8 Tidal ellipse for the neap tide at Buoy 1.

The current vectors at the neap tide are shown in Figure 3.9. It can be seen that the neap tidal currents in general do not exceed 1.0 m/s over the entire domain. Tidal currents do not exceed 0.5 m/s towards the coast and over the bank.

Table 3.2 Summary of Current at the survey sites

Location	Tide Type	Max U	Min U	Max V	Min V	Max Speed	Mean Speed
Buoy 2	Mean neap	0.27	-0.27	0.66	-0.64	0.71	0.45
	Mean spring	0.69	-0.60	1.64	-1.66	1.78	1.16
Buoy 1	Mean neap	0.26	-0.23	0.62	-0.59	0.67	0.42
	Mean spring	0.57	-0.51	1.50	-1.45	1.61	1.04

Figure 3.10 shows the current vectors for Arklow during the maximum of the spring tide. The pattern of the energetic flow areas is similar to that of the neap tide. The current speeds, however, are significantly higher, with values exceeding 2.0 m/s in places. A notable feature in both of these figures is the

area of increased current speed to the north east of the domain. This not likely to be a real feature of the flow as it appears more like a numerical error. However, the process of extending the domain at the north, south and east boundaries moved this apparent numerical error away from the area of interest near the Arklow Bank.

Table 3.2 shows a comparison between the neap and spring tides at the Task 3 survey locations.
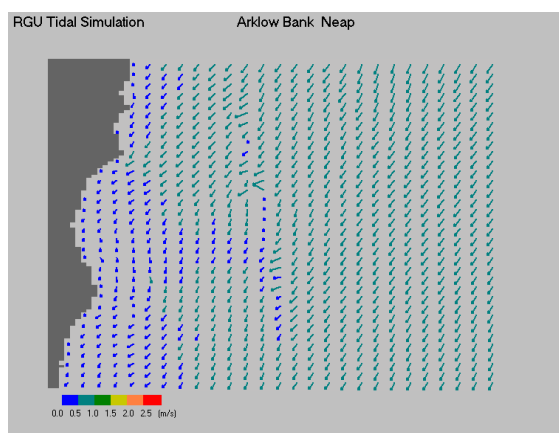
Figure 3.9 Mean neap maximum tide at Arklow.
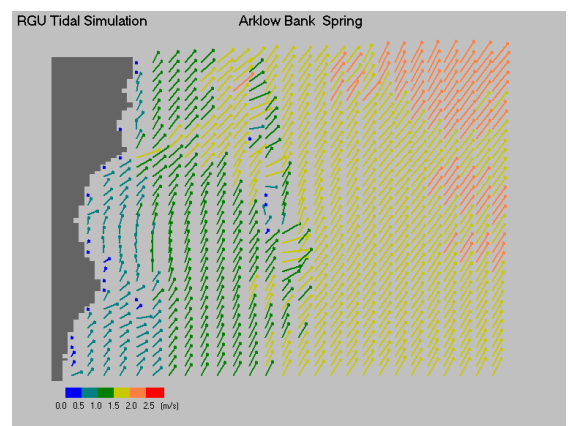
Figure 3.10 Mean spring maximum tide at Arklow.

Figure 3.11 and Figure 3.12 show the comparison of modelled and measured current speed at the neap tide. It can be seen that there is a reasonable agreement between the two data sets. The model over predicts the measured data for the Southern site and under predicts for the northern site. However, if we take into account the natural variation in tidal current magnitude, the predicted results are a good approximation on which to base design optimisation.
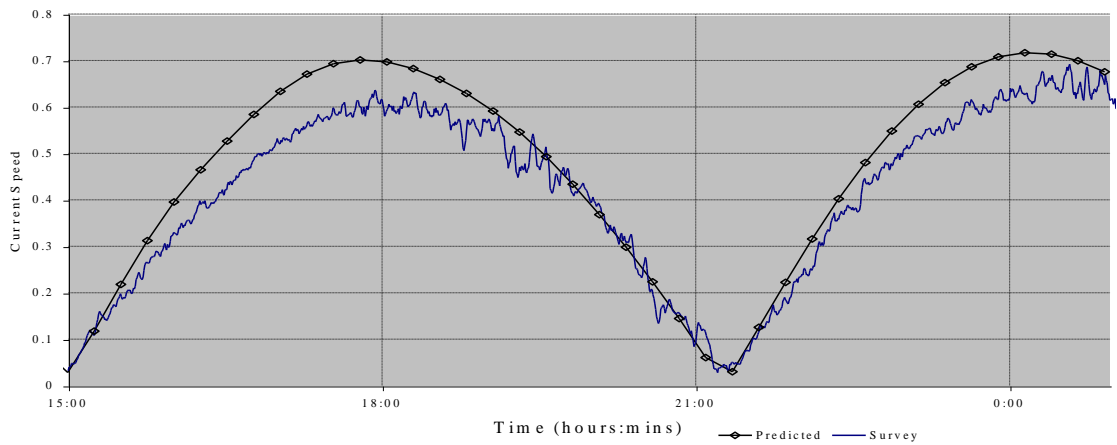
Figure 3.11 Comparison between mean neap model and measured current speed at neap tide at Buoy 1
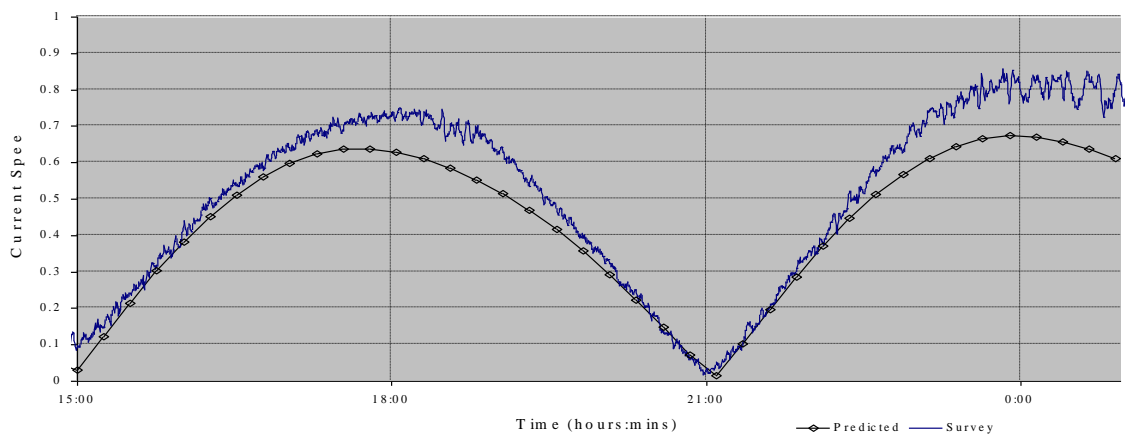
Figure 3.12 Comparison between mean neap model and measured current speed at neap tide at Buoy 2

Good agreement can also be seen in the comparison between the predicted and measured results for the spring tide (Figure 3.13).
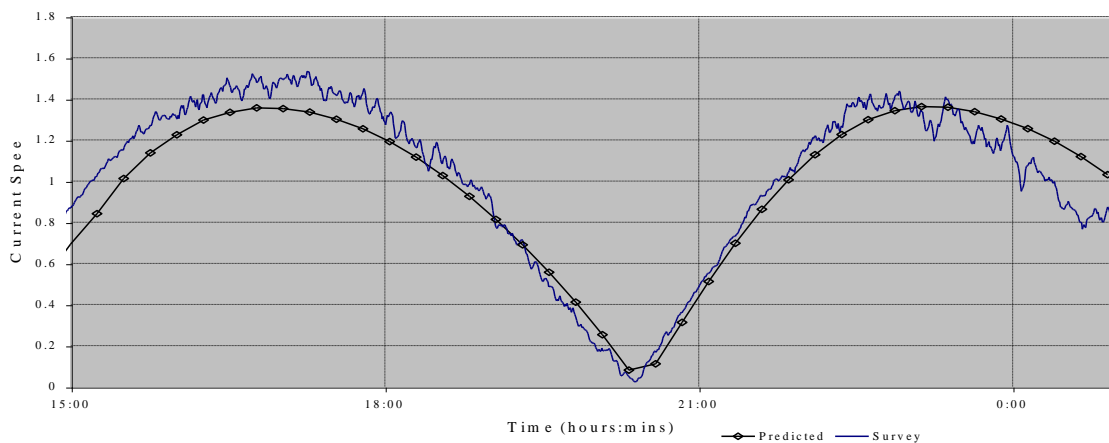
Figure 3.13 Comparison between mean spring model and measured current speed at spring tide at Buoy 1

These apparently good results give confidence in the model flow prediction in other regions of the domain close to the Arklow Bank. After all the purpose of the model is not to show that it is possible to create a model that matches measured values, but to use the measured values to give confidence that the flow predicted away from the measured values is a reasonable approximation also. Thereby giving confidence in any tidal energy calculations carried out away from the measured position. In this particular instance, the tidal flow model was to provide flow data for the cost optimisation part of the OPTCurrenT.

In producing this model it has been necessary to extend the domain away from the area of interest. The extended areas continue the boundary topography away from the boundary. As such, a simplified artificial domain is created. The boundary conditions were derived from tide tables (Clarke 1999), tidal diamonds (Haslam 1978) and the co-tidal chart (Hall 1971). The artificial extended domain will have varied from these real measured values. Thus the boundary condition values had to be interpolated from the data available. This, in itself, shows the importance of having measured data within the domain. It would not have been possible to create and verify this model without it.

3.4.2 Yell Sound, Shetland

The location of Yell Sound is described in Section 2.3.

3.4.2.a   Topographical model

The topographical model uses data direct from the Admiralty charts of Yell (Haslam 1980). The northern and eastern boundaries for the model were selected as the northern and eastern entrances to Yell Sound. The eastern and southern boundaries were selected so as to include the full extent of the voes which come off the sound in a south easterly direction.   The inter-island channels in this area are complex and some channels not directly connected to Yell Sound were included in the domain. These areas were treated as flat land of zero depth.   The gridding method used a structured rectangular grid superimposed on an unstructured triangular mesh as described in Section 3.2.8.

The method allowed for rapid generation of grids, which had different sizes and levels of refinement.

The final grid of the area had a 150 m resolution in both x and y directions in the far field and a 90 m x 90 m resolution in the locale of the narrow channels around Bigga and Samphrey, where the highest currents are found. Five layers where used in the sigma dimension. Overall the grid contained 18195 points.

3.4.2.b The Boundary Conditions

The boundary conditions for Yell can be seen in Figure 3.14. The open-sea boundary conditions control how the interior responds.   Therefore, these conditions are varied to make the interior match the survey data.
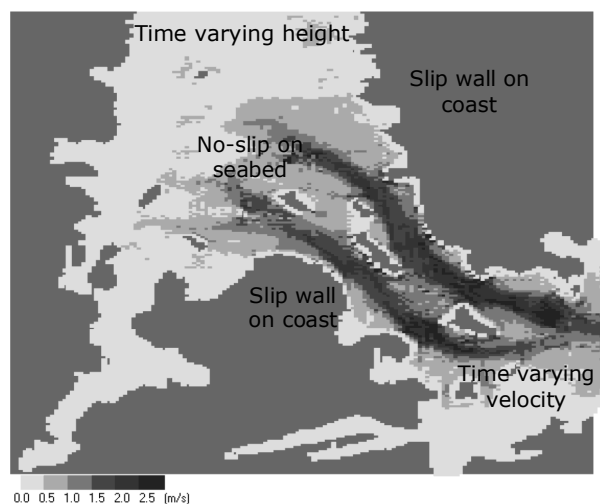
Figure 3.14 Boundary conditions for Yell Sound Model

In the case of Yell Sound, Admiralty Charts gave sufficient information about the water depth and the nature and phase of tidal elevations and currents at the boundaries of the Sound to allow the formulation of a preliminary numerical model. These data sources are designed for shipping safety and the surveys were often carried out many years ago with simple equipment. They are based on average readings over a long period of time. If located near the boundary, however, they can provide an indication of the flow conditions. The model was initially operated using flow velocity data, based on tidal diamond "A" on UKHO Chart 3298 (Morris 1986) describing the flow at the northern boundary (60° 34.49' N, 1° 16.92' W) and tidal amplitude data describing the eastern boundary based on tidal heights at Burra Voe (60° 30' N, 1° 03' W) (Clarke 1999). From these initial values, the values of velocity, amplitude and phase difference are varied to achieve an acceptable agreement with survey measurements throughout the interior and more especially near the area of interest for tidal energy development.

The model was run to determine the tidal flow conditions at both spring and neap tide.

3.4.2.c   Model Predictions and Preliminary Validation

It is necessary to validate the model with known survey data in order to process the results from the model with any degree of certainty. This is an on-going process during the model development, as the boundary conditions are adjusted to bring the model values closer to the measured survey data. It is, however, unlikely that the there will be an exact match between the data sets. The UKHO tidal amplitude data is given as mean values for high and low water at spring and neap tides. These are derived from long term observations at coastal water depth stations. Tidal current surveys are expensive, thus the tidal diamond current speed and direction are averages of surveys, or, alternatively, drawn from a single survey, over a shorter duration that the amplitude surveys. The measurement techniques used (Bell 2003) are a source of error in areas of high currents.   Although the model uses both these data sets as boundary conditions, the interaction between amplitude and velocity in the interior and the different measurement techniques means that the model cannot match both data sets and a judgement must be taken on matching the data within acceptable limits.

In the comparisons of tidal current data, there will also be discrepancies as the model velocities are taken at mid-water and the surveys usually measure near the surface, although measurement depths are not given. Assuming a one-seventh power law relationship, the water speed at mid-water is approximately 91% of the flow near the surface.

In addition to the comparisons shown, the model was also compared with commercial survey data, which is not available for publication.

Although for the purposes of tidal energy development, only the tidal current speeds are of interest, it is important also to consider the tidal amplitudes for the purposes of model validation.   There are only three tidal amplitude measuring stations within the Yell Sound area. These are at Burra Voe, Toft Pier (60° 28' N, 1° 12' W) and Sullom Voe (60° 27' N, 1° 18' W) (Morris 1986). Burra Voe is at the edge of the computational domain on the Eastern boundary

and, therefore, was used as an indication for amplitude condition on this boundary. Sullom Voe is out of the main channel on one of the spur Voes. The most suitable point for amplitude validation near the area of interest is Toft Pier, which is off the southern channel near Samphrey. The results for spring and neap are given in Figure 3.15.
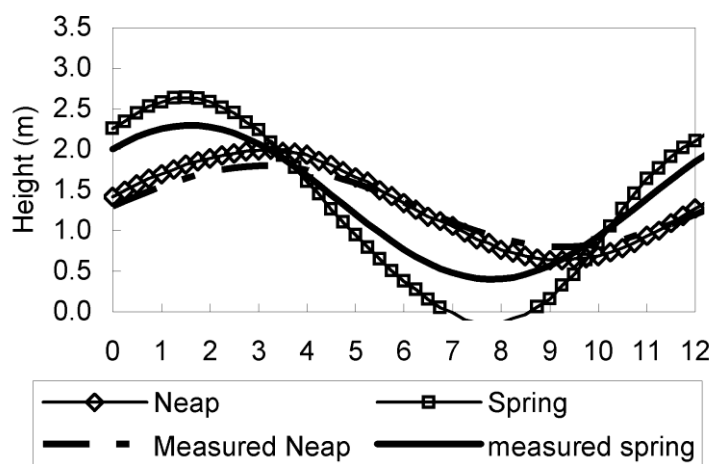
Figure 3.15 Comparison of survey and predicted amplitudes at Toft Pier for mean spring and mean neap tides

The neap tide bears very good agreement between the model and measured results. There is not as good an agreement between the spring tide results. They are considered, however, to be within acceptable limits, given the time averaged nature of the measured values.

These results show comparison of the model results with two tidal diamonds located at 60 29.47' N, 1 12.22' W (Diamond F on Chart 3298) and 60 29.87' N, 1 10.12' W (Diamond J on Chart 3298) as shown in Figure 3.16.
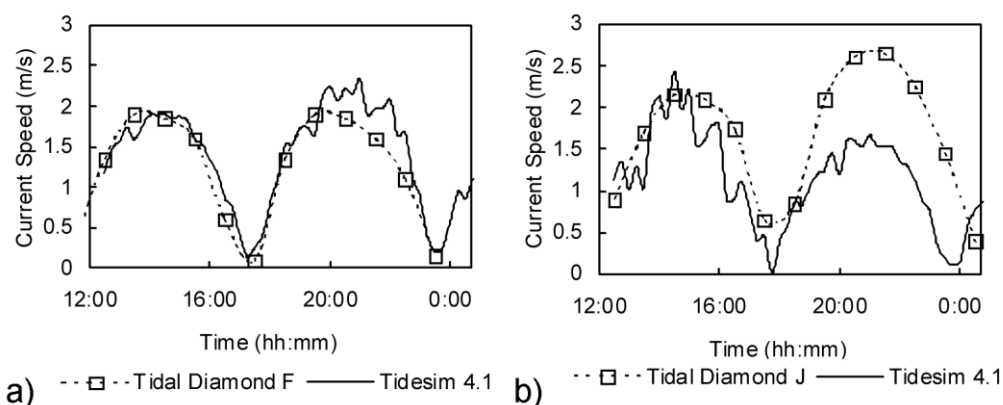
Figure 3.16 Comparison of survey and predicted current speed at tidal diamond F (a) and J (b) at mean spring tide
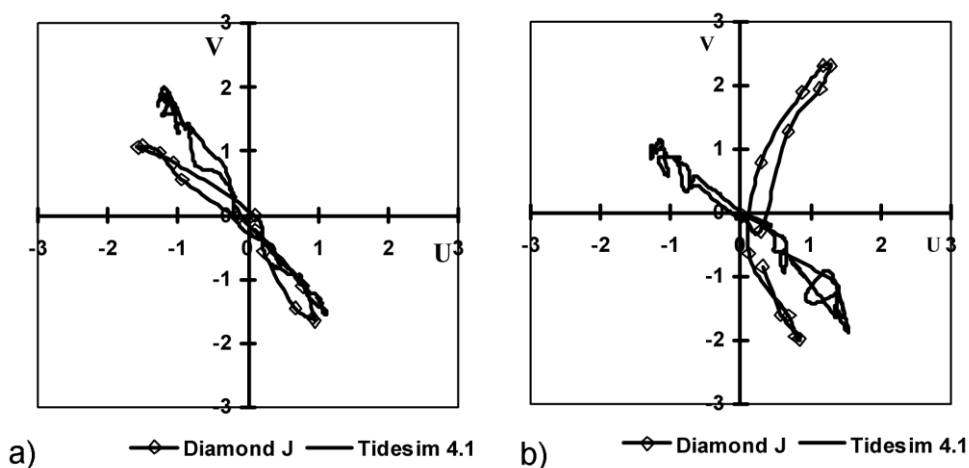
Figure 3.17 Comparison of survey and predicted tidal ellipses at tidal diamonds F (a) and J (b) at mean spring tide.

Figure 3.16(a) and Figure 3.17(a) show the comparison between simulated and chart data at Diamond F during the spring tide. There is acceptable agreement at both measurement points, taking into account the expected differences between averaged and instantaneous data.

The data for the diamond J (Figure 3.16(b) and Figure 3.17(b)) shows good agreement on the flood tide, but does not compare well on the ebb tide where a strong northerly flow is suggested by the survey data heading through the

shallow channel between the islands. The model predicts a weaker current passing through the deeper channel parallel to the coast. Intuitive analysis would suggest that the modelled flow through the deeper channel is more likely and that there is possibly a localised topographical feature causing the measured northerly flow in the diamond survey.

An acceptable comparison can be seen between the measured and modelled current speed time series for the neap tide (Figure 3.18). There is again a disparity in the ebb tide for Diamond J. The probable reasoning is as for the Spring tide analysis above.
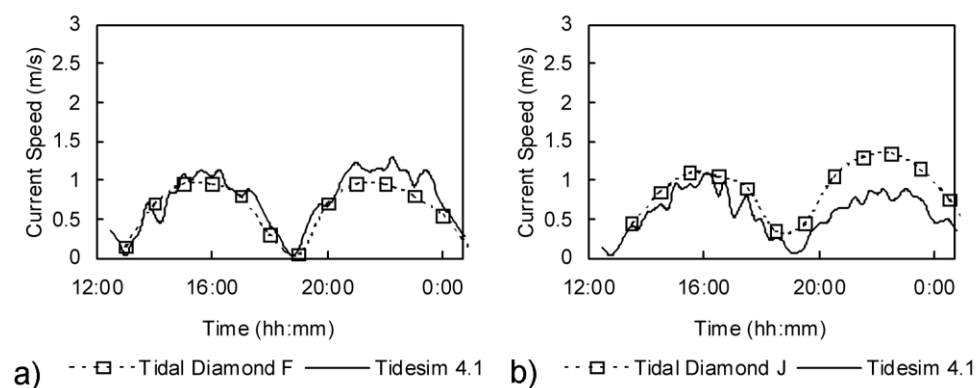
Figure 3.18 Comparison of survey and predicted tidal speed at tidal diamonds F (a) and J (b) at mean neap tide.

3.4.2.d   Observations on the Numerical Modelling

The hydrodynamic model of Yell Sound appears to produce results compatible with pre-existing available survey data. It is, therefore, reasonable to assume that the tidal current predictions elsewhere in the computational domain are a good indication of those in the respective area of Yell Sound. It should, however, be appreciated that the predictions were based on available data and, as such, the data sets produced can only be assumed as accurate as the validation data sources.

The magnitude and direction of tidal currents is of key importance when determining a suitable location for a tidal power device. The Stingray system

produced for the demonstration project responds to currents from one direction only as it has an asymmetric hydrofoil and does not rotate to face the prevailing tide. The hydrofoil is positioned near the seabed during the reverse tide so as to minimise drag. However, commercial systems will be designed to yaw or otherwise reverse the hydroplanes so as to act on both tides.

Predicted tidal vectors can be seen in Figure 3.19 and Figure 3.20. A strong bi-directional reciprocating current is indicated in the narrows either side of the islands of Samphrey and Bigga. At either end of the narrows, a unidirectional 'jetting' effect can be seen, i.e. on the ebb tide there is a significantly greater tidal current speed to the north of the narrows.

0.0 0.5 1.0 1.5 2.0 2.5 (m/s)
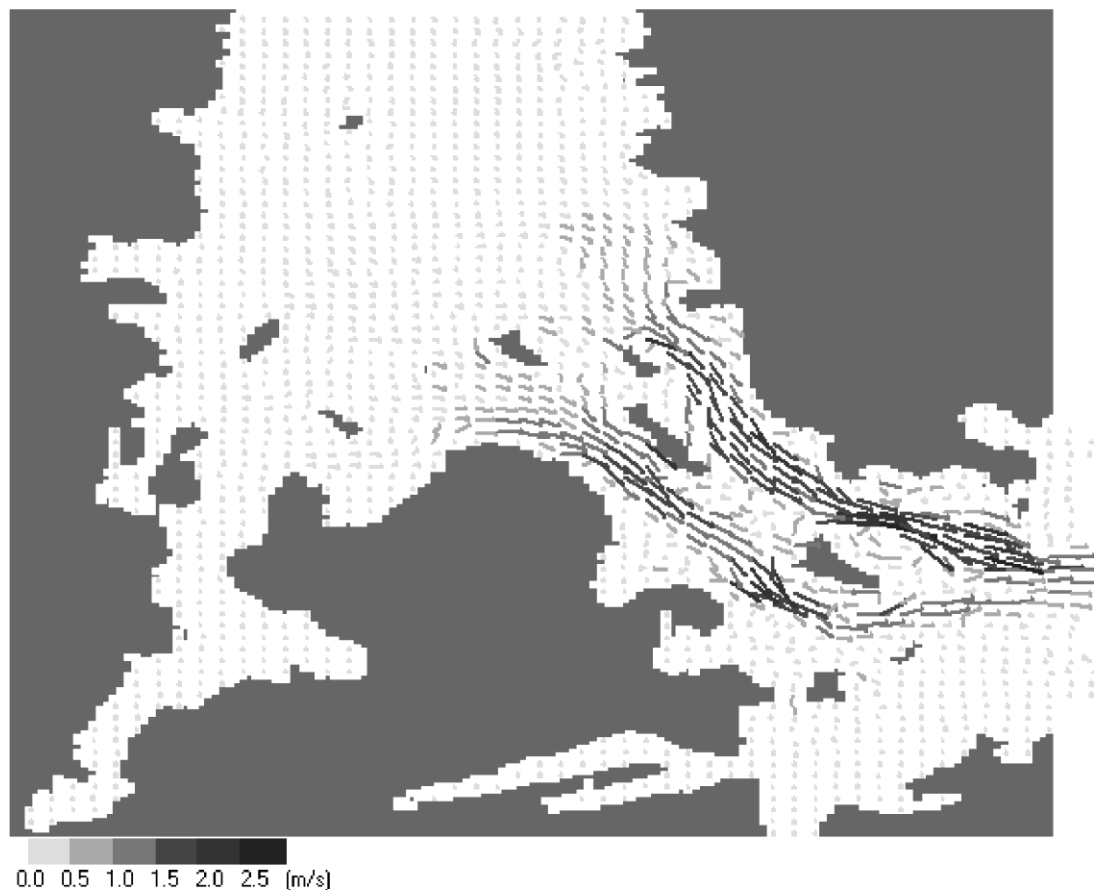
Figure 3.19 Predicted tidal vectors during the flood tide at Yell Sound
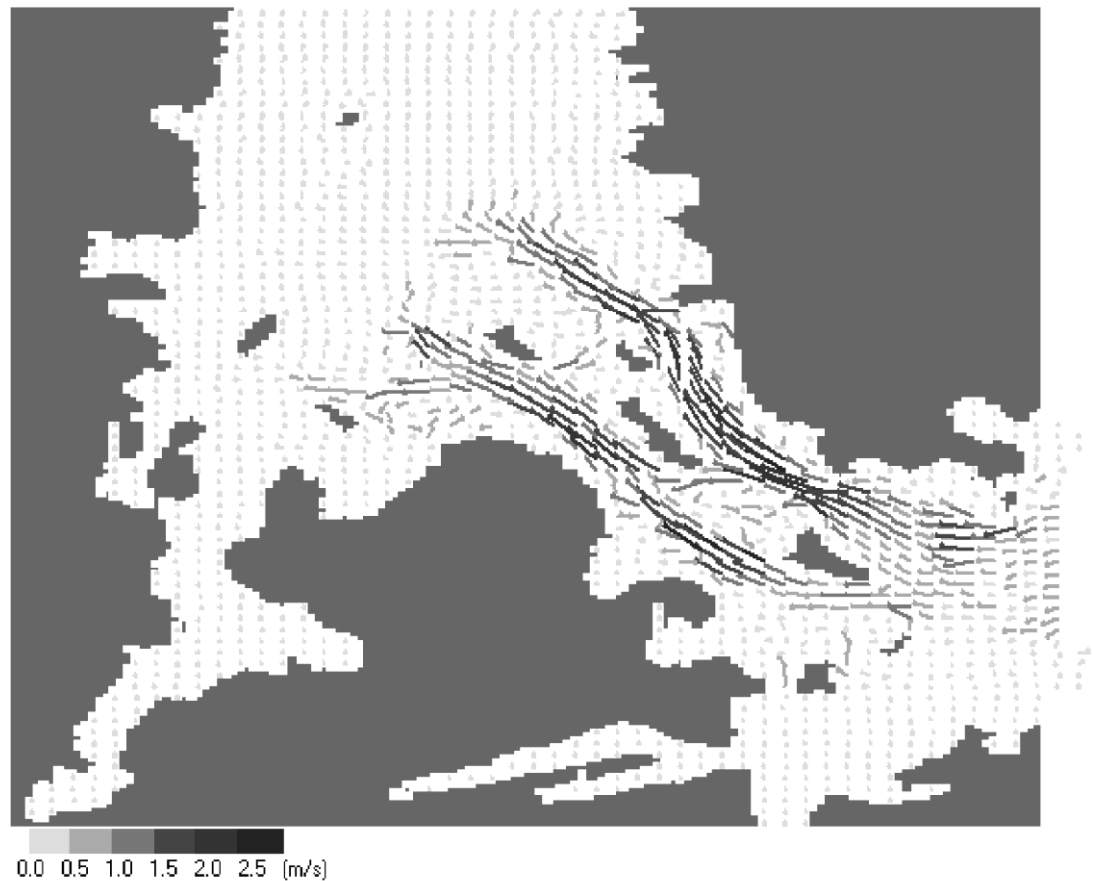
Figure 3.20 Predicted tidal vectors during the ebb tide

As might be anticipated, the fastest currents are in the narrows around the island of Samphrey and Bigga (Figure 3.21). At spring tide, maximum currents are predicted in the range of 2.5m/s to 3.0m/s. During the neap tide in these energetic zones, the current is greater than 1.0m/s for most of the tidal cycle. These current characteristics make the regions well suited for tidal power generation. The model predicts four distinct energetic areas - two either side of Bigga and another two either side of Samphrey.

0.0 0.5 1.0 1.5 2.0 2.5 (m/s)
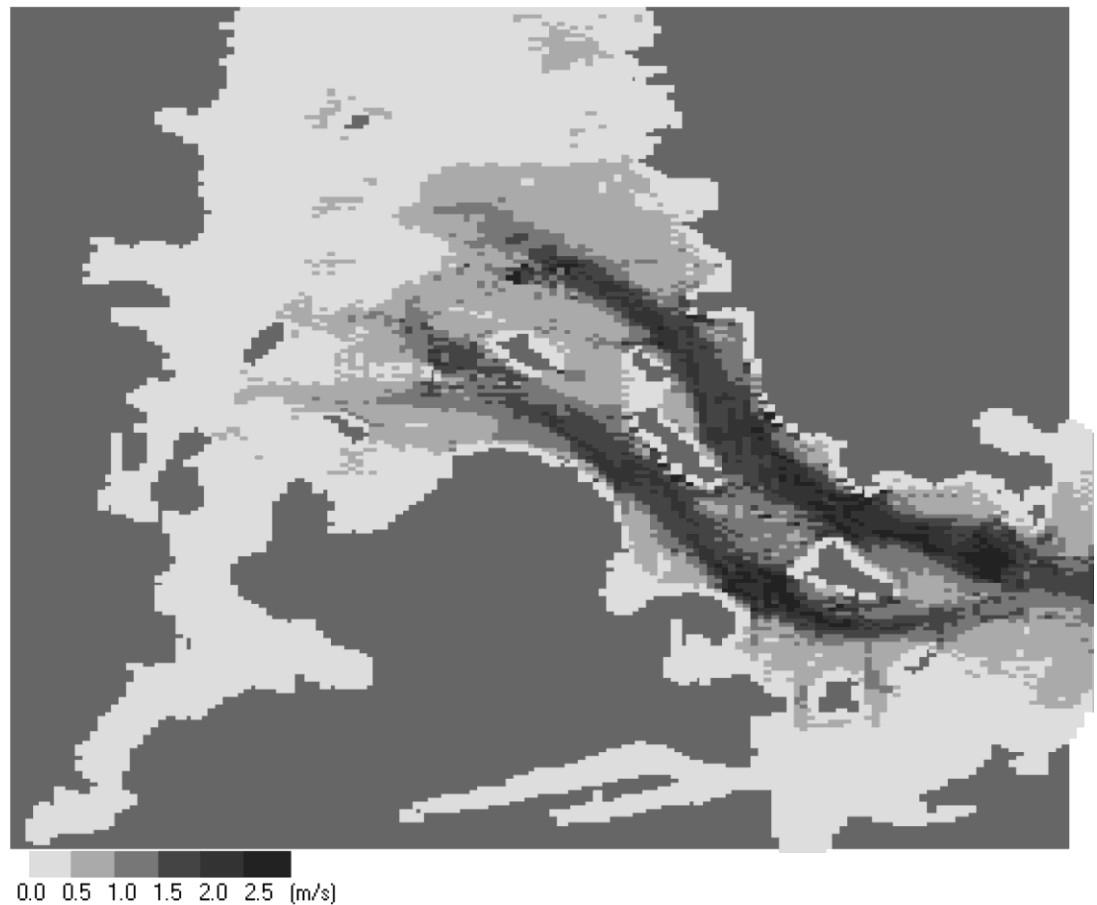
Figure 3.21 Predicted maximum current speeds during the mean spring tide

Current speed is not, however, the only factor that needs to be taken into consideration when selecting a suitable site for a tidal current energy generator (Bryden, INaik, Fraenkel et al., 1998). The technology used on the Stingray prototype device allows for placement in 25 to 35 metres of water. There are other limitations based on shipping lanes, pipelines, subsea cables, other sea users and environmental constraints.

Figure 3.22 and Figure 3.23 show the predicted maximum tidal current speeds where the depth is between 25 m and 35 m. It can be seen that the area on the western coast of Bigga is the largest zone of high-energy currents under these depth criteria. However, like the area on the western coast of Samphrey,

this area is in the south shipping lane approach to Sullom Voe, which is home to a large petroleum terminal. Thus, these two areas are unsuitable due to the possible hazard to shipping safety.
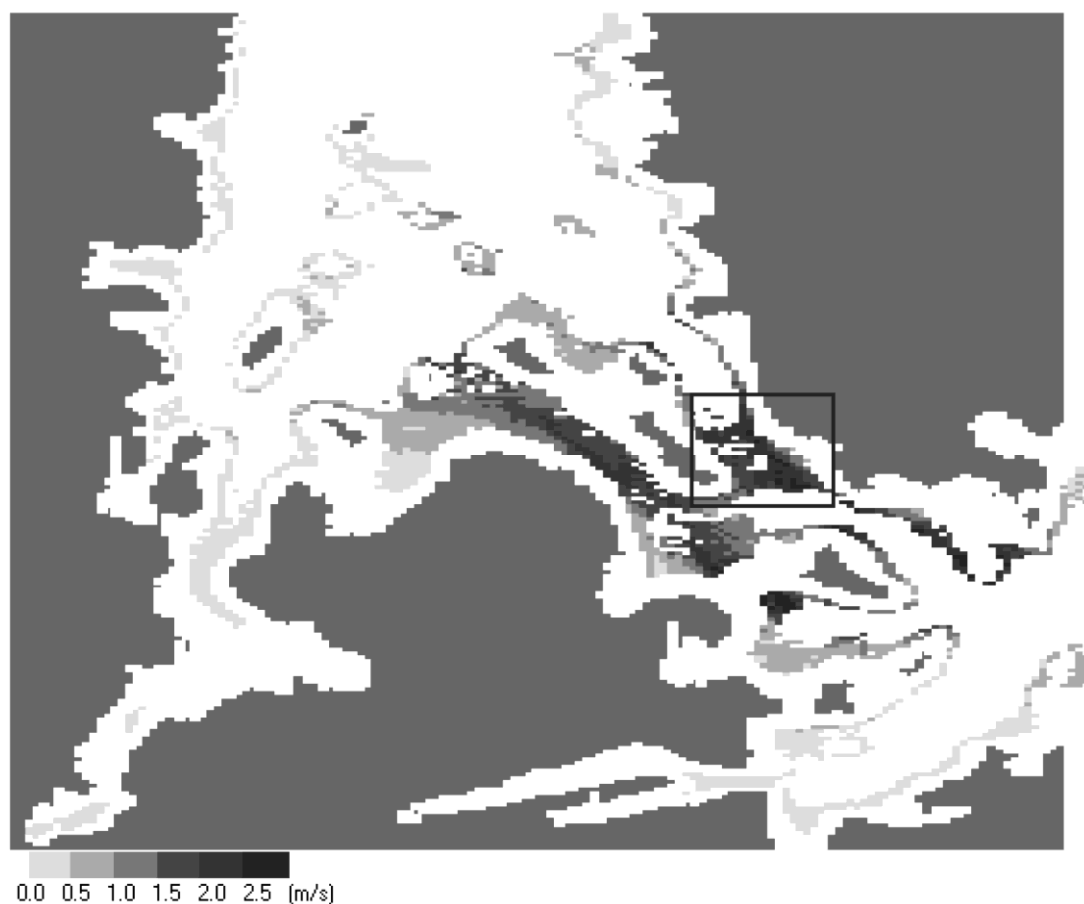
Figure 3.22 The maximum mean current speed at depths between 25 m and 35 m with the most favourable area for tidal power indicated.

The two most suitable areas have been marked. The most appropriate area (the marked area on Figure 3.22) is located between 60° 29.094' N and 60° 30.3762' N and 1° 9.06498' W and 1° 11.0439' W. It is considered most suitable as it contains a larger area of energetic flow. Within this area, the predicted peak spring current is approximately 2.7m/s.
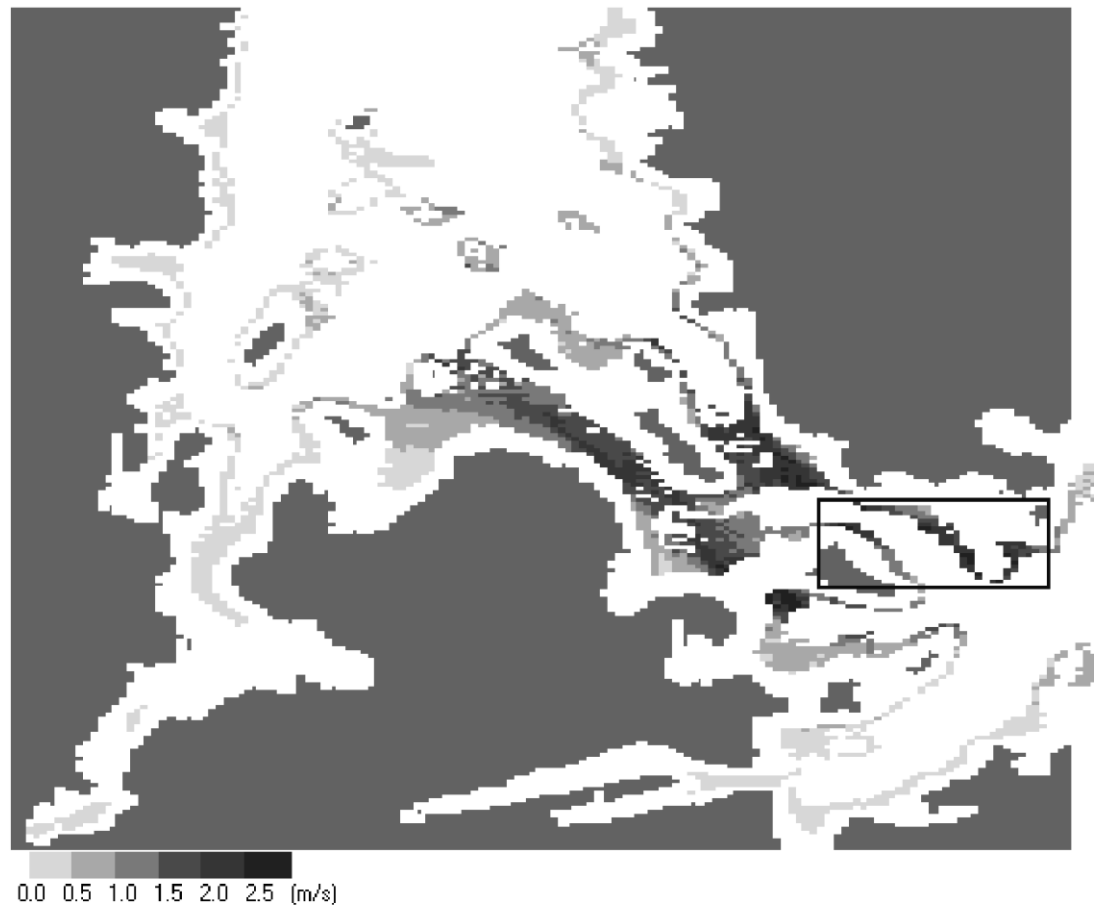
Figure 3.23 The maximum mean current speed at depths between 25 m and 35 m with the second most favourable area for tidal power indicated.

The Yell study permitted a further validation of the model via the ADCP current survey.

A comparison between current speed predictions from the numerical model and field measurements taken during the two spring tides experienced during the field study is presented in Figure 3.24. The first six hour period represents the more energetic NW to SE flow and the second six hours represent the SE to NW flow. There is a reasonable match between the predicted and measured data. The model, which based its boundary descriptions on a mean spring tide, under-predicts the first peak of the first spring tide, but is in good agreement with the second spring tide. The model over-predicts both tides for the second peak.

Much of the difference is most likely accounted for by local topographical effects, causing the asymmetrical return tide, the data for which was not available for the region at the time of modelling.

Figure 3.24 Comparison between ADCP and hydrodynamic model for two spring tides

A comparison between current speed predictions from the numerical model and field measurements taken during the two spring tides experienced during the field study is presented in Figure 3.24. The first six hour period represents the more energetic NW to SE flow and the second six hours represent the SE to NW flow. There is a reasonable match between the predicted and measured data. The model, which based its boundary descriptions on a mean spring tide, under-predicts the first peak of the first spring tide, but is in good agreement with the second spring tide. The model over-predicts both tides for the second peak. Much of the difference is most likely accounted for by local topographical effects, causing the asymmetrical return tide, the data for which was not available for the region at the time of modelling.

The model results presented in Figure 3.24, and others, are perhaps not as smooth as might be expected from smooth sinusoidal boundary conditions. These are most probably an indication of in stabilities in the model. The model

does not have 2nd order horizontal stress terms. In handling horizontal shear stress, these can increase numerical dissipation and add stability to the model. However, these instabilities do not greatly affect the results in terms of how the magnitude and direction compare to the measured values. Indeed it could be argued that there is a greater sense of reality in terms of the turbulent variation seen the measured ADCP data.

3.5 Conclusions

These case studies demonstrated the benefits of flow modelling of the Arklow Band and Yell areas. These benefits may be extended in generality to the modelling of other areas for the purposes of tidal energy resource analysis. The models have provided tidal information over a large area where otherwise tidal information is sparse. The tidal diamonds from the chart of Yell Sound (Hall 1971) follow the line of the shipping lane to the oil terminal at Sullom Voe. A tidal current energy development would not be permitted within the shipping lane. However, there is no indication of the flow in the north-easterly channel away from the shipping lane. The model results indicate that the flow in this channel is suitable for a tidal current energy development and the combination of the depth data indicated suitable regions with appropriate depth and current combination. This would not have been possible without hydrodynamic modelling work. However, the case studies also demonstrate the failings of tidal current modelling. The boundary conditions are based on tidal diamonds. These only provide hourly values of near surface currents. There is neither indication of flow variation with depth, nor flow variations between the hourly measurements. In addition, admiralty charts do not describe the seabed topography at a high resolution as the charts are designed for navigational safety. Although other authors have gone to great efforts to produce mathematically accurate tidal models (Couch & Copeland , 2003). This is arguably unnecessary for modelling tides in areas where the boundary conditions and topography are poorly prescribed. The mathematically simple model used in this study performed well against the validation points available on the chart. The UKHO is not the only source of boundary condition data available in the United Kingdom (UK). The Proudman Oceanographic Laboratory (POL) produced a tidal atlas for the UK continental shelf for the Department of

Trade and Industry (DTI), now called Department of Business, Enterprise and Regulatory Reform (DBERR). The atlas was produced for a study on marine energy resources for the UK (DTI 2004). This has tidal current magnitude at nautical mile (1800 m) resolution. This data is available as public source. This data set was available for purchase from POL prior to this report. The resolution of the data set is poor for coastal areas with intricate channels where the majority of the tidal resource lies in the UK (CENEX 1996, Bryden, Delure, DeNat et al., 2002). However, it can provide more detailed far field boundary conditions. The drawback of this data is that the model domain has to be extended into deeper open water where baroclinic variations can exist and the shallow water approximation do not apply.

More detailed bathymetry is also available. In sites such as Yell, tidal current developers perform bathymetric surveys in order to get detailed topography for planning the deployment of their devices. This data may be introduced into models if produced in the correct format. However, it is very often at a different datum and can disagree with the UKHO data in some cases. The disagreement is due to the age or the data on the UKHO surveys and differences in measurement techniques. However, modelling work is largely immaterial once at this stage of the project. From circa 2006, Seazone™ began leasing licenses to use far higher resolution bathymetric survey data. This is good quality depth data from which accurate topological models can be constructed. Especially as many areas, such as Orkney, have been resurveyed more recently – perhaps levered by the need to determine the available tidal energy resource at UK government level. The disadvantage of this data is that it is expensive. A quote gained by the author for data covering the Orkney Islands in early 2007 was in excess of £20,000.

The use of more complex models, such as those of Couch & Copeland (2003) can be judged to be of greater value when such more refined topology is available. However, at this point another issue is encountered – that of timescale. The present developer and government funding strategy are aimed at a two year design to deployment and testing strategy. This two year period is also partly economic, to maintain investor confidence and return on investment. More detailed modelling uses higher computational effort in

topology, grid generation, initial condition definition, running the model and processing the results. The author's experience is that the developers do not have the time, or the expenditure to invest in detailed hydrodynamic modelling. Hydrodynamic modelling is seen by its practitioners as a fast tool to obtain guidance as to where to perform a tidal current survey prior to device installation. However, the author believes that the developers' misgivings are probably justified given the sources of error discussed here. Especially as they envisage the modelling to provide far more detailed accurate flow than can be described by the model. That said the modelling work described in this chapter met its goals in providing data for a proof-of-concept economic optimisation model, in the Arklow case, and narrowing the choices of potential deployment sites in the case of the Yell Sound work.

CHAPTER 4   ENERGY RESOURCE ANALYSIS

4.1 Introduction

Analysis for the purposes of determining the potential of a site for development for tidal current energy generation is a surprisingly complex process. This chapter demonstrates the effects of applying different methods of resource calculation and how this affects the value of the estimate of energy production produced. Aspects of this work have been previously presented by the author (Melville, Couch & Bryden, 2007) and as the authors contribution to commercial report (Black & Veatch Ltd 2005).

Overall Energy Flux

The simplest method of resource analysis is to estimate the gross maximum energy flux. This method uses data on peak tidal flows and a broad estimate of channel topography. The energy flux is calculated from

$$P = \tfrac{1}{2}\rho A U^3 \qquad\qquad\qquad\qquad 4.1$$

where P is the power produced, ρ is the water density, A is the flow area and U is the water flow velocity (Bryden, Naik, Fraenkel et al. 1998).

This method is commonly used as an initial appreciation of the energy available in a site.   It is, however, an over-estimate of the energy available for extraction. Firstly, because it assumes a peak power and does not take into account the variation of tidal flow with time and, secondly, the power calculated assumes complete extraction of the energy. Despite this, it is probably the most common indicator used in tidal current energy resource assessment.

4.2 Energy Flux with Tidal Harmonics

As discussed in greater length in Section 2, tidal currents vary with time. The harmonic nature of the tides renders them extremely predictable and tidal

amplitudes and speeds can be predicted many years in advance. This is the other great advantage of tidal current power over wave and wind energy. It does, however, mean that the average energy flux is significantly less than the maximum flux.

One short-cut method used for energy approximation is using the mean of the mean spring and mean neap tide speeds (National Energy Institute, Triton Consultants). The current speed during a spring-neap tidal cycle where the spring peak is 2.5m/s and the neap peak is 1.25 m/s and can be seen in Figure 4.1. In this case the average velocity would be 1.875 m/s. The resultant energy flux would be 3375 W/m^2.

The mean energy flux is given by:

$$\overline{P} = \tfrac{1}{2}\rho A \int_T \frac{|U|^3}{T}\, dt \tag{4.2}$$

Where T is the total time, which is usually one Spring-Neap cycle, and t is time. Bryden and Melville (2004) propped a discretised simplification of Equation.4.2:

$$\overline{P} = \tfrac{1}{2}\rho A U_{cmc} \tag{4.3}$$

Where U_{cmc} is the cube-root mean cube speed given by Equation 4.4

$$U_{crmc} = \overline{U^3}^{\,\frac{1}{3}} = \sqrt[3]{\sum_T \frac{|U|^3}{T}\,\Delta t} \tag{4.4}$$

Where Δt is time interval between measurements.

The cube-root mean cubed velocity is plotted alongside the transient tidal velocity in Figure 4.1 at a value of 1.487 m/s. The maximum energy flux density for such a site would be 8000 W/m^2 using Equation.4.1 compared to an average power density of 1687 W/m^2 applying Equation.4.3
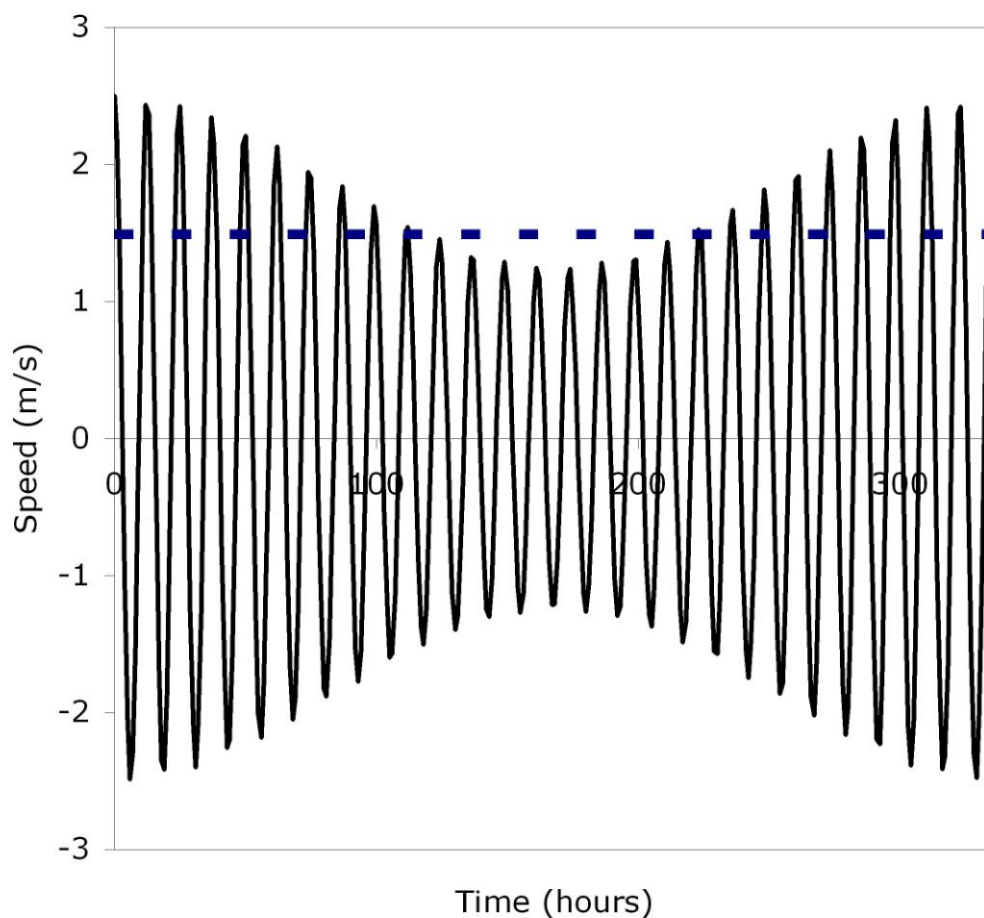
Figure 4.1 Time-series for theoretical spring-neap cycle showing value of cube-root mean cubed velocity

Although using the cube-root mean cubed velocity is perhaps a better approximation of the energy flux in a site, it does not give an indication of the actual energy available to the developer. A refinement could be to consider that the power is taken only from the swept area of the device. Equation.4.3 would become Equation.4.5:

$$\overline{P} = \tfrac{1}{2}\,\rho A_{device} U^3_{crmc}$$

4.5

Where A_{device} is the swept area of the device.

The swept depth range for an initial measure, where no particular device is being considered, would be from 5 m above the seabed to 10 m below the sea surface (to allow surface clearance for shipping and storm surge). If the channel was only 30 m deep to start with, these considerations would have reduced the available energy estimate by approximately 50%, although in deeper water, the effect is obviously less dramatic. The wakes from tidal turbines were numerically analysed in order to optimise the layout of tidal current developments (MacLeod, Barnes & Rados 2001, Melville, Bryden, Rados et al. 2004). The analysis determined that the optimum device spacing, assuming a staggered row arrangement, would be two turbine diameters in the radial direction and 5 diameters in the axial direction. From this, it can be deduced that the energy available across the channel along the radial plane will reduce by another factor of 50%. The power flux using the scenario above reduces to 421 W/m². It is useful to note at this point that the extractable energy from the hypothetical system is 5.26% of the original estimate based on the spring peak current.

4.3 Considerations of Power Curves

Generators are not 100% efficient. Energy is lost in the capture of the fluid flow to mechanical motion, in gearbox mechanisms and in the electrical generator. The level of these energy losses usually varies with the speed of the incident fluid. A device performance or *Cp* curve relates the ratio of the device speed to incident water speed (tip speed ratio) to the power efficiency of the device (Bryden, Naik, Fraenkel et al. 1998, Bryden and Melville 2004, Boyle 2004). The power efficieny, *Cp*, is given by

$$Cp(u) = \frac{P_{device}(u)}{P_{area}(u)} \qquad\qquad 4.6$$

Where $P_{device}(u)$ is the power produced by the device at current speed u and $P_{area}(u)$ is derived from Equation 4.1.

$$P_{area} = \tfrac{1}{2}\, \rho A_{device} U^3 \qquad\qquad 4.7$$

Equation.4.1 becomes Equation.4.8 for a particular water speed.

$$P_{device} = \tfrac{1}{2}\, \mu Cp \rho A_{device} U^3 \qquad\qquad 4.8$$

Where μ is the product of the efficiencies of gearbox, power train and transmission cable. Similarly, Equation.4.3 becomes Equation 4.9 when Cp is assumed to be constant with respect to speed.

$$\overline{P}_{device} = \tfrac{1}{2}\, \rho A U_{cmc} \qquad\qquad 4.9$$

However, the control systems of many devices are set such that they have a cut-in speed under which they do not operate and a rated speed, above which the rated power is produced and there is no further increase in power produced with increased current speed. This upper limit is governed by the torque from the gearbox to the generator. The result of the combination of Equation 4.8 and these control parameters is a power curve relating water speed to output power.

It is possible to take this speed varying Cp into account when using Equation 4.2, producing Equation 4.10.

$$\overline{P} = \tfrac{1}{2}\, \mu \rho A_{device} \sum_{T} \frac{Cp(U)\lvert U\rvert^3}{T}\, \Delta t \qquad\qquad 4.10$$

With $Cp(U)$ being evaluated at each time interval.

The alternative approach is to use the probability density function, $\Phi(U)$.

Where $P(U)$ is given by equation 4.8. Equations 4.10 and 4.5 should produce the same result given the same current speed time series data. When

attempting to match a flow regime to a device, it is less computationally intensive to calculate *Φ*. This method is explored in detail in Chapter 3. The two methods should give the same result given suitable discretisation.

Applying a cut-in speed of 0.75 m/s to the hypothetical case considered here made very little difference to the average power flux (in the order of 1%). This is not because of the low amount of time that the flow is less than 0.75 m/s. Indeed the flow is below 0.75 m/s for 28% of the time. Rather, it is because of the cubic relationship with velocity causing very little power to be produced at velocities less than unity, i.e. sea water flowing at a speed of 0.75 m/s has a power flux of 216 W/m^2, and this is without the consideration of device efficiency as discussed earlier. Some device developers are attracted by the significant opportunities of fast tidal current flows around the UK, in the order of 1 m/s to 1.5 m/s. If a hypothetical moderate energy site is considered having a peak spring current of 1.5 m/s and peak neap current of 0.75 m/s then 37% of the flow is below 0.75 m/s, the maximum power flux is 1728 W/m^2 and the average is 574 W/m^2. The average power flux drops by 3.7% if the cut-in speed is 0.75 m/s. Again, the device efficiencies are not taken into account in this case. A developer considering exploitation of these moderate energy sites would have to maximise efficiency and minimise cut-in speed to make best use of such sites. However, there may be benefits gained from installation in a less harsh environment and the location of sites closer to areas of urban development. The trend in average power flux with spring current speed assuming neap current is half the spring current can be seen in Figure 4.2. The trend is described by the cubic equation:

$$p = 75.388U^3 - 9.1308U^2 + 224.08U$$

4.11

The trend in Equation 4.11 is still cubic in order, but with a significantly decreased cubic coefficient and a large linear contribution. Although the developer of a moderately energetic site loses significantly on the peak currents, the losses are less significant where average energy is concerned.

The chart shows Power flux W/m² (y-axis, 0 to 6000) against spring current speed (x-axis, 0 to 5) with the polynomial trend:

$$y = 75.388x^3 - 9.1308x^2 + 224.08x$$

Legend: Power flux W/m²   polynomial trend
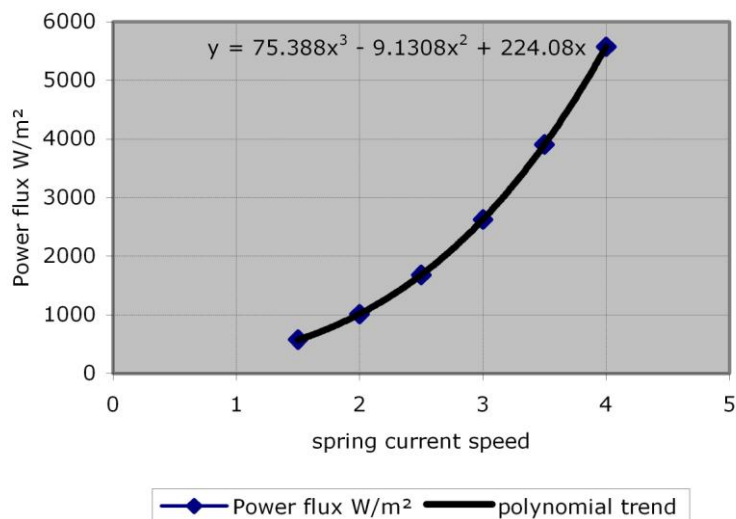
Figure 4.2 Trend in average power flux with spring peak current speed

A common simplification in using this technique is to assume a constant power coefficient during the power varying stage of the power curve. However, power coefficient varies with tip speed ratio (Bryden, Naik, Fraenkel et al. 1998, Piggot 1997). The form of the variation varies with the design of the blade and the efficiency of the pitch control mechanism used to optimise the blade performance. Bryden, Naik, Fraenkel et al. (1998) demonstrated that power output could be optimised to the site flow characteristics by correct selection of the blade power coefficient, rated speed and rated power level. Analogy with wind turbines (EUROS 2007) would indicate that blade design and correct selection of rated rotor speed can be key in the choice of the optimum tip-speed ratio and the on-set of the sub-optimal tip-speed ratio. Other researchers continue to investigate the design of tidal turbine blades, where the effects of the denser and more viscous medium will contribute to blade design and the resultant hydrodynamics.

In practice, the choice of rated speed and rated power is an economic choice in matching the design loads against the small amount of extra energy at current velocities near the maximum spring value. The selection of a rated speed of 2.0 m/s for a device in the hypothetical case discussed above results in a further 13% drop in the average energy produced by the turbine.

This hypothetical case has demonstrated the extent to which resources may be, and have been, over-estimated. From an original estimate of 8 kW/m^2, the available energy has dropped to 156 W/m^2. That is 2% of the original estimate and 9.2% of the unaltered average power flux.

Reductions in available power result from the topology. Without reference to charts, as a quick approximation, the depth is often assumed to be of a rectangular profile. This is not often the case and dramatic reductions can result.

Further reductions in the resource estimate arise from the depth velocity profile in that the commonly quoted tidal currents, such as tidal diamonds or tidal atlases, are near surface currents. As also discussed in Section 2, the velocity profile may be assumed to be of 1/7th power law, but in practice varies from site to site and through the tidal cycle from uniform to other power laws. Indeed, it has become more common amongst energy resource consultants to now use the 1/7th power law to determine the flow at hub height, and use this as the average flow over the swept area of the turbine. In reality the average flow would be as given in Equation 4.12 or Equation 4.13 (Bryden, Naik, Fraenkel et al. 1998) for a horizontal axis turbine.

$$\overline{U} = U_{msx} \int_{-y}^{+y} \left(\frac{y + z_0}{H_{msx}} \right)^{\frac{1}{7}} dy$$

4.12

$$\overline{U} = \frac{U_{msx}}{A} \int_{-r}^{+r} \cos\left[\sin^{-1}\left(\frac{y}{r} \right) \right] \left(\frac{y + z_0}{H_{msx}} \right)^{\frac{1}{7}} dy$$

4.13

Where r is the turbine radius, z_0 is the hub height, and y is the height above the sea-bed.

Integrating the general form in Equation 4.12, the average velocity is obtained as

$$\overline{U} = \frac{7 U_{msx} H_{msx}}{8} \left(\frac{y + z_0}{H_{msx}} \right)^{8/7}$$

4.14

4.4 Extraction limits

Other overestimates of extractable tidal current energy resources stem from the assumption that the area being considered could either be saturated with converters or that the channel was divided into discrete blocks, in the order of 1 km square and that all these blocks could be saturated with devices (Binnhe, Black and Veatch Ltd 2001), sometimes taking into account topology (Dacre & Bullen, 2001). In recent years, extractable limits have come under investigation stimulated by results from the SUPERGEN-Marine consortium. Here is found another application for hydrodynamic modelling in the field of tidal current energy systems.

4.4.1 Method

The method followed is that developed by Bryden (Bryden and Melville, 2004, Bryden, Couch, Owen et al. 2007). The technique may be applied to 1D, 2D, 3D and time-varying models. In this case it was applied to a 1D, steady-state model. The basic flow dynamics are modelled using the open channel flow equations (Equation 4.15).

$$\left(1 - \frac{Q^2}{\rho g A^2} \right) \frac{\partial h}{\partial x} = \left(\frac{-U^2}{gb} \right) \frac{\partial b}{\partial x} - \frac{1}{\rho g A} P_{er} \tau_0$$

4.15

Where Q is the volumetric flow rate; h is the water depth; g is the acceleration due to gravity; P_{er} is the wetted perimeter; A is the cross sectional area; τ_0 is the bed friction shear stress term given in Equation 3.21.

The energy extraction is introduced as an additional drag term (Equation 4.16).

$$\tau_{ex} = \tfrac{1}{2}\rho f \frac{Q^2}{A^2}\frac{R}{\Delta x}$$

<div align="right">4.16</div>

Where f is the fraction of the kinetic flux being extracted; and R is the hydraulic radius given by Equation 3.22 and Δx is the length over which the energy is being extracted.

Equation 4.17, which incorporates the energy extraction, is thus derived from Equation 4.15.

$$\left(1 - \frac{Q^2}{\rho g A^2}\right)\frac{\partial h}{\partial x} = \left(\frac{-U^2}{gb}\right)\frac{\partial b}{\partial x} - \frac{1}{\rho g A}P_{er}\left(\tau_0 + \tau_{ex}\right)$$

<div align="right">4.17</div>

The flow is assumed to be stationary at the inlet boundary. The acceleration of the flow at a distance Δx into the domain can be taken from the Bernoulli energy balance (Chin 2000) is given by equation 4.18

$$\Delta h_{inlet} = \frac{U_1^2}{2g}$$

<div align="right">4.18</div>

This boundary condition relies on the assumption that the channel is at the exit of a stationary body of water such as a sea loch, or that the body of water feeding the channel is large such that the flow in the body is negligible. Thereby, the assumption for the model is that the flow is static head driven.

The water depth is set at the channel outlet boundary. An initial volumetric flow rate is assumed as the starting point of a bi-section iterative method.

4.4.2 Results and Discussion

A range of cases were run as follows

- Channel depths (m): 20, 30, 40, 50

- Height drop along channel (m): 0.001, 0.02, 0.04, 0.06,080, 0.10,0 0.15, 0.20, 0.25, 0.3

- Channel length (m): 4000

- Channel width (m): 1000, 2000, 3000, 4000

4.4.2.a Effect on channel flow

The results of this model with energy extraction levels ranging from 0% to 100% of the raw energy can be seen in Figure 4.3 and Figure 4.4. The change in velocity relative to that at the channel entrance can be seen in Figure 4.5. It can be seen that the energy extraction results in a decrease in the general height gradient either side of the extraction point with a step head change across the area of energy extraction. There is a corresponding reduction in channel current velocity with a rapid acceleration across the point of energy extraction.

It is notable that there is flow in the channel at extraction of 100%. On face value this would seem impossible. However, the raw energy is defined in terms of kinetic energy of the flowing water in the channel. The energy extraction term (Equation 4.17) applies increased shear stress which removes momentum from the system. As commented previously, this extraction of energy causes a hydraulic step to occur at the point of extraction. This step means that there is a build up of potential energy at this point. At 100% of the original kinetic energy extracted, the step is approximately the head difference between the ends of the channel. This potential energy head continues to drive flow down the channel. Such levels of energy extraction are in conflict with the maximum level of extraction proposed by Betz (Boyle 2004) for wind energy. However, wind turbines remove energy from the very bottom of the boundary layer and do not impact on the potential energy of the atmospheric system.
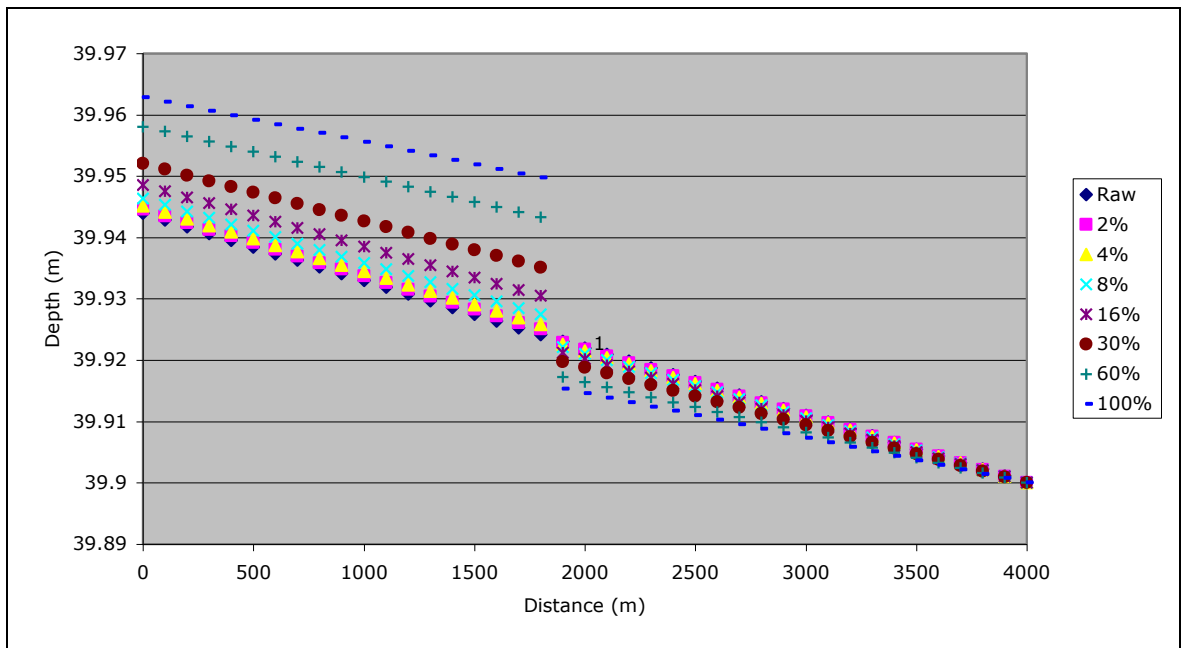
Figure 4.3 Height profiles along the length of a rectangular channel with various levels of energy extraction
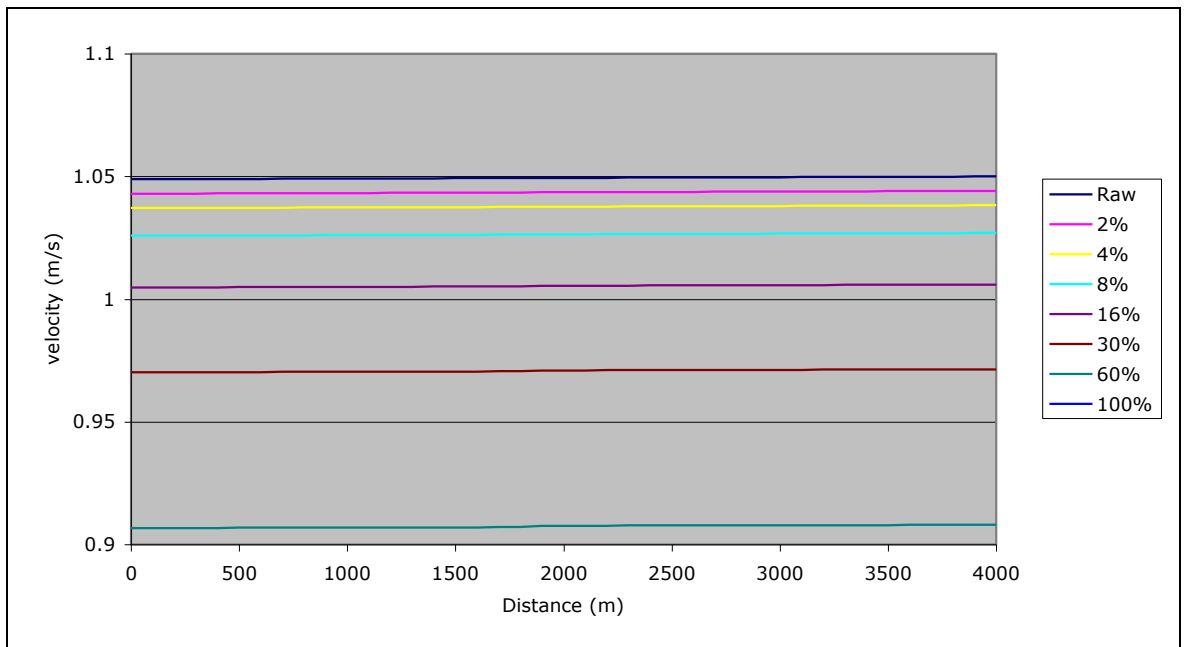
Figure 4.4 Velocity profiles along the length of a rectangular channel with various levels of energy extraction
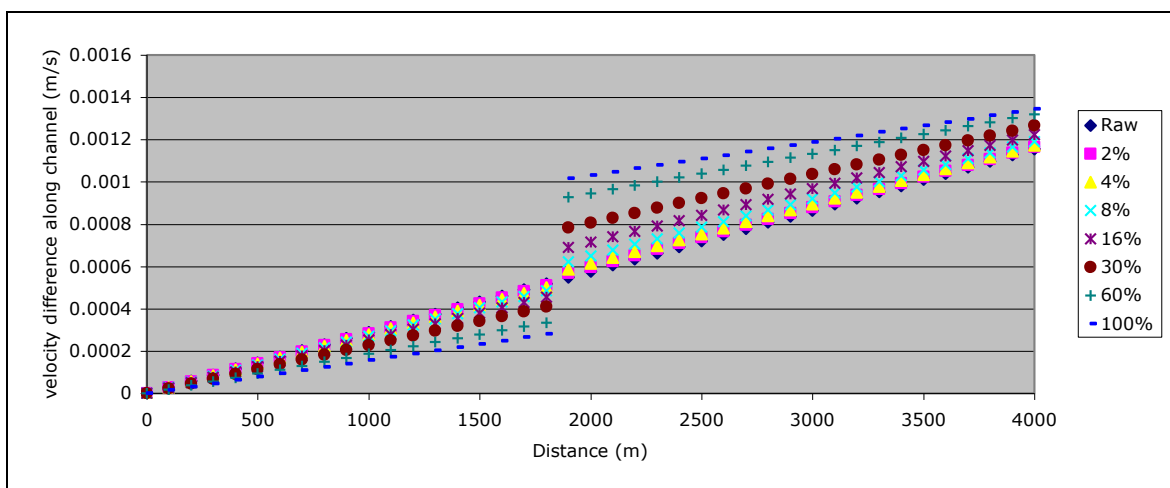
Figure 4.5 Velocity profiles along the length of a rectangular channel with various levels of energy extraction

The relationship between the fraction of raw power extracted, i.e. the total power available in the channel by Equation 4.1, and the fractional velocity deficit can be seen in Figure 4.6.
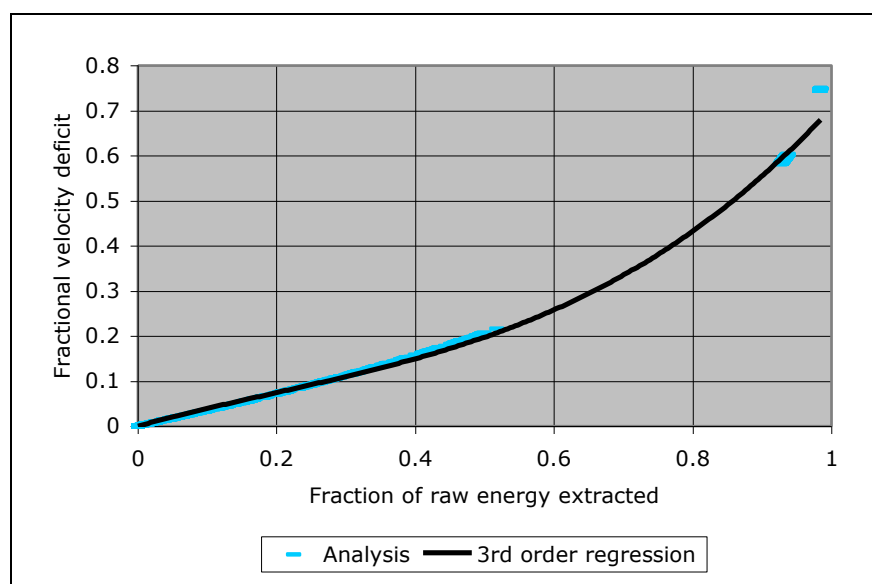
Figure 4.6 Relationship between the fractional velocity deficit and fractional power extracted relative to raw power

This relationship is independent of channel shape and head drop. A cubic regression was carried out on the data of 1.0 based on velocity deficit with values up to 0.6, can also be seen alongside the calculated data. The equation of this cubic correlation is given in Equation 4.19.

$$\frac{\Delta u}{u_r} = C_3 \left(\frac{\Delta P}{P_r}\right)^3 + C_2 \left(\frac{\Delta P}{P_r}\right)^2 + C_1 \left(\frac{\Delta P}{P_r}\right)$$

4.19

Where Δu and ΔP are the differences in velocity and power between the raw value and that after power extraction; and the subscript r signifies the raw value. The regression coefficients C_3, C_2 and C_1 had values of 0.40, -0.08 and 0.36 in this analysis.

The correlation is a good match, if a little conservative, at lower extraction levels, but under-estimates at the high end of extraction. However it is unlikely for developers to consider such high levels of energy extraction.

It has been shown in Section 4.3 that up 11.25% of the raw power can be extracted by a row of 15 m turbines in 30 m water depth at any given current speed given depth restrictions and a power coefficient of 0.45. It can seen from Figure 4.6 that this level of extraction would reult in a 4% decrease in velocity using this model. However, the developer may wish to extract more than this amount of energy. From Figure 4.6, doubling the power extraction level to 22.5% would cause a drop in velocity of 8%. However, the energy would have to be extracted from a larger area as only half this power could be extracted from one row. The model was adapted to extract the energy from a number of consecutive cells in order to see how this affected the relationship between power extracted and velocity deficit. The resultant relationship can be seen in Figure 4.7. This relationship is not greatly different from the single cell extraction and therefore it can be assumed that Equation 4.19 still applies and that it can be utilised more generally for velocity deficit calculations.
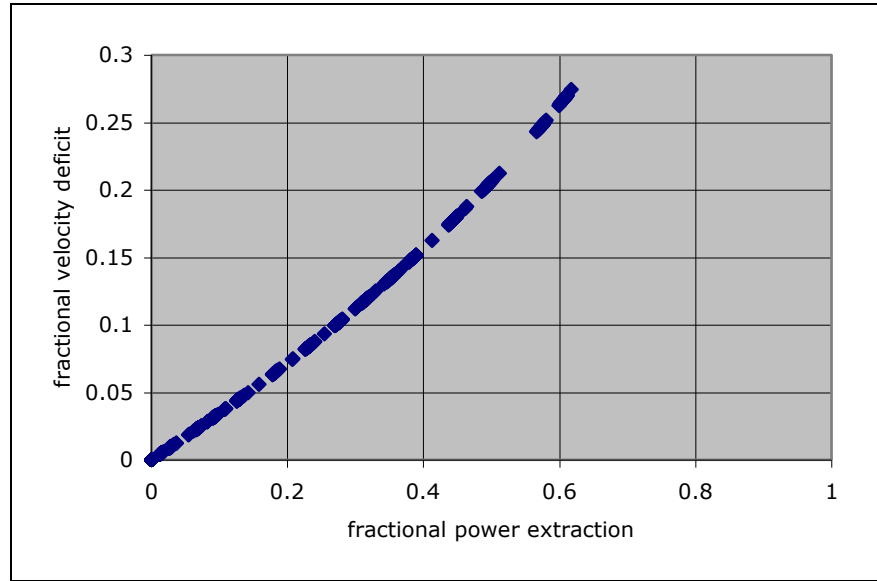
Figure 4.7 Relationship between energy extraction and velocity deficit with extraction of power from two rows

4.4.2.b   Effect on power available

Developing this concept, it should be possible to produce a relationship for average power production based upon Equation 4.19 and Equation 4.10 represented by Equation 4.20.

$$\overline{P} = \tfrac{1}{2}\,\mu\rho A_{array} \sum_{T} \frac{Cp(U)}{T}\left|U_r\left(1 - \left[C_3\left(\frac{\Delta P}{P_r}\right)^3 + C_2\left(\frac{\Delta P}{P_r}\right)^2 + C_1\left(\frac{\Delta P}{P_r}\right)\right]\right)\right|^3 \Delta t \qquad 4.20$$

Where *N* is the number of devices and other variables are as defined in Equations 4.10 and 4.21. The relationship presented in Equation 4.20 appears to give a tidy relationship from which the actual average power after installation can be determined from the intended power extraction level. Importantly, it implies that there is a difference between the expected and actual average energy. Notably, the form of the velocity term means the average power available reduces as the intended power extraction level increases.

4.5 Conclusions

This chapter has examined a number of methods of determining the energy resources available to potential tidal energy developers. It has demonstrated the ways by which resources may be severely over-estimated by the use of calculations that make simplistic assumptions. A one dimension open channel flow model has been used to examine the effects of tidal energy extraction and an equation developed to determine the average power available once energy has been extracted.

The analysis has shown that is possible to over-estimate a resource by 98% from considering the maximum peak flow as compared to a method that takes into account temporal tidal current variation and the power curve for the tidal device, and that this may be even greater once topology is taken into account. In doing so it has been shown that the relationship between spring current velocity and average power is of cubic order, but the cubic coefficient is reduced and lower order terms make a significant contribution. This would tend to suggest that development of lower current velocity sites could be preferable given the penalties involved in design and logistics for more extreme current sites.

The analyses using the 1D model indicate that it is possible to develop simplified correlations relating energy extraction to the true energy resource after extraction. They have also demonstrated that the method by which energy was extracted from only one cell in the domain does hold for extraction of energy over a greater proportion of cells in the domain thereby validating the use of single cell extraction in the analysis. However, the model used may be too simplistic to transfer these correlations to the topologically complex real environment. Further, the boundary conditions employed were for a particular case – that considering flow from a large static body of water with fixed head boundaries, and may not transfer well to other tidal regimes. In addition, the one-dimensional nature of the model does not enable extraction of energy at different levels in the water column or extraction from part of the channel width.

CHAPTER 5   ECONOMIC MODELLING OF TIDAL ENERGY CONVERSION SYSTEMS

5.1   Introduction

This chapter considers the economic modelling of tidal current energy conversion systems. It is based on the work carried out by the author during the Optimisation the Performance (Electrical and Economic) of Tidal Current Turbines funded in part by the European Commission FPII Non-Nuclear programme (Bryden, Delure, DeNat et al., 2001, Melville 2000, Melville 2004, Melville 2004a).   The chapter considers the formulation of the optimisation toolbox and looks at methodologies and results of analysis using the toolbox. The modelling work used in the case study was the model of Arklow Bank produced by the author and considered in Chapter 3.

Economic modelling is important in developing technologies. It is required by developers to demonstrate to investors that the economics of the project being undertaken and seeking investment will prove profitable for all those concerned. In the burgeoning tidal energy industry it is important to demonstrate that tidal energy can produce a reasonable return on investment. This has become even more important in more recent years as there are many more developers coming into the market vying for a limited investment pool and ultimately market share. The economic model developed here went a step further and proposed a method of optimisation whereby the importance of correct device placement within a development area could have a big influence on the return of investment or cost of electricity produced.

5.2   Method

An economic model needs to be robust in order to stand the scrutiny of investors. All aspects of the costs of a development need to be considered. Total costs take account of the capital expenditures and the operational expenditures over the lifetime of the proposed development. The capital expenditure includes the cost of:-

1. the tidal device;

2. the support structures;

3. electrical connection to the shore,;

4. control and monitoring system and

5. the cost of the installation/removal operations.

The operational expenditures include the maintenance cost; the cost of the onshore operating station and the cost of personnel (Bryden, Delure, DeNat et al., 2001, Melville 2004, Melville 2004a). It is necessary to formulate mathematical equations that describe these components to the model. During the OPTCurrenT project, these equations were researched by Thetis SpA (Bryden, Delure, DeNat et al., 2001). However they were implemented in the model by the author.

The tidal energy conversion system considered as a basis for the optimisation model was the Marine Current Turbines' (MCT) Seaflow design (Marine Current Turbines 2005). This design consists of a horizontal axis rotor connected to a gearbox and AC generator contained inside a naecel. The naecel is mounted on a steel pile. The naecel is raised to the surface for maintenance. The pile is installed by drilling into the sea bed with a civil engineering jack-up rig. Cables are laid across the sea bed to a shore based grid connection point. Although this tidal turbine design was used in the model development, the techniques developed could be applied over the broad spectrum of tidal current energy conversion system designs.

5.2.1   Cost model components

5.2.1.a Turbines

Cost estimates were based on the prototype costs experience of the Seaflow project (Marine Current Turbine 2005) and on contemporary wind turbine

technology costs. These were provided to the project by IT Power Ltd and were implemented into the model by the author.

The model contained data on pitch controlled, single or twin rotor, and single rotor stall controlled turbines, with diameters ranging from 10 to 20 m and rated current speeds from 1.6 to 2.8 m/s. The cut-in speed for all designs was taken as 1 m/s. These were taken as hypothetic off-the-shelf designs to minimize computational effort in the optimisation process.

5.2.1.b Support structures

A simplified pile design was implemented into the model. The cost of the structure was considered as the cost of a steel tube, the design of which could withstand the static stresses placed upon it by the current interacting with the turbine. The parameters considered in the design were:

1. Water depth (for length and naecel loading position)

2. Sea bed type (sand, rock, clay or composite)

3. Thrust produced by the turbine was based on the maximum tidal current speed as calculated from Equation 5.1.

$$F_{Thrust} = \frac{1}{2} x C_{Trust} \rho A u_{max}{}^2 \qquad\qquad 5.1$$

where F_{Thrust} is the thrust , C_{Trust} is the trust coefficient; A is the swept area of the TCEC; ρ is the water density and u_{max} is the maximum velocity component normal to the swept area encountered by the TCECS.

These parameters were incorporated into Equations 5.2 to 5.4 (standard civil engineering texts, Thetis SpA, 1999) to determine the dimensions of the supporting pile.

$$\frac{D}{T} \leq 0.18 \frac{C_s E}{C_D \sigma_{lim}} \qquad\qquad 5.2$$

Where D is the pile diameter, T is the wall thickness of the pile, σ_{lim} is the elastic limit stress, C_s is the safety factor defining the maximum allowable stress in the pile, E is the modulus of elasticity, and C_b is the safety factor for buckling.

The embedded length, free length (from the seabed to the axis of the turbine) and the pile diameter are governed by the thrust from the turbine and the soil mechanics of the seabed. For consolidated sediment the following are used:

$$\frac{\sigma_{lim}}{C_s} \geq F_{Thrust} \frac{D\left(L_F + 0.54\left(\frac{F_{Thrust}}{\rho_b DK_p}\right)^{\frac{1}{2}}\right)}{2\pi T\left(\frac{D-T}{2}\right)^3} \qquad 5.3$$

Where ρ_b is the seabed sediment specific weight, K_p is the Rankine passive load coefficient = $\tan^2(45°+\Phi/2)$, Φ is the internal friction angle of the seabed sediment.

$$F_{Thrust} \leq 0.5\rho_b DK_p \frac{L_i}{L_f + \underline{L_i}} \qquad 5.4$$

Where L_I is the approximate imbedded pile length (L_I = 1.2 $\underline{L}_I$)

Similar constraints define the parametric design for piles erected in clay and rock bed types.

The cost function for the pile is defined by

$$PC = UC(LF + LI)\ \rho s\ \pi DT \qquad 5.5$$

Where P_C is the pile cost, U_C is the unit cost per unit weight of steel, L_F is the free standing length of the pile, L_I is the imbedded length of the pile, ρ_s is the steel specific weight, D is the pile diameter, and T is the pile thickness.

The model used Microsoft™(MS) Solver.xla addin in MS Excel to solve for the length, thickness and diameter by minimising Equation 5.5 subject to the

design constraints of Equations 5.2 to 5.4. The scaled-variable option was selected to allow for the large order of magnitude difference between the dimensions.

5.2.1.c Electrical connection to the shore

The electrical cable network linking an array of devices to the shore consisted of a single cable from the shore to distribution unit feeding local connections to termination units at each device.
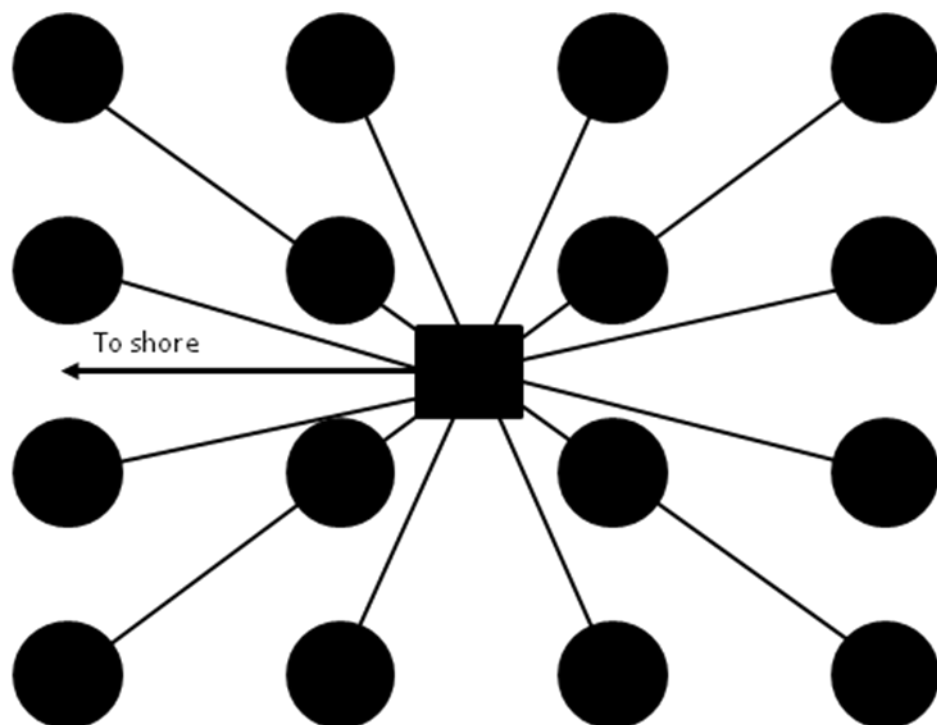
Figure 5.1   Array layout for cable length calculations (not to scale)

The costs of the cables and connectors system consisted of:

1. fixed costs for termination and distribution units;

2. variable cost per metre for each cable within the array and to shore;

3. the surface termination and connection to grid;

The model selected the closest straight line distance from a shore hypothetical grid connection point to an array location within the computational grid as obtained from results provided by the topographical modelling (Section 3). Equation 5.6 describes the cost of connection to the grid of a single turbine.

CC = KC + ACL + TS + TU   5.6

Where K_C is the cost constant for cable manufacture start up, A_C is the cost per metre for the cable, T_S is the surface termination unit cost, and T_U is the underwater termination unit cost.

The length of cable within the grid was based on a centralised star distribution feeding to either in-line or staggered rows of devices. A discrete roots of a quadratic equation as in Equation 5.7 was used to determine the number of devices in each row.

$$Nr = \text{int}\left(-\tfrac{3}{5} + \tfrac{1}{5}\sqrt{5 + 9 \cdot Nt}\right) + 1$$ 5.7

where Nr is the number of rows required for the number of turbines, Nt.

The length of cable for the intra-array connections in a single row or the middle row of an array are given by Equations 5.8 and 5.9 for odd and even number of devices in a row respectively.

$$L_{row} = 2\alpha D\left\lfloor N_m\left(\frac{N_m}{2} + 1\right)\right\rfloor$$ 5.8

$$L_{row} = \alpha D N_m{}^2$$ 5.9

Where L_{row} is the length of the cable in the row, a is the axial spacing factor, D is the diameter of the rotor and N_m is the number of devices in the row. The length of cable required to connect the other rows to the distribution unit is

given by application of Pythagoras' theorem. For example, Equation 5.10 gives the length (excluding the middle row) for an array with an odd number of rows and mills per row.

$$L_{array} = 4D \sum_{j=1}^{\frac{N_m}{2}} \sum_{i=1}^{\frac{N_r}{2}} \sqrt{\alpha j^2 + \beta i^2} \qquad\qquad 5.10$$

Where L_{array} is the length of cable in the array, D is the rotor diameter, N_r is the number of rows, N_m is the number of devices in each row and α and β are the radial and axial spacing of the devices.

For a turbine array, the cost of the cable (C_c) and connection system is given by:

$$CC = KC + AC*L1 + TS + AC*Larray + 2\ Nm\ TU + KSDU \qquad\qquad 5.11$$

Where K_c is the fixed cost, A_C is the cost of cable per unit length, T_S is the cost of the cable termination, N_m is the number of devices in the array, T_U is the cost of array termination units, *KSDU* is the cost of the subsea distribution unit, and L_1 is the length of array to shore cable.

The device spacing was based on that for wind turbine arrays, i.e. two diameters in the radial direction and ten diameters in the axial direction.

5.2.1.a Vessel Requirements

The model considered the costs of a number of specialist vessels involved in the installation, maintenance and decommissioning of a tidal array. These were:

- Cable laying vessel

- Civil engineering jack-up

- Work ship, used in installation and maintenance

- Diving support vessel – diving vessels were included in the model, but given zero cost during the analyses as it was believed that divers could not be used in the tidal regimes in which they would have had to work. However some device developers have used them successfully in prototype installation and maintenance since the model was developed (Hammerfest Strøm 2008)

The costs of each of these included a fixed mobilisation/demobilisation element and variable elements for working and waiting on weather duration as in Equation 5.12.

$$\text{Cost} = (V + DV)(MD + I + WOWD) \qquad\qquad 5.12$$

Where V is the installation vessel cost per day, DV is the support vessel cost per day (if required), MD is the mobilisation/demobilisation days, I is the installation days, and $WOWD$ is the number of waiting on weather days.

The installation time of an array can be described by Equation 5.13.

$$I = \text{nit} (8Nm\ 0.92) \text{ for } Nm \leq 36$$

$$I = 6Nm \text{ for } Nm > 36 \qquad\qquad 5.13$$

Where I is the total number of days for array installation and N_m is the number of devices being installed.

This allows for the speed up in installation with a greater number of devices due to experience. The weather component was taken as a percentage or a minimum fixed value.

5.2.1.b Decommissioning

Decommissioning costs were calculated in a similar manner to installation. In-line with many modern development rules the decommission costs were set

aside at the start of the project to guarantee their availability at the end of the project.

5.2.1.c Annualised capital cost

The total capital cost for the tide array is the sum of these costs. The annual contribution (AC) of the capital cost is given by Equation 5.14.

$$AC = CAPEX \frac{\left(\dfrac{r}{100}\right)}{\left[1 - \left(1 + \dfrac{r}{100}\right)^{-T}\right]}$$

5.14

Where *CAPEX* is the total capital investment, *r* is the discount rate and *T* is the lifetime of the project.

5.2.1.d Maintenance

The model scheduled maintenance to occur on an annual basis with a more prolonged work-over every five years. In both cases the cost of work vessels involved were considered as in Section 5.2.1.a. The annual cost of equipment was taken as a fixed percentage of the device cost (excluding support structure).

5.2.1.e Grid connection

The shore electricity distribution network charges for connection to their grid. A fixed cost was set into the model for this.

5.2.1.f Onshore operations

Costs for operating engineers and technical personnel were included at a variable rate.

5.2.1.g Total annual cost

The total annual cost is then the sum of the annualised capital cost and the annual costs presented in sections 5.2.1.g to 5.2.1.i.

5.2.2 Estimated Power Production

In order to optimise the economic performance of a tidal energy array, or farm, it is necessary to estimate the annual energy production in addition the cost.

IT Power Ltd provided design power curves for the 'off-the-shelf' turbines that the provided costs for in Section 5.2.1. using Equation 4.9 was used to calculate the power generating sector of the velocity range and constant power above the rated speed. An example can be seen in Figure 5.2.
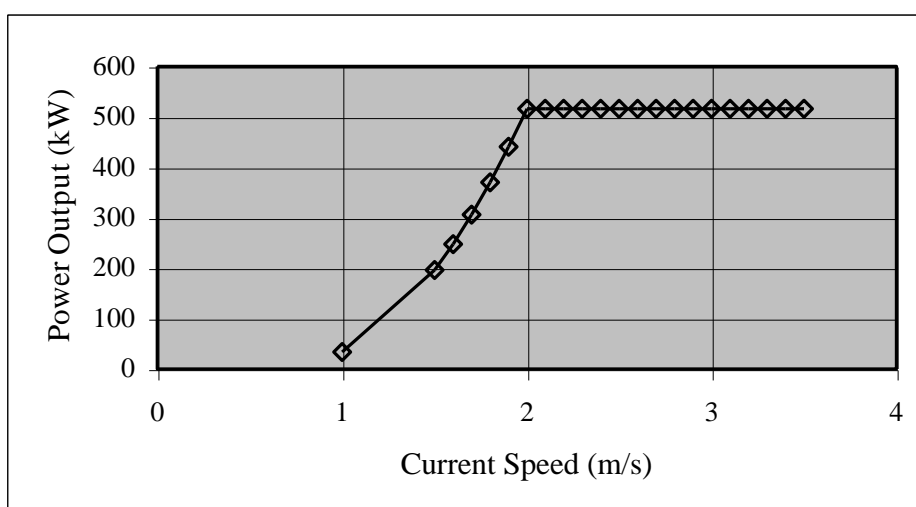
Figure 5.2 Sample power curve for a pitch controlled 20m turbine with a nominal power velocity of 2.0m/s.

These power curves are used in conjunction with the flow velocity to calculate the annual energy at a location with the study domain.   A rigorous hydrodynamic model or the site of interest simulating an entire array lifetime, or even a year, of tidal information is too computationally intensive. Instead, a parametric equation is used to generate tidal velocity components (Equation

5.15). The coefficients A, B and C are derived from the peak currents in both the ebb and flood directions during the mean spring and mean neap tides. It is sufficient to use the mean tides because the production lifetime of an array, at approximately 15 to 20 years, covers the period of the longest tidal harmonic, and is long compared to the periods of the diurnal and semi-diurnal tidal harmonics that cause the majority of tidal flow variation. The merits of such simplified tidal modelling are discussed in Chapter 2.

$$\Phi = A + \left(B + C\cos\left(\frac{2\pi t}{T_1}\right)\right)C\cos\left(\frac{2\pi t}{T_2}\right) \qquad\qquad 5.15$$

Where A, B and C are constants defining the range of the tide, Φ is the horizontal velocity component or tidal amplitude, t is the time, T_1 is the spring-neap tide period, and T_2 is the ebb-flood tide period.

The coefficients are obtained by solving the system of equations in Equation 5.16 to Equation 5.18. These are derived from substituting the appropriate value of the cosine terms in Equation 5.15 for the values at mean spring-flood, mean spring-ebb and mean neap-flood tides.

$\Phi sf = A+B+C$ $\qquad\qquad\qquad\qquad\qquad\qquad\qquad\qquad$ 5.16

$\Phi se = A-B-C$ $\qquad\qquad\qquad\qquad\qquad\qquad\qquad\qquad$ 5.17

$\Phi nf = A+B-C$ $\qquad\qquad\qquad\qquad\qquad\qquad\qquad\qquad$ 5.18

Where Φ_{sf}, Φ_{se} and Φ_{nf} are the horizontal velocity components or tidal amplitude at mean spring-flood, mean spring-ebb and mean neap-flood tides respectively. These flows are calculated using a hydrodynamic model of the site over the mean spring and neap tides.

The energy production for a particular turbine in a particular cell can be estimated by calculating the velocity at intervals through the spring-neap cycle, finding the equivalent power output from the performance curve (Figure 5.2) by linear interpolation.

The cost of energy production in p/kWh, or €/kWh, is estimated by Equation 5.19

CE = total annual cost / annual energy production   5.19

5.2.3 The Optimisation Mechanism

The optimisation model consists primarily of an MS Access™ database and a MS Excel™ with MS Visual Basic™ controlling the sub-programs and providing the graphical user interface (GUI) and FORTRAN 90 dynamic link libraries (dll) performing higher mathematical calculations. The process of data flow can be seen in Figure 5.3.
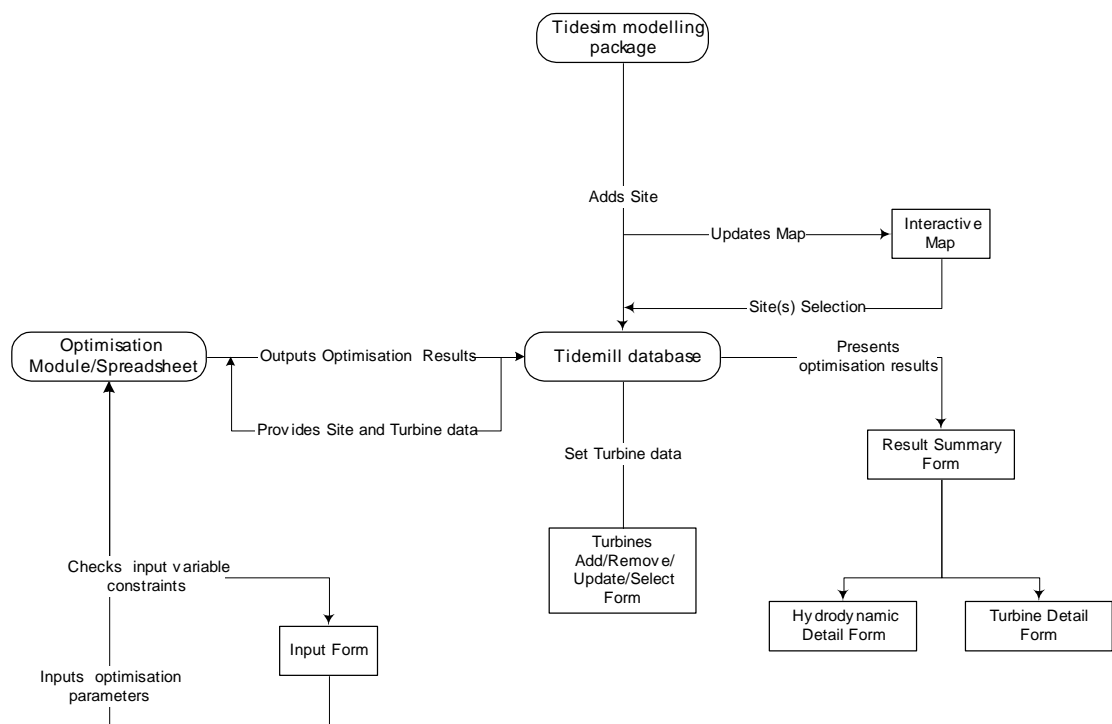
Figure 5.3 Features of the OPTCurrenT application

The database stores all the data regarding the site under development and the results.   The database structure can be seen in Figure 5.4. The database storage allows quick data retrieval for input/ output to the optimisation routines and the results output via AODBC database communication.
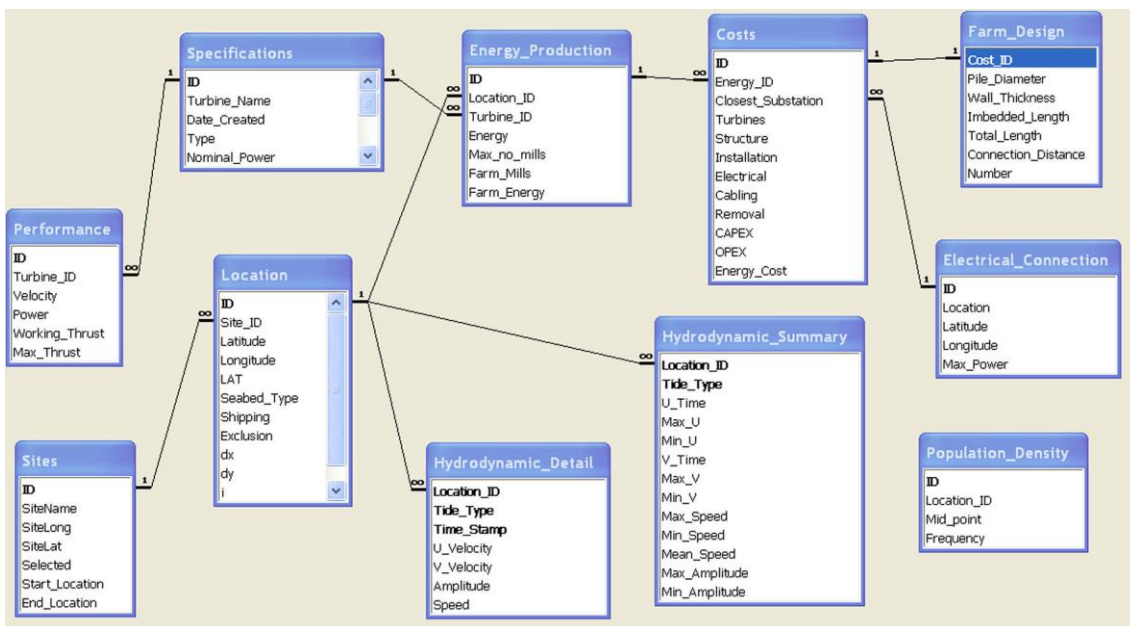
Figure 5.4 The Model database structure

5.2.3.a Spreadsheet

The spreadsheet stores the input values for the economic calculation. A list of these input values as used in the case study can be seen in Appendix B. These values were obtained by Thetis SpA (1999). The input data is of prime importance to an economic model in order to preserve its validity. Some commercial costs are notoriously difficult to obtain for research based projects as commercial organisations want to preserve their competitive edge. However, the inputs used were considered be within the correct order of magnitude at the time of the original study. The spreadsheet calculates the optimum parametric design for the pile support structure as described in Section 5.2.1.b.

5.2.4 Optimisation Procedure

Dimla, Bryden & Rados (2000) discussed the methodology for determining whether a channel or other stretch of water is suitable for tidal current turbines. Factors to be considered include the magnitude of the tidal current, environmental impact, topography, the presence of shipping, and the structure

of the local supply grid. These factors are also important in filtering suitable sites within the chosen area.

The first stage of the actual optimisation process is to filter out the areas of the site that are not suitable for tidal turbine construction or operation. The filtering parameters are depth, current velocity, and other environmental impact considerations.

The turbine requires sufficient clearance from the seabed so as not to be damaged by moving sediments or be affected by the boundary layer. The seabed clearance is given to be 5m. Clearance above the turbine is required to take account of waves, storm surge, shipping and the boundary layer. Thus, the minimum possible depth suitable for tidal turbine operation is 19m, assuming the smallest blade diameter of 5m.

The maximum depth criterion is based on the practicalities of pile construction and is assumed to be 50m. The maximum suitable current is also governed by the practicalities of construction and is determined to be 5m/s. There is also a lower bound velocity criterion. This is somewhat arbitrary and is imposed to ensure the turbine is above its minimum production velocity of 1m/s, for a reasonable proportion of the tidal cycle.

Although a full environmental impact assessment has not been carried out on tidal turbines, it is accepted that they should not be placed in spawning ground or other areas of importance to marine life. Busy shipping lanes should also be avoided.

A database query is used to select all the cells in the study domain that meet these criteria. The cost and energy calculations for each turbine that fits within the valid depth envelope is calculated for these cells only. A database query is then used to select cell-turbine combinations that have a high capacity factor (Equation 4.6), and a low cost of energy.

CF = actual power / rated power   5.20

5.3   Sensitivity Study

A sensitivity study of the optimisation model was performed. This work was reported by the author (Melville, Bryden, Rados et al., 2004; Melville, Bryden, Rados et al. 2004a).   The study used idealised data for locations, varying current speed (both spring and neap), topology, and farm layout.   A range of spring current speeds from 2m/s to 3.5m/s was studied.   This range has been generally accepted as the viable range for tidal current power generation. Neap currents were considered in the range one-third to two-thirds of spring-peak speed. In terms of topology, a depth range of 20 to 35 m is studied. This has the effect of limiting the choice of size of turbine and the amount of energy available for extraction. The assumption is that any one power plant consists wholly of one turbine design. The model used does not feed back the effect of the energy removed from the tidal stream into the hydrodynamic model. That is, the given flow velocity is not affected by the presence of the tidal plant. In reality, this is not the case.

The layout parameters for the tidal farm are taken from the wind energy industry. The distribution of generators per row and number of rows is given by the roots of Equation 5.7. This equation was developed to minimise the loses due to wake effects and to some extent optimises the cable usage on a plant that is not constrained by topology. A range of layouts was considered by varying the coefficients of this equation in order to consider the effect of narrow topology on the economics.

5.3.1.a Results and discussion

5.3.1.b Site depth

The depth of the site has three main influences on tidal current plant development. The energy flux in a site is proportional to the depth. Thus in a deeper channel there is potentially more power available for extraction, given the appropriate technology. However, channel depth can place restrictions on the choice of technology and represents a significant influence on the cost of energy extraction. In order to avoid large shear stress on turbine blades and minimise possible damage from rocks carried along in the current, the turbine

should be mounted clear of the sea-bed. Ideally, this would be as high as possible in the water column, where the fastest current is located. However, there is also a need to avoid damage and stress through wave action, storm surge and shipping. Suitable clearances are taken as 5m from the seabed and 9m from the surface. With these constraints, clearly a device must be placed in water that is a minimum of the diameter plus 14m.
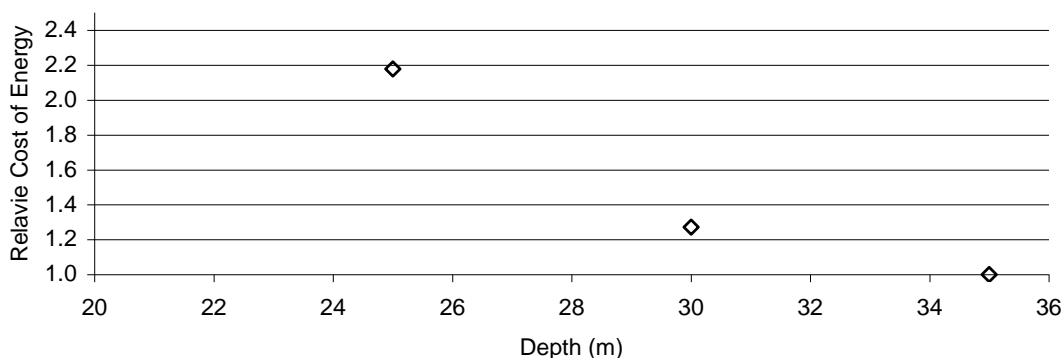
Figure 5.5 Seabed depth against relative cost of energy. Spring current 3m/s, neap current 1.5m/s, nominal 2.0MW plant

Deep water also places a restriction in that jack-up drilling technology, currently being used for pile installation, has a maximum operating depth. The minimum relative cost of energy (RCE) is plotted in Figure 5.5. It can be seen that the RCE decreases with increasing depth. This is primarily because the larger turbines that can be used in the deeper water are more cost effective.

5.3.1.c Farm size

The model was run on a one-kilometre square channel with a square depth profile of 35m. This geometry allows the model unrestricted choice of turbine size and to the number of turbines. A range of installed capacities was considered from 500kW up to 25MW. The results (figure 2) indicate that increasing plant installed capacity increases cost efficiency. As can be seen in Figure 5.6   the cost efficiency increases with installed capacity. This is also true of increasing turbine generation capacity.
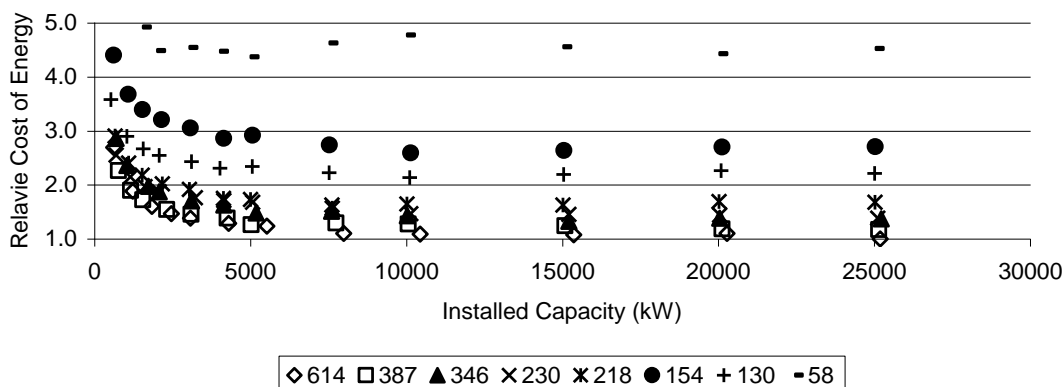
Figure 5.6 Installed capacity against the relative cost of energy for a range of turbine capacities (MW)

Both these results are explained, in part, by economies of scale. There are fixed costs, which do not vary, or vary only slightly, with increased scale of production in the installation of plant and the manufacture of turbines. The capital cost breakdown for a variety of plant capacities can be seen in Figure 5.7. The overall installation costs (installation, cabling, electrical connection etc) reduce as a proportion of the overall capital with increasing plant size, from 65% for a 500kW to 41% for a 25MW (614 kW turbine). There are economies of scale in large farms, though hese do not outweigh those of increasing turbine power capacity. Thus large farms or many small turbines are significantly less cost efficient.

Installation and removal are the most significant of the capital costs, at all plant capacities (Figure 5.7). This is an indication of one of the greatest challenges to tidal power development, that of reducing these costs. Various technical solutions are being considered to deal with this within the industry. For example Owen and Bryden (2005) proposed a lightweight support structure that used down-force produced by hydrofoils to overcome the overturning moment produced by the tidal currents. Reduction of these costs would greatly improve the economics of small-scale plant for local remote power distribution.
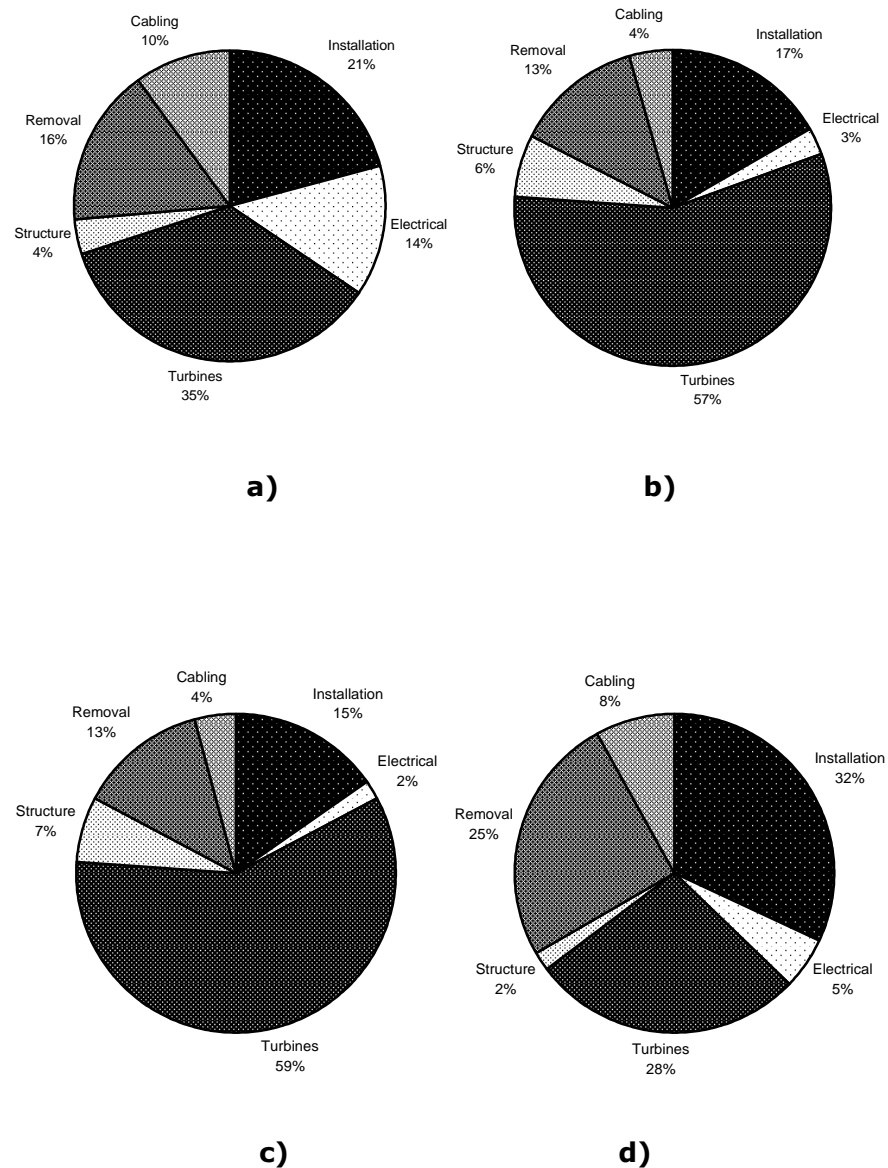
Figure 5.7 Capital cost breakdown for a) 614 kW turbine, 614kW plant; b) 614kW turbine, 7.5MW plant; c) 614kW turbine, 25MW plant and d) 37kW turbine, 10MW plant

5.3.1.d Site energy

The effects of current speed and therefore available energy in a site were examined considering a nominal 7.5MW plant in a depth of 35m over a range of maximum spring currents from 2m/s to 3.75m/s. In each case the neap maximum was half that of the spring maximum. As would be expected there is an increase in cost efficiency with increasing current (Figure 5.8 and Figure 5.9). The variation is not as great as indicated from the theory, in which the

power available varies as the cube of the velocity (Equation 4.1). The cost efficiency would be expected to vary by a factor of 6.6 over this speed range based solely on maximum spring current speed. However it varies by a factor of three when the complete tidal cycle is taken in to account.
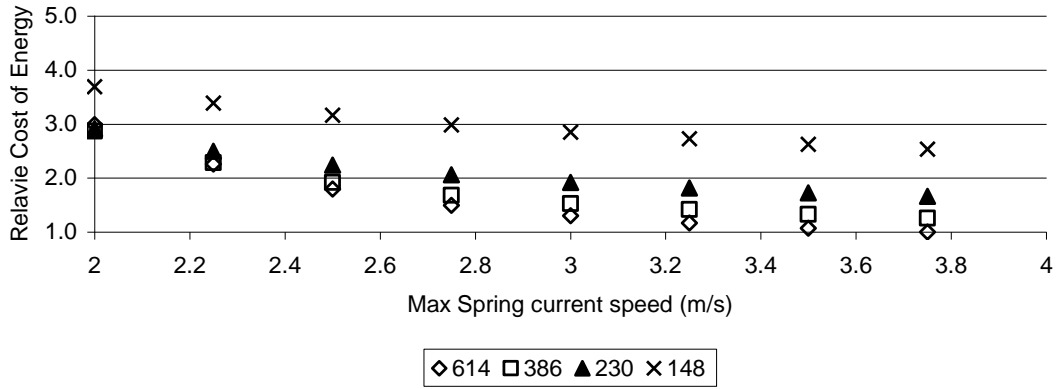
Figure 5.8 Variation of relative cost of energy with spring current speed for a range of turbine capacities (kW)
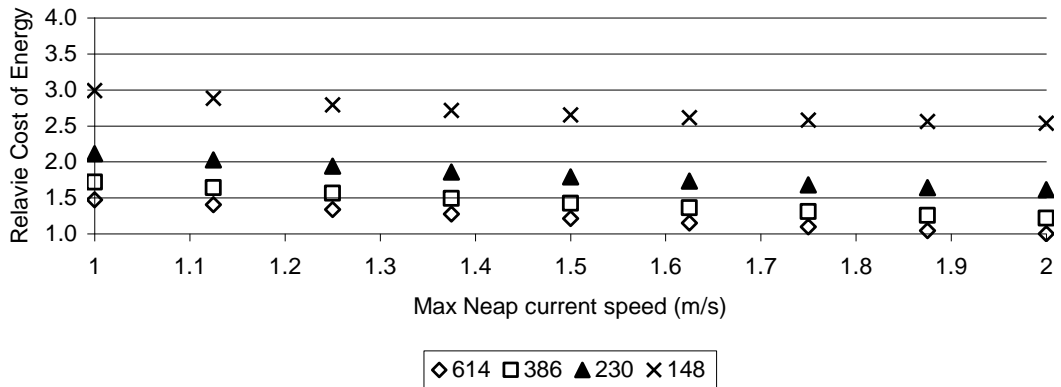
Figure 5.9 Variation of relative cost of energy with neap current speed. 3m/s spring current.

These effects can be assigned to two factors: the harmonic nature of tidal flow, which means that the plant is not producing energy at a constant rate and, probably more significantly, the power curve of the turbines. The sinusoidal current profile means that the overall average power available is less than the

maximum power by approximately 20% to 30% depending on the tidal harmonics. This supports the observations on resource availability reported in Chapter 4.

The cut-in speed for all the turbines is 1m/s. Earlier work by Bryden, Naik, Fraenkel et al. (1998) indicated the importance of matching power curves to efficiency of power output, with the purpose being to maximise the capacity factor (Equation 4.6).

However, when economics is taken into account, it appears more cost efficient to use large generators even at currents well below their rated speed. The variation of the relative cost of energy against capacity factor can be seen in Figure 5.10. There is no clear correlation, as small turbines operating at high capacity are less economic than some larger turbines operating at a lower capacity factor. However there is an optimum level around at approximately 35% of capacity factor if only the lower bound of the results envelope is considered.
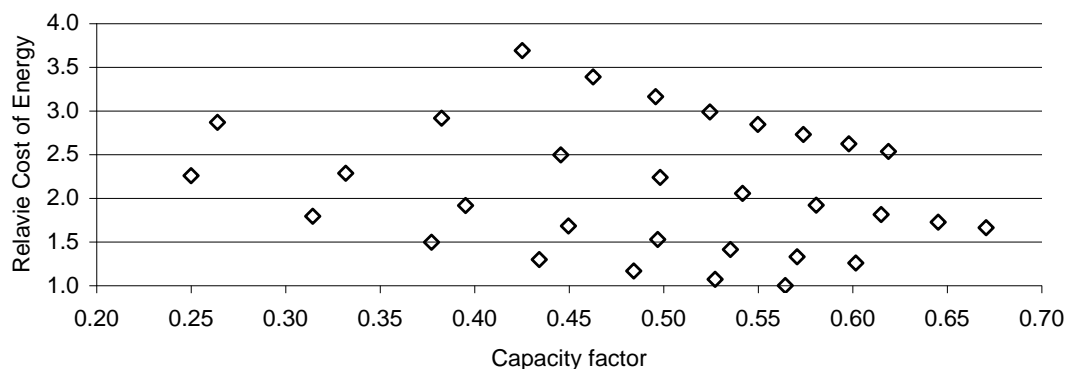
Figure 5.10 Variation of capacity factor for a range of turbines against the relative cost of energy

5.3.2   Other sensitivities

5.3.2.a Cost sensitivity

The analysis presented above considered the sensitivities of the optimisation model to topographical effects. There are other issues that affect cost and the balance of costs. The input cost data is presented in Appendix B. Many of these costs including installation vessel and cable laying vessel costs have a large range of values depending on the market at the time of installation. The effect of such changes in cost could be large on the optimisation process.

5.3.2.a Weather sensitivity

Many of the costs involved in the installation of tidal arrays incorporate an element for waiting on weather. The weather affects the ability of installation vessels to get on site, lay cable and permit divers to dive. Many of the areas proposed for tidal current energy are in remote areas, which are exposed in some degree to extreme weather. The effect of wind acting against strong tidal currents can cause severe sea states in winds which would not otherwise produce such heavy seas. Whilst many tidal areas are in channels that pose an element of protection from many wind directions, others, such as Arklow Bank and the Pentland Firth are far more exposed. A decrease in site availability could have a substantial effect on installation and maintenance costs.

The energy produced is also affected by availability. The model included an assumption for availability in determining the overall annual energy production. However, breakdown during long periods of weather in which maintenance vessels cannot operate could have a significant effect on the energy produced and the cost of energy. However, tidal devices are less prone to such availability issues than other offshore renewable sources. This is because they do not rely on strong wind, i.e. bad weather, to generate power. For wind and wave loss of power production during periods of strong wind has a greater effect on productivity.

The effect of vessel costs and availability has not been investigated here, but would be interesting further work.

5.4   Application to Case Study

The economic optimisation process was carried on the Arklow Bank area, the location of which is described in Chapter 2. The economic model used the inputs as provided in Appendix B and used tidal data produced by the Arklow Bank hydrodynamic model described in Chapter 3. The study case used data in which the peak current wasf 2.5 m/s (5 knots) and the neap peak was approximately 1.25 m/s (2.5 knots). This data set was exaggerated relative to the actual flows for the Arklow area where peak currents are approximately 1.5 to 2.0 m/s. However, such flows are not outside the realms of feasible currents for other areas that may be considered for tidal current energy exploitation.

5.4.1   Results

The available area for the tidal energy development can be seen in Figure 5.11. The result of applying filtering of depth between 20 m and 50 m; spring maximum speed <= 5 m/s; and mean neap speed > 0.5 m/s can be seen in Figure 5.12.
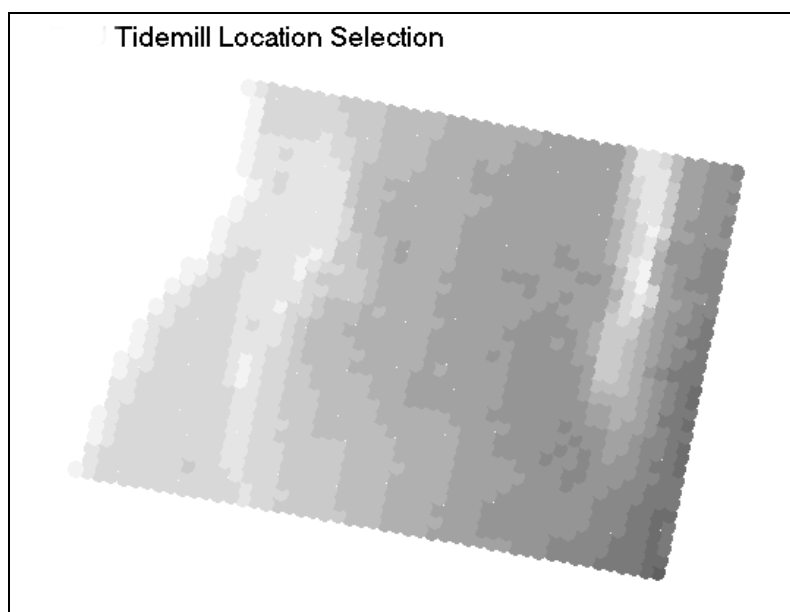
Figure 5.11 Available Area for Device Optimisation
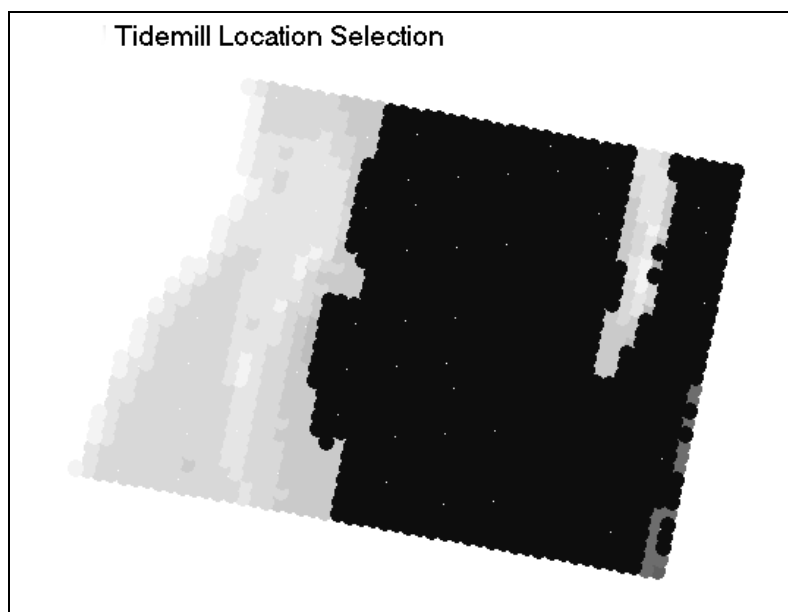
Figure 5.12 Filtered Locations for energetic low regime (Available Locations Shown in Black).

The effect of this filtering is more noticeable if a hypothetical low velocity tidal regime is applied to the area. The results of this can be seen in Figure 5.13.

It can be seen that there remained many possible location and turbine combinations with the highly energetic currents. The optimisation reduced 15864 location-turbine combinations to 9312 combinations which had an energy cost less than 20 p/kWh and a capacity factor of greater than 20%. The capital cost of the arrays ranged from approx. £18.7 million (eleven 10 m diameter turbines) down to £11.25 million (five 20 m diameter turbines) producing 117 kW and 906 kW respectively. Figure 5.14 shows the distribution of mills by energy cost where the energy cost is less than 20 p/kWh. It can be seen from this that the bulk of the location/turbine combinations cost 6 p/kWh.
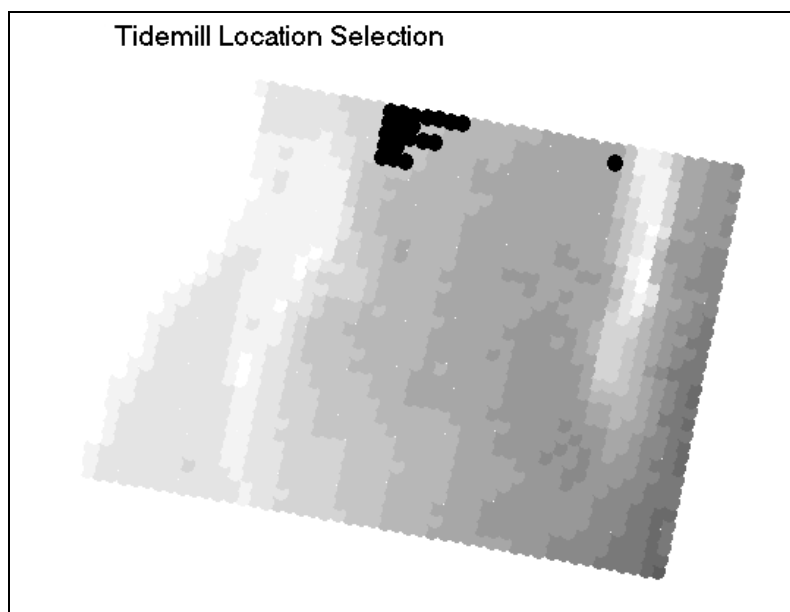
Figure 5.13 Filtered Locations for less energetic flow regime (Available Locations Shown in Black)

The optimal solution was 20m pitch-controlled turbine (5 in the array), that produced 960kW with a capacity factor of 35%. The energy cost for this design was 3.1p/kWh. The CAPEX for the array was £11.25 million.

The lower energy potential of Case B resulted in a reduction of the feasible location/turbine combinations from 15864 to 64.

A series of optimisations were carried out on this data set representing the placement and design of tidal current arrays with capacities of 2.5, 5.0, 7.5 and 10.0 MW.
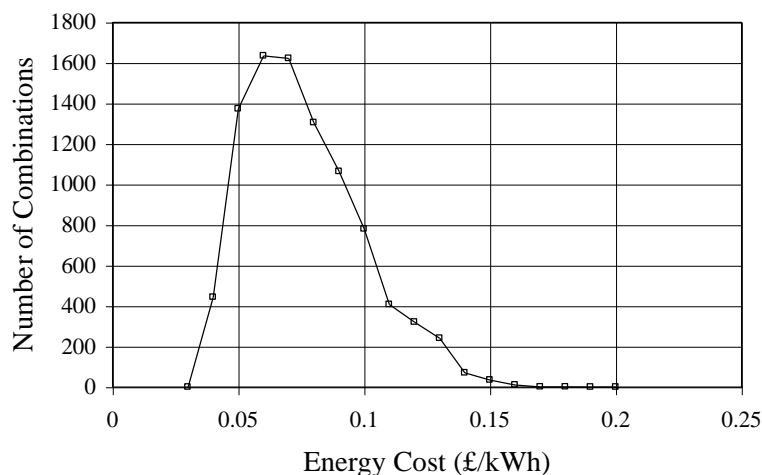
Figure 5.14 Distribution of Location/Turbine Combinations with Respect to Energy Cost(Energy Cost < 20p/kWh, Capacity Factor > 20%).

The optimal result for each plant, in terms of chosen design and location energy produced and the cost of energy produced, are given in Table 5.1.

With the exception of the 12.5MW plant, the same type of turbine has been selected. The optimal solution for the Arklow Bank based on this data is a 10.0MW capacity plant comprising of eleven 20m twin-rotor turbines arranged in two rows. The energy cost from this plant is 6.6 p/kWh (8% discount rate over 20 years). The large rise in energy cost between the 10MW and 12.5MW is explained by a lack of contiguous cells of the right depth and energy. The model selected the smaller turbine, which requires more turbines, but these can fit into a smaller area. However, the smaller turbine produces less power per turbine so the cost of energy increased.

It can be seen that here too that there is an optimal size (by number of devices in the array and energy anticipated production. The cost of energy reduces with increased size up to the 25.2 GWh array and then increases again for the 31.1 GWh farm with 23 devices. The figures are not necessarily important here, as the input cost data has a degree of unreliability as discussed previously. It is the trends that are important. The developer not only has to consider the optimum location in developing a site, but also needs to consider the optimum size of the development.

Table 5.1 Optimal designs for Arklow Bank

Capacity (MW)	Diameter (m)	Rated Speed (m/s)	Number of mills	Annual Energy Production (GWh)	Energy Cost (p/kWh)
1.25	20	2.0	2	4.61	11.0
2.5	20	1.6	6	11.1	9.5
5.0	20	20	6	13.8	7.6
7.5	20	2.0	8	18.4	7.1
10.0	20	2.0	11	25.2	6.6
12.5	15	20	23	31.1	10.2

a) 2.5MW Plant

b) 5.0MW Plant

c) 7.5MW Plant
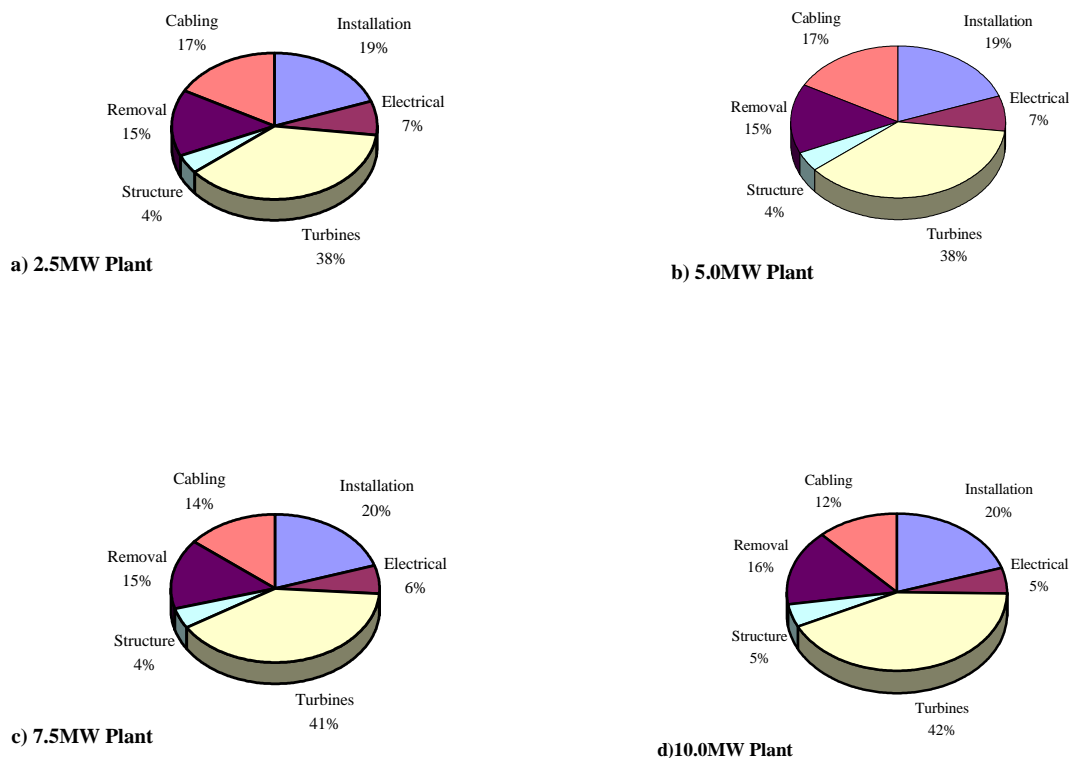
d)10.0MW Plant

Figure 5.15 Breakdown of costs for the optimum selections for 2.5, 5.0, 7.5 and 10.0MW tidal current plant at Arklow

The cost breakdown can be seen in Figure 5.15. Caution should be taken in the analysis these results by the reader. The results were produced from the costs presented in Appendix B. The true costs may be a lot higher. However, these results demonstrate the effect of economy of scale. This is especially applicable when the devices are located long distances from the nearest electrical connection point. For the 5.0MW plant, the cost of connecting to the grid (cable installation and hardware) contributes 24% of the total capital cost. The respective costs for the 7.5MW plant contribute 20%.   All other cost contributions increased. A point here is that the proportion of the cost for the structure is only around 4 to 5 per cent of the total cost. A large part of the effort of this computational model went into the optimisation of the parametric design of the structure. This resulted in a ball park design of the structure. Since an actual detailed design would have to be done, this is of little value to the designers. It would probably have been more efficient to assume a set cost

for the design of approximately 3% of the total cost of the installation and remove this computationally intensive part from the model. However, this result would not have been noticed if it had not been included in the model in the first instance.

The cost of cable laying, installation and decommissioning are all affected by access to site. Many of the intended sites, including those in this study (Chapter 2) have issues of availability due to exposure during bad weather. The equations for installation costs (Equation 5.12) include an element for waiting on weather. A decrease in availability would have an effect on the proportion of costs attributable to installation work. This type of sensitivity analysis was not done during this work, and it would be an interesting follow-on study.
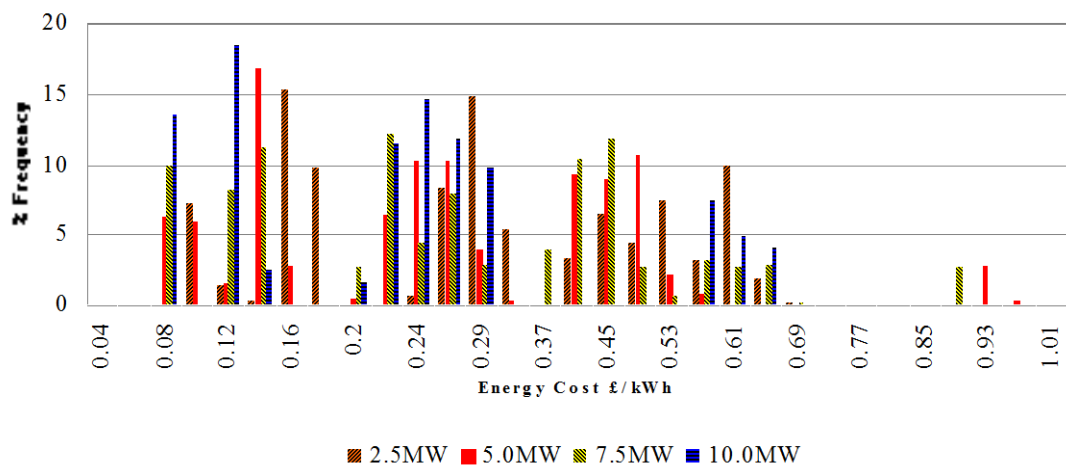
Figure 5.16 Frequency distribution of results for 2.5, 5.0, 7.5 & 10.0 MW Tidal current plants in Arklow
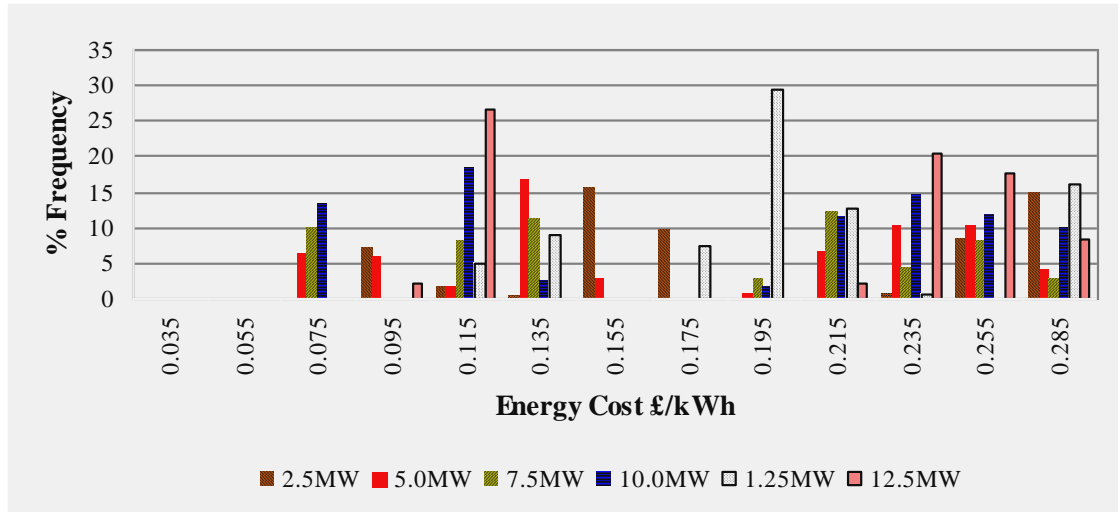
Figure 5.17 Frequency distribution of results for 2.5, 5.0, 7.5 & 10.0 MW Tidal current plants in Arklow (Energy cost <0.3 £/kWh)

The frequency distribution of results with respect to energy cost can be seen in

Figure 5.16 and Figure 5.17. The multi-peak profile that can be seen is caused by the optimisation selecting different types of turbine coupled with the discontinuous nature of their power output. The selections for the 7.5MW and 10.0MW plants can be seen in Figure 5.18.
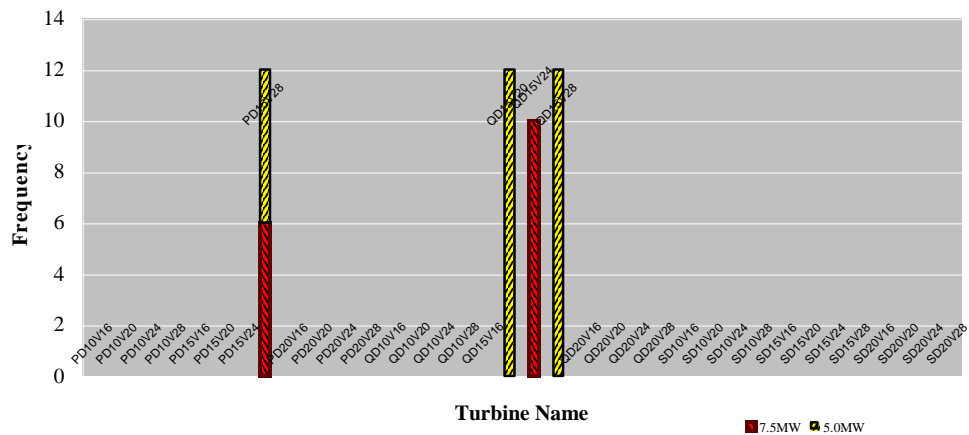
Figure 5.18 Distribution of turbine selection for 5.0MW and 10.0MW tidal current plants at Arklow

Only 16 of the selections fell with in the 20 p/kWh and had a capacity factor of greater than 20%. The optimal solution in this case was a stall controlled 15 m turbine with an energy cost of 10 p/kWh and a capacity factor of 24%. The array contained 7 turbines and produced 220kW. The capital cost for this array was £12.4 million. The modal energy cost for this case was 14 p/kWh. Again the actual cost values are not important here. The significance comes from the variation in costs depending on the choice of turbine, location and size of array and this the cost optimisation has selected a location, type of turbine and the size of the array from this multitude of combinations some of which have a far lower economic efficiency. Such results would not have been realised without the application of the cost optimisation model.

5.5   Conclusions

This chapter has explored the use of an optimised economic model for tidal current turbines. It has set out a mechanism for the process of optimisation and analysed the results with a sensitivity study and case study. The case study demonstrated that the best use of a resource, given the choice of a range of devices with rated speeds from 1.5 m/s to 2.0 m/s, was to use the largest rated power available in all circumstances, and that a long thin tidal array was more cost effective than a wider one with fewer rows. This assumed a 'centrally distributed cable network within the array. It was also demonstrated that a larger number of devices in an array improved the economic efficiency, in terms of cost of unit energy, by bringing economies of scale in the installation process. The model employed a parametric design optimisation process for calculating the size and cost of the supporting pile. It was concluded that this optimisation was unnecessary and computationally expensive and that a fixed size would be a better use of computational resources. However, this would not have been determined without the performing the optimisation process in the first place.

The case study demonstrated the importance of the optimisation process in analysing a site intended for development. It demonstrated that there could be a large cost variation within a site depending on available depth, current and distance from shore. To some extent this was in disagreement with the sensitivity study which determined the largest, most powerful turbine to be the

most economic.   However, the case study brought in an added element of topology and found that an array for smaller turbines could be better placed to exploit a resource due to energy availability and proximity to shore.

Both of the studies demonstrated economics of scale.   However, restricted topology in the case study meant that there was an optimum level of array size. However the case study only employed one cable structure within the farm and only one array layout structure.   Perhaps better economy could have been achieved with a long narrow layout as the sensitivity study found that long narrow arrays were better for the cable distribution employed.

Both studies demonstrated that the installation and decommissioning costs of an area were the most significant part after turbine cost. Cost reduction due to scale of manufacture was not applied to the capital costs of the turbine (rotor, gearbox and generator). These costs could have been reduced for larger arrays. However, it is apparent that the cost of installation with this form of support structure is significant.   These costs would need to be reduced as a necessary process in making tidal current energy more economic.   This could be done by different methods of support. In saying this, the economics of other structural supports has not been carried out and other designs may well have other considerations in terms of cost.

There are some tidal current energy device designers considering devices that can capture energy at less energetic sites in order to avoid the high costs of installation in high energy sites. Exploitation of sites with slower currents would open large areas of the world's coastlines for tidal current energy development. More importantly, areas of coastline near centres of population and industry could be exploited. The author believes that the economic argument presented here does not support the development of such devices.   It has been demonstrated that support structure costs are a minor contribution to overall cost of development. The energy yield from devices with higher rated powers does not yield the cubic relationship as first perceived from a quick look at the power-velocity relationship. However, it is clear from the data that larger devices will be more economic that smaller ones in unrestricted topology. Following the installation costs, the next largest are those of the turbine itself. It is unlikely that large cost savings could be made in this area. The costs used

here were based on the SeaFlow prototype turbine produced by MCT. However, the costs provided by IT Power took into account a degree of mass production as costs would be in a mature industry rather than those of a prototype development.

This examination of tidal current energy conversion economic does not include the effects on current speed due to the extraction of energy. These were discussed in more detail in Section 4. It was observed, using the 1-D open channel model, that the overall channel velocity decreased with the rate of energy extraction, but there was a local acceleration around the area of energy extraction. Indeed, this local acceleration meant that subsequent regions of energy extraction experienced a lesser energy drop than one region extracting the same overall fraction of energy. The question to be asked is what does this mean for the economics of tidal power energy? There are a number of combating effects:

The overall reduction in channel speed would mean less energy available to turbines.

It has been demonstrated that reduction in current speed has a lesser effect on energy production than first expected due to the transient nature of tidal flow and the power curve of the turbine, which extracts less energy than that available once it has reached its rated speed.

The economy of scale may overcome the rate of loss of energy production.

A law of diminishing returns should manifest as the current speed drops off fast at higher rates of energy extraction.

The open channel flow model utilised in the energy extract discussion describes a particular tidal flow regime and other channel types have different responses to tidal energy extraction and therefore effects on its economics.

Unlike wind power the extraction of tidal energy is not limited by that apparently available as kinetic energy as a potential head builds up extending the limit of total energy extraction (Chapter 4).

It is not possible to conclude on the economic effects of large scale tidal developments at this stage and further work is required on the effects of energy extraction and the incorporation of this into tidal models.

Another issue in the consideration of the validity of this economic model is the level of error in the results. There are several sources of error, most of which are difficult to quantify.

Errors arising from the hydrodynamic model from which the current velocity data is taken. Chapter 3 considers this in more detail, however, the main sources are in the boundary conditions and topographical model on which the flow model is based.

The economic model used here applied a further simplification on a pure form of the lunar semi-diurnal tide and the lunar fortnight tide. This differs from the real case, as discussed in Chapter 2.

The design and installation costs can be seen in Appendix B. Many of the costs have a large range of valid cost. Many costs, such as cabling and installation barge costs cannot be easily quantified by research projects due to the lack of information produced by a competitive commercial environment.

CHAPTER 6   CONCLUSIONS AND FURTHER WORK

This work contributes to knowledge in a number of areas:-

1. It is the first published work on survey data analysis prior to deployment of a large-scale prototype tidal current energy conversion system;

2. At the time that the work was carried out, it was the first published work considering the use of the least-squared harmonic method for prediction of energy output from a tidal current energy device;

3. It is the first work to propose a directional power coefficient in the process of resource analysis for a tidal current energy conversion system;

4. The work on economic modelling was the first to produce an optimised economic model for tidal current energy conversion systems (TCECS);

5. It is the first work to use an optimised economic model for TCECSs to demonstrate the effect of device placement on cost of energy produced;

6. It is the first work to use an optimised economic model for TCECSs to demonstrate that the cost of energy for TCECSs is minimised by maximising the rated power, given no topographical impedance;

7. It proposes a method to determine the energy resource available including energy extraction;

Chapter 2 has examined a number of techniques used in the deployment of ADCJPs in extreme current areas and methods of the resultant data analysis in order to obtain statistics that are of use to the tidal energy developer and those involved in researching tidal energy.

It has been noted that the method of deployment in these fast currents has a strong influence on the quality of data recovered. These are summarised below:

The choice of marker buoy and securing arrangement can present a source of anomalous data. The recommended arrangement, concluded by the author,

would be a lead buoy, appropriately positioned at a vector normal to the ADCP unit with sufficient buoyancy and line to remain on the surface during the majority of the tide and a good anchorage weight and chain. An acoustic release marker may be attached to the ADCP frame for security of recovery.

The mounting frame and gimbals are another source of data corruption, as seen in both the Arklow and Yell surveys. The frame should be well weighted to prevent vibration and movement. It is recommended by this author that the gimbals' operation should be locked for operation of ADCP units in extreme currents. The ADCP unit's software can cope with up to 26° of slope on the sea bed terrain and so measurement should not be affected provided that the placement is correct.

After the physical design of the survey placement, the biggest contribution to effective ADCP operation is the sampling and time-averaging period combined with the bin size. A variety of combinations were used on the case studies considered. The Arklow survey used a coarse bin size that led to poor resolution of the vertical depth profile. Simultaneous velocity-depth profiling is one of the major benefits of acoustic measurement. Although it was not strictly required for the future data use in the hydrodynamic model, it is felt that an opportunity was lost not to be able to characterise the velocity profile at a higher resolution at such an early stage in the development of tidal current power. It is accepted that concessions had to be made on the memory available for data storage at the time of this survey, and that temporal resolution was more important. The Yell data was collected at higher temporal and spatial resolution. This gave a good picture of these variations in the tidal flow. It is unfortunate that the data during the fastest tides was corrupted by the sensor movement as discussed previously. The Warness surveys used a variety of spatial and temporal resolutions, though it was not clear as to the reasoning for this. The longer of the surveys at station 7 had higher depth resolution (smaller bin size) and higher temporal resolution (shorter time ensembles) than those of the survey at station 6 that had a shorter overall duration. The result was that the S6 survey produced little constructive information aside form an indication of the peak flows at the time of the survey. The harmonic analysis applied to the Yell and Warness data demonstrates the importance of the survey duration. The 30 day survey period proved more

reliable in generating tidal harmonics with which to predict future tidal currents and energy production. The author was not involved in the prescription of these surveys. It was believed by those performing the surveys that the short term surveys would yield the required information faster given a short time line to installation of the first devices a the tidal test centre.

The author recommends a minimum duration of 30 days with 10 minute time averaging and 1.0 m bins in order to capture the flow field and yield suitable data for planning a tidal energy development. This is easily achievable given the modern advances in data storage memory and reduction in its cost in recent years.

Surveys with a 10 minute ensemble are not suitable for analysing the degree of turbulence in these extreme tidal currents. Variations can be seen in the data that may be associated with turbulence, but the data is time averaged over the ensemble period and many higher frequency variations that could be directly related to turbulence are averaged out. Determining turbulence will be a key contributor to designing devices for longer survivability and longer maintenance intervals. It is recommended by the author that shorter duration / very high resolution surveys should also be undertaken, as carried out at Yell and subsequent to the analysed surveys at Warrness. It is recognised that there is unpublished work by other authors on the turbulence of high velocity tidal flows, but more work will need to be carried out and placed in the public domain if designers are to refine their tidal device designs for lower capital and maintenance costs.

Chapter 2 demonstrated a number of techniques that are of value to the tidal energy developer in assessing the suitability of a site to their design. The tidal rose and tidal ellipse are important in determining the directional nature of the flow. This is important as many designs do not yaw and so are limited to recti-linear flow. It can be seen that the statistical measures of occurrence and exceedence can be used to develop an indication of the raw energy available at a particular site. The author developed the technique for considering only the flow normal to the plane of the device, in effect using a directionally dependant power coefficient (Cp). The driver for this was the Stingray device for which the work was done on Yell Sound. However, this work has demonstrated the

impact of assuming a non-directionally varying *Cp* can have on over-estimating the potential of a site.

The work done here on tidal harmonic prediction demonstrates the importance of carrying out longer term surveys (30 days) in order to perform longer term predictions of velocity probability density and so raw energy potential with the summation of longer period harmonics and conjunction of semi-diurnal harmonics adding to the velocities produced by the basic assumption of semi-diurnal and fortnightly variation. The true importance of the harmonic modelling lies in the ability to predict the time and magnitude of the tide into the future. It is often said that the key benefit of tidal power is its predictability. However, this work has demonstrated that this is not accurate when predictions are based on surveys less that 30 day duration. It is a feature of high energy tidal sites that, in the past, they have been avoided due to navigational safety and thus the tides are not well mapped. This, in itself, sets the requirement for surveys and the need for the surveys, when performed, to produce as much useable data as possible.

The case studies in Chapter 3 demonstrated the benefits of flow modelling of the Arklow Band and Yell areas. These benefits may be extended in generality to the modelling of other areas for the purposes of tidal energy resource analysis. The models have provided tidal information over a large area where otherwise tidal information is sparse. However, the case studies also demonstrate the failings of tidal current modelling. The boundary conditions are based on tidal diamonds. These only provide hourly values of near surface currents. There is neither indication of flow variation with depth, nor flow variations between the hourly measurements. In addition, admiralty charts do not describe the seabed topography at a high resolution as the charts are designed for navigational safety. Other authors have gone to great efforts to produce mathematically accurate tidal models (Couch & Copelands 2003). This is arguably unnecessary for modelling tides in areas where the boundary conditions and topography are poorly prescribed. The mathematically simple model used in this study performed well against the validation points available on the chart. The UKHO is not the only source of boundary condition data available in the United Kingdom. The resolutions of some of these other data sets are poor for coastal areas with intricate channels where the majority of the

tidal resource lies in the UK (CENEX 1996, Bryden 2002). However, it can provide more detailed far field boundary conditions. The draw back of this data is that the model domain has to be extended into deeper open water where baroclinic variations can exist and the shallow water approximation do not apply.

More detailed bathymetry is also available. In sites such as Yell, tidal current developers perform bathymetric surveys in order to get detailed topography for planning the deployment of their devices. This data may be introduced into models. However, modelling work is largely immaterial once at this stage of the project. From circa 2006, Seazone™ began leasing licenses to use far higher resolution bathymetric survey data. This is good quality depth data from which accurate topological models can be constructed. Especially as many areas, such as Orkney, have been resurveyed more recently – perhaps levered by the need to determine the available tidal energy resource at UK government level. The disadvantage of this data is that it is expensive.

The use of more complex models, such as those of Couch (Couch & Copeland 2003) can be judged to be of greater value when such more refined topology is available.

The present developer and government funding strategy are aimed at a two year design to deployment and testing strategy. This two year period is also required to maintain investor confidence and return on investment. More detailed modelling uses higher computational effort in topology, grid generation, initial condition definition, running the model and processing the results. The author's experience is that the developers do not have the time, or the expenditure to invest in detailed hydrodynamic modelling. Hydrodynamic modelling is seen by its practitioners as a fast tool to obtain guidance as to where to perform a tidal current survey prior to device installation. However, the author believes that the developers' misgivings are probably justified given the sources of error discussed here. Especially as they envisage the modelling to provide far more detailed flow than can be described by the model. That said the modelling work described in this chapter met it's goals in providing data for a proof-of-concept economic optimisation model, in the Arklow case, and

narrowing the choices of potential deployment sites in the case of the Yell Sound work.

The use of an optimised economic model for tidal current turbines was explored in Chapter 5. It has set out a mechanism for the process of optimisation and analysed the results with a sensitivity study and case study. The case study demonstrated that the best use of a resource, given the choice of a range of devices with rated speeds from 1.5 m/s to 2.0 m/s, was to use the largest rated power available in all circumstances, and a long thin tidal array was more cost effective than a wider one with fewer rows. This assumed a centrally distributed cable network within the array. It was also demonstrated that a larger number of devices in an array improved the economic efficiency, in terms of cost of unit energy, by bringing economies of scale in the installation process. The model employed a parametric design optimisation process for the calculating the size and cost of the supporting pile. It was concluded that this optimisation was unnecessary and computationally expensive and that a fixed size would be a better use of computational resources

The case study demonstrated the importance of the optimisation process in analysing a site intended for development. It demonstrated that there could be a large cost variation within a site depending on available depth, current and distance from shore. To some extent this was in disagreement with the sensitivity study which determined the largest, most powerful turbine to be the most economic. However, the case study brought in an added element of topology and found that an array for smaller turbines could be better placed to exploit a resource due to energy available and proximity to shore.

Both of the studies demonstrated economics of scale. However, restricted topology in the case study meant that there was an optimum level of array size. However the case study only employed one cable structure within the farm and only one array layout structure. Perhaps better economy could have been achieved with a different layout.

The installation and decommissioning costs were the most significant part after turbine capital cost. It is apparent that the cost of installation with piled support structures is significant and these costs would need to be reduced as a necessary process in making tidal current energy more economic. In saying

this, the economics of other structural supports has not been carried out and other designs may well have other considerations in terms of cost.

There are some tidal current energy device designers considering devices that can capture energy at less energetic sites in order to avoid the high costs of installation in high energy sites. Exploitation of sites with slower currents would open large areas of the world's coastlines for tidal current energy development. More importantly, areas of coastline near centres of population and industry could be exploited. The author believes that the economic argument presented here does not support the development of such devices. It has been demonstrated that support structure costs are a minor contribution to overall cost of development. The energy yield from devices with higher rated powers does not yield the cubic relationship as first perceived from a quick look at the power-velocity relationship. However, it is clear from the data that larger devices will be more economic than smaller ones in unrestricted topology. Following the installation costs, the next largest are those of the turbine itself. It is unlikely that large cost savings could be made in this area. The costs used here were based on the SeaFlow prototype turbine produced by MCT. However, the costs provided by IT Power took into account a degree of mass production as costs would be in a mature industry rather than those of a prototype development.

This examination of tidal current energy conversion economics does not include the effects on current speed due to the extraction of energy. There are a number of combating effects:

1. The overall reduction in channel speed would mean less energy available to turbines.

2. It has been demonstrated that reduction in current speed has a lesser effect on energy production than first expected due to the transient nature of tidal flow and the power curve of the turbine, which extracts less energy than that available once it has reached it's rated speed.

3. The economy of scale may overcome the rate of loss of energy production.

4. A law of diminishing returns should manifest as the current speed drops off fast at higher rates of energy extraction.

The open channel flow model utilised in the energy extract discussion describes a particular tidal flow regime and other channel types have different responses to tidal energy extraction and therefore effects on its economics.

Unlike wind power the extraction of tidal energy is not limited by that apparently available as kinetic energy as a potential head builds up extending the limit of total energy extraction.

It is not possible to conclude on the economic effects of large scale tidal developments at this stage and further work is required on the effects of energy extraction and the incorporation of this into tidal models.

Another issue in the consideration of the validity of this economic model is the level of error in the results. There are several sources of error, most of which are difficult to quantify.

Errors arising from the hydrodynamic model from which the current velocity data is taken. Chapter 3 considers this in more detail, however, the main sources are in the boundary conditions and topographical model on which the flow model is based.

The economic model used here applied a further simplification on a pure form of the lunar semi-diurnal tide and the lunar fortnight tide. This differs from the real case, as discussed in Chapter 2.

Many of the cost inputs have a large range of valid cost. Many costs, such as cabling and installation barge costs cannot be easily quantified by research projects due to the competitive commercial environment.

Overall, computational modelling of tidal current energy conversion systems can have a significant contribution to their design and site development with due regard to the limitations of the modelling technique and the input data provided.

CHAPTER 1   REFERENCES

Bell, C., and Carlin, L., (2003), *"The generation of UK tidal stream atlases from regularly gridded hydrodynamic modelled data"*, http://www.pcmaritime.co.uk/comm/library/ProudmanTidalPaper.pdf, Proudman Oceanographic Laboratory, Liverpool, Accessed date 2005

Black & Veatch Ltd, (2005), Tidal Stream Energy Resource and Technology Review,, Carbon Trust.

Binnhe, Black and Veatch Ltd, (2001), "The Commercial Prospects for Tidal Stream Power", DTI

Bourke, P, (1989), *An Algorithm for Interpolating Irregularly-Spaced Data with Applications in Terrain Modelling*, http://local.wasp.uwa.edu.au/~pbourke/papers/triangulate, presented at Pan Pacific Computer Conference, Beijing, China. Accessed date October 2007

Boyle, G, (2004), *"Renewable Energy Power for a Sustainable Future"*, 2nd Edition, Oxford University Press, Oxford

Bryden, I. G., (1998) personal communication

Bryden, I. G., Naik, S., Fraenkel, P. and Bullen, C. R., (1998), *"Matching Tidal Current Plants to Local Flow Conditions"*, Energy: The International Journal, vol 23, no. 9

Bryden, I. G., (2000) personal communication

Bryden, IG and MacFarlane DM, (2000), The utilisation of short term energy storage with tidal current generation systems, Energy, Vol 25, Issue 9, pp 893-907

Bryden, IG, Delure, Y, DeNat, L, Gravili, D, Holmes, B, Lewis, A, Melville, G and Thake, J, (2001), "*Optimising the performance (electrical and economic) of tidal current turbines*" Contract JOR3CT980205, European Commission, Luxembourg

Bryden, IG and Melville, GT, (2004), "*Choosing and Evaluating Sites for Tidal Current Development*", Proceedings of the IMechE, Part A: Power and Energy, December 2004, Vol 218, No. A8, pp 567 – 578

Bryden, IG, Grinstead, T, and Melville, GT, (2005), "*Assessing the Potential of a Simple Tidal Channel to Deliver Useful Energy*", Applied Ocean Research, Vol 26, Issue 5, July 2004, pp 198-204

Bryden, IG, Couch, SJ, Owen, A, and Melville, G, (2007), "*Tidal current resource assessment*", Proceedings of the Institution of Mechanical Engineers, Part A: Journal of Power and Energy, Vol 221, No. 2 / 2007, pp 125-135, Professional Engineering Publishing.

Chin D. A., (2000), *Water resources engineering*, Prentice Hall, New Jersey, ISBN 0-201-35091-2, p. 146.

Chanson H, (2004), *The Hydraulics of Open Channel Flow*, pp 81-82, Butterworth Heinmann, Oxford, ISBN: 0750659785.

Clarke, JP, (1999), Admiralty Tide Tables Volume 1 2000 United Kingdom and Ireland (including European Channel Ports, United Kingdom Hydrographic Office, Taunton

Commission of the European Community (CEC), (1995), CENIX: — tidal and marine currents energy exploitation (JOU2-CT-93-0355), CEC-DGXVII

Couch, SJ and Copeland, GJM, (2003), *Tidal Straining, Mixing and Lagrangian Flow Residuals Around Headlands*, Journal of Marine Environmental Engineering, vol 7, no. 2, pp 25-45.

Dacre, SL and Bullen, C, (2001), *Pentland Firth Tidal Current Energy Feasability Study – Phase I*, RGU and ICIT, Aberdeen and Orkney (unpublished report).

Davies, AM, and Furnes, GK, (1980), "*Observed and computed M2 tidal currents in the North Sea.*" J. Phys. Oceanogr., vol 10, No. 2, pp 237–257

Dimla, D E Snr, Bryden, I G, Rados, K G, (2000), 'Site Assessment Methodology for Offshore Tidal Current Plants: A Preliminary Investigation', Proc. ISOPE 2000, pp 478-483, Seatle

Doodson, AT and Warburg, HD, (1941), *Admiralty Manual of Tides*, HMSO, London.

Drago, M and Lovenitti, L, (2000), "σ-Coordinates hydrodynamic numerical model for coastal and ocean three-dimensional circulation", Ocean Engineering Vol 27, pp 1065–1085

Eling Tide Mill Trust Ltd, "Eling Tide Mill History", http://www.elingtidemill.wanadoo.co.uk/hist.html, accessed 23 March 2008.

Environmental Systems Research Institute Inc., (1998), *ESRI Shapefile Technical Description An ESRI White Paper*, Environmental Systems Research Institute Inc, New York

EUROS Gmbh, (2007), *On the influence of design tip speed ratio on turbine performance*, www.euros.de/on_the_influence_of_TSR-opt.pdf, accessed: 08 November 2007

Foreman, MGG, (1978 revised 2004), "*Manual for Tidal Currents Analysis and Prediction"*, Institute Of Ocean Sciences, Patricia Bay Sidney, B.C.

Frau, J.P., (1993), "Tidal energy: promising projects: La Rance, a successful industrial-scale experiment", Energy Conversion, IEEE Transaction on, Vol 8, Issue 3, pp 552-558

Langdon, J, (2004), "Mills in the Medieval Economy: England 1300-1540", Oxford University Press, Oxford, pp 78 – 79.

Lewis, T, and Holmes, B, (2000), "Optimising the performance (electrical & economic) of tidal power turbines (OPTCurrenT) Task 3 Final report", European Commission contract JOR-CT98-0205

Youyo Lu, and Lueck, R.G., (1989), *"Using a Broadband ADCP in a Tidal Channel. Part I: Mean Flow and Shear"*, J Atmospheric and Ocean Tech, Vol 16, November 1999, pp 1556 - 1579

Marine Current Turbines Ltd, (2005), "*Development, installation and testing of a large scale tidal current turbine*, DTI contract T/06/0021/00/REP, URN 05/1698, Department of Trade and Industry, London

Hall, GPD, (1971), "Co-tidal and Co-range Lines - British Isles and Adjacent Waters", Tidal series, No. 5058, HMSO, Taunton

Hammerfest Strøm, Technology and Environment, *www.hammerfeststrom.com/content/view/48/78/lang,en/*, Accessed date 13 May 2008

Haslam, DW, (1978), "*Arklow to the Skerries Islands"*, Standard Navigational Chart series, No. 1468, HMSO, Taunton

Haslam, DW, (1978), "*Carnsore Point to Wicklow Head*", Standard Navigational Chart series, No. 1787, HMSO, Taunton

Haslam, DW, (1980), "*Shetland Islands North-East Sheet*", Standard Navigational Chart series, No. 3282, HMSO, Taunton

Haslam, DW, (1981a), "*Orkney Islands - Western Sheet*", Standard Navigational Chart series, No. 2249, HMSO, Taunton

Haslam, DW, (1981a), "*Orkney Islands - Eastern Sheet*", Standard Navigational Chart series, No. 2250, HMSO, Taunton

Haslam, DW, (1983), "*Cape Wrath to Pentland Firth and the Orkney Islands*", Internatonal Chart series, No. 1954, HMSO, Taunton

Howarth, M. J., (1981), "Intercomparison of AMF VACM and Andera current meters moored in fast tidal currents", Deep Sea Research, Vol 28A, No 6, pp 601-607.

Koutitas, C. G., (1988), Mathematical Models in Coastal Engineering, Pentech Press Ltd, London, pp. 49-82

MacLeod, A J, Barnes, S. & Rados, K G, (2001), Wake effects in tidal current turbine farms. Proceedings of the MAREC Conference, Newcastle, September 2002, p. 49–53

Melville, GT, Couch, SJ and Bryden, IG, (2007), *"Hydrodynamic Modelling and Survey Data Analysis for the Fall of Warness, Eday, Orkney"*, project report produced for the European Marine Energy Centre

Melville, GT, Bryden, IG, Rados, KG, and Macleod, AJ, (2004), "*Tidal power resource analysis and the consideration of development economics*", Littoral, 20-22 September, Aberdeen, UK

Melville, GT, Bryden, IG, Rados, KG, and Macleod, AJ, (2004a) "*Tidal power resource analysis and the consideration of resource economics*", Marine Renewable Energy Conference (MAREC), Blythe, UK, IMarEST

Melville GT, Bryden IG and Lomax, CD, (2002), "*Hydrodynamic Modelling of Yell Sound*", Marine Renewable Energy Conference (MAREC), Newcastle-upon-Tyne, UK, IMarEST,

Melville, GT, Rados, KG, and Bryden, IG, (2001), "*A Model to Optimise the Electrical and Economic Performance of Tidal Current Energy Conversion Systems*", Marine Renewable Energy Conference (MAREC), Newcastle-upon-Tyne, UK, IMarEST

Morris, RO, (1986), "*Yell Sound*", Standard Navigational Chart series, No. 3298, HMSO, Taunton

Morris, RO, (1987), "*Approaches to Stretto di Messina*", Standard Navigational Chart series, No. 1018, HMSO, Taunton

Owen, A and Bryden, IG, (2005) *Prototype Support Structure for Seabed Mounted Tidal Current Turbines,* Proceedings of the Institution of Mechanical Engineers, Part M: Journal of Engineering for the Maritime Environment, IMechE, Vol 219, No 4, pp 173-183

Pawlowicz, R, Beardsley, B and Lentz, S, (2002), "*Classical Tidal Harmonic Analysis Including Error Estimates in MATLAB using T_TIDE*", 2002, Computers and Geosciences, 28, pp 929-937.

Piggott, H (1997), Wind Power Workshop, Centre for Alternative Technology Publications, p 13

Press, WH, Teukolsky, SA, Vetterling, WT, Flannery, BP, (1992), *Numerical Recipes in Fortran 77*, 2nd Edition, Cambridge University Press

Pugh, DT, (1987), "Tides, Surges and Mean Sea-level: a Handbook for Engineers and Scientists", Wiley, Chichester (out of print)

RDI Instruments Ltd, telephone conversation

The Engineering Business Ltd, (2003), *Stingray tidal stream energy device – phase 2*, DTI contract T/06/00218/00/REP, URN 03/1433, Department of Trade and Industry, London

Thetis SpA, (1999), Private communication

White, FM, (1999), *Fluid Mechanics, Fourth Edition*, McGraw-Hill, Singapore, p 334

APPENDIX A   TIDAL RECORDS TIME-SERIES
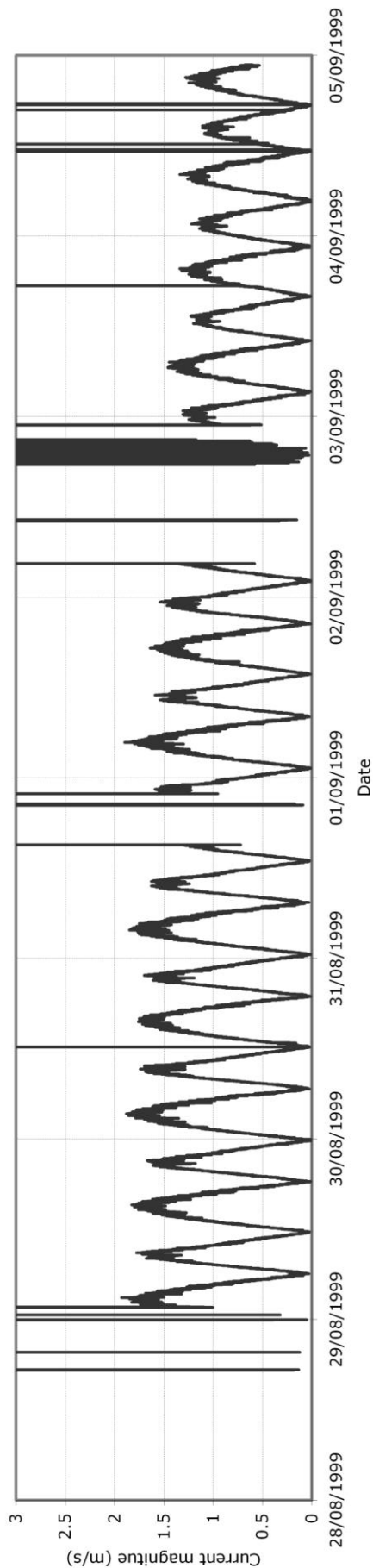
Figure A.1(a) The current magnitude time-series for the Arklow Bank North survey
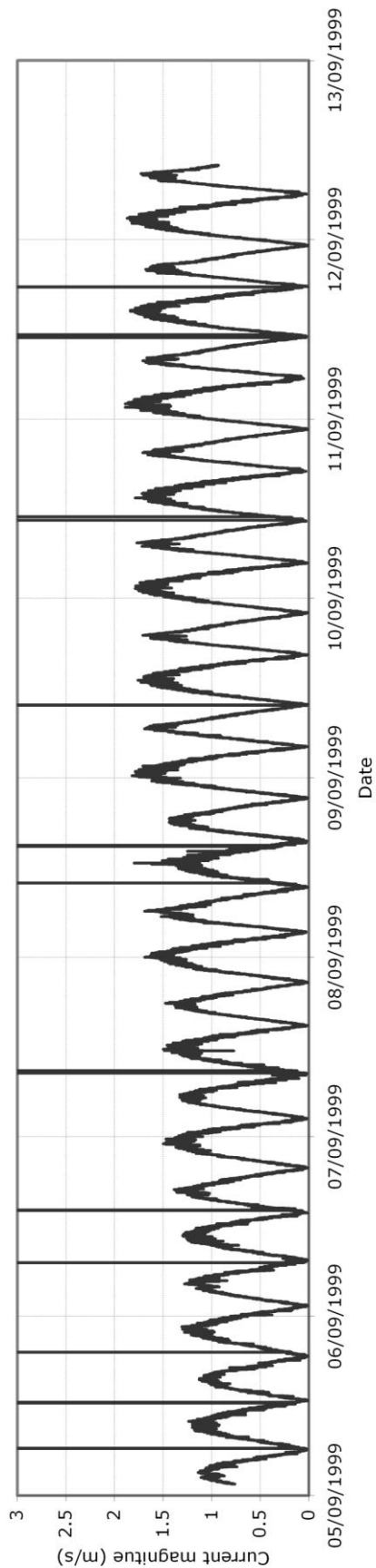
Figure A.1(b) The current magnitude time-series for the Arklow Bank North survey
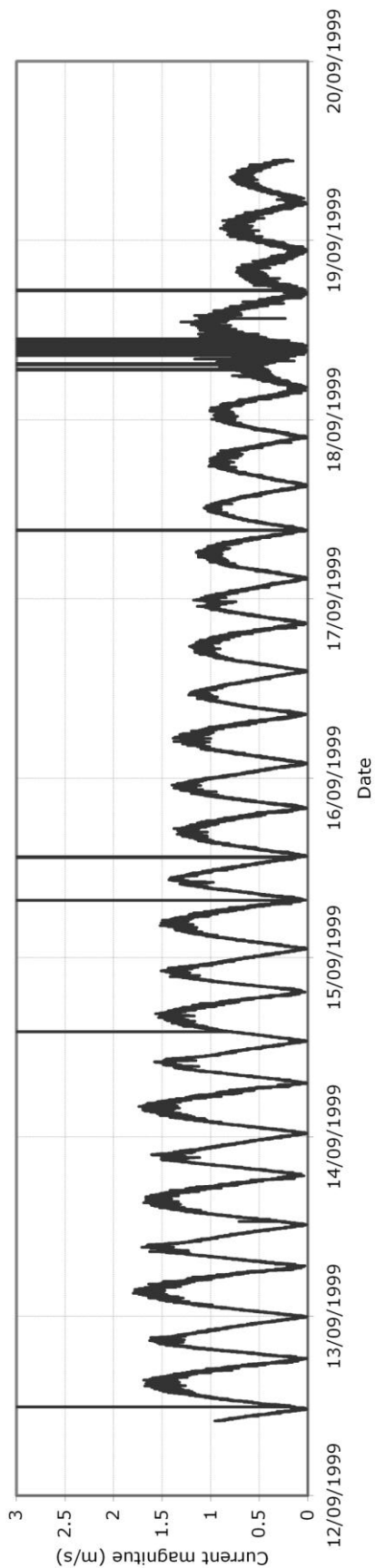
Figure A.1(c) The current magnitude time-series for the Arklow Bank North survey
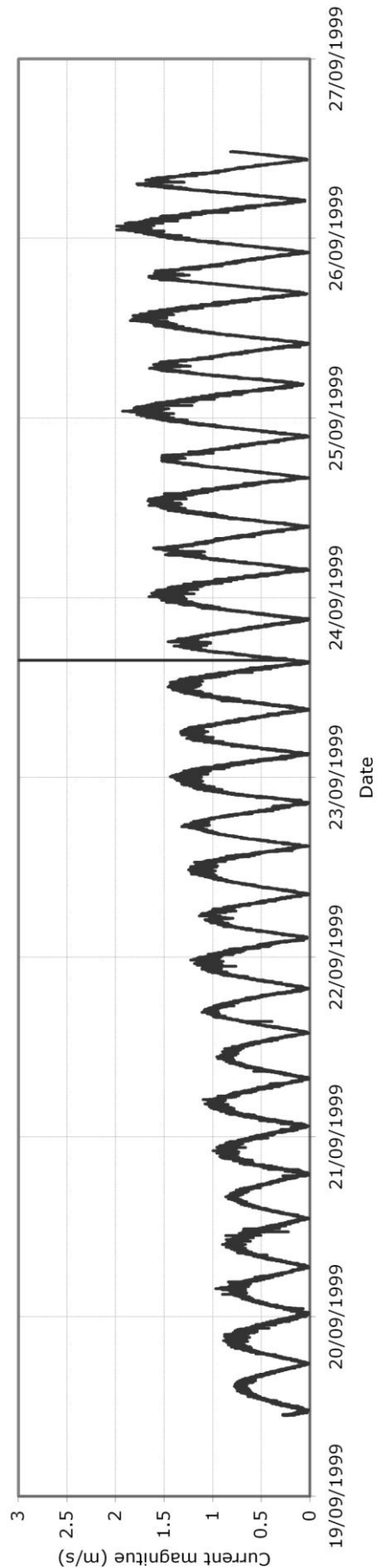
Figure A.1(c) The current magnitude time-series for the Arklow Bank North
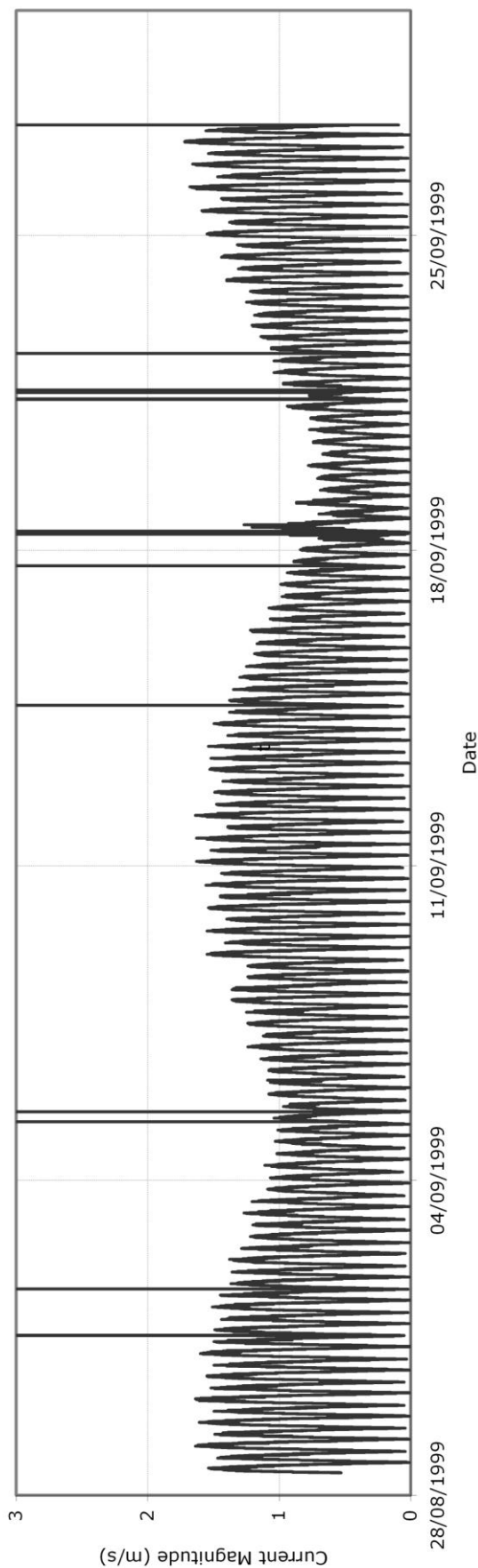
Figure A.2 The current magnitude time-series for the Arklow Bank South survey
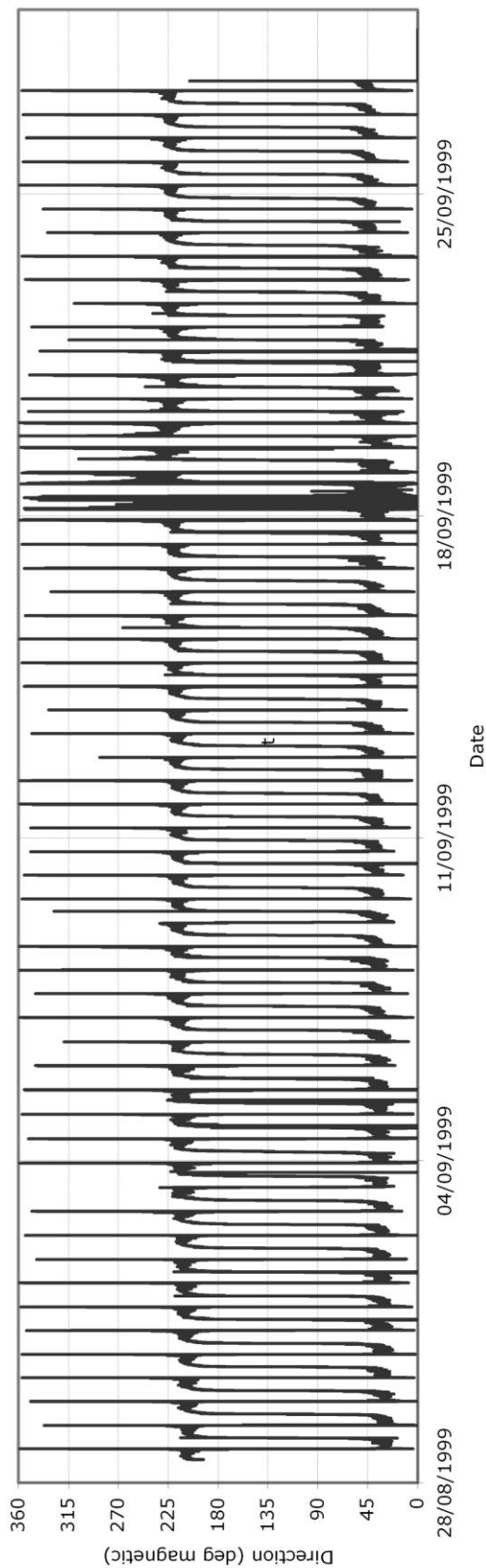
Figure A.3 The current direction time-series for the Arklow Bank South survey
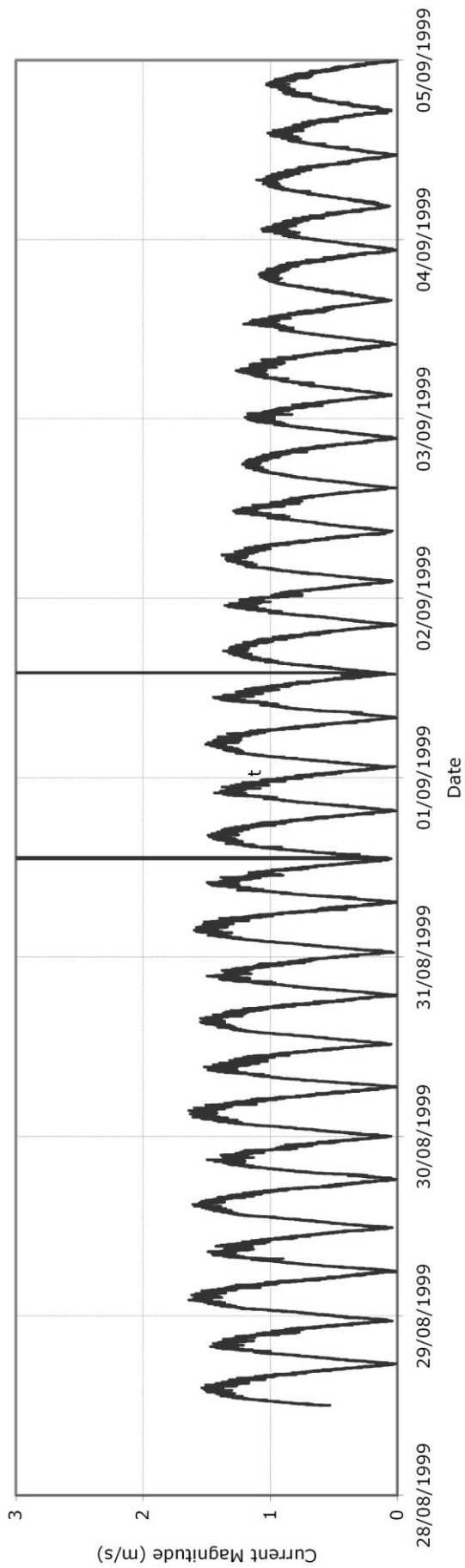
Figure A.4 The current magnitude time-series for the Arklow Bank South survey from 28/8/99 to 5/9/99
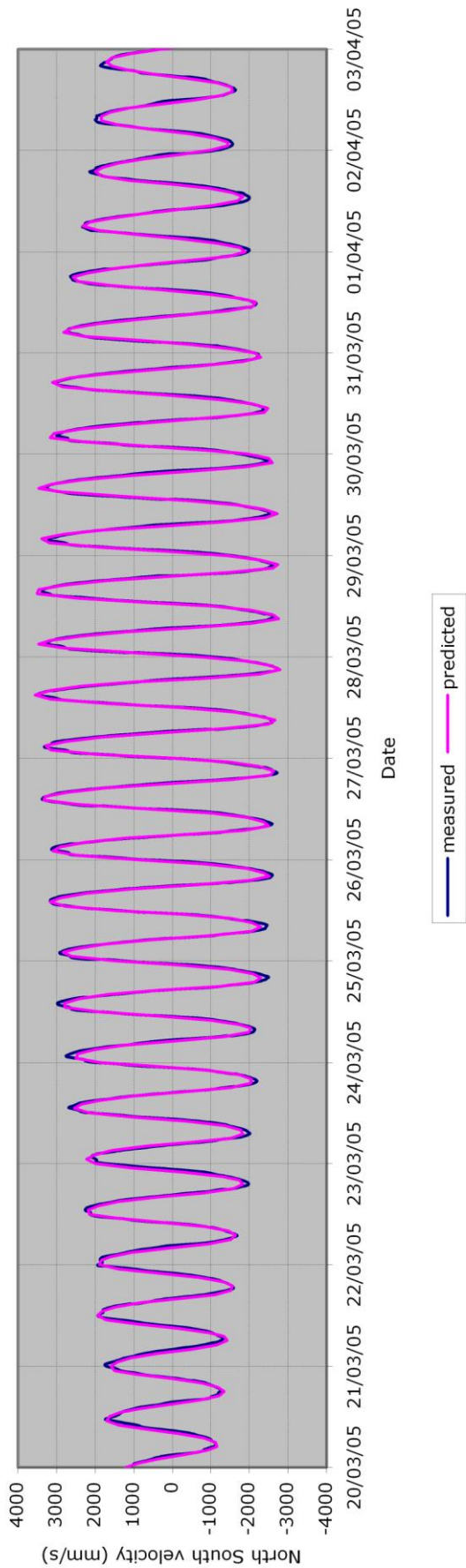
Figure A.5 Comparison of LSRM prediction against measured velocity for Survery 7 at Warrness
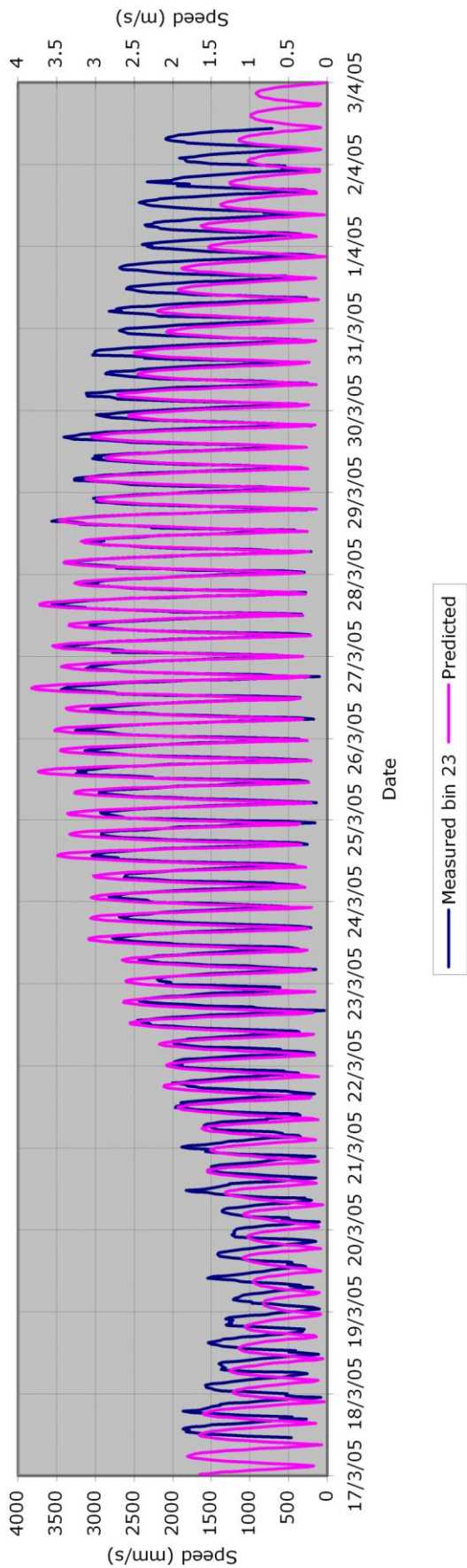
Figure A.6 Comparison of LSRM prediction against measured velocity for Survery 6 at
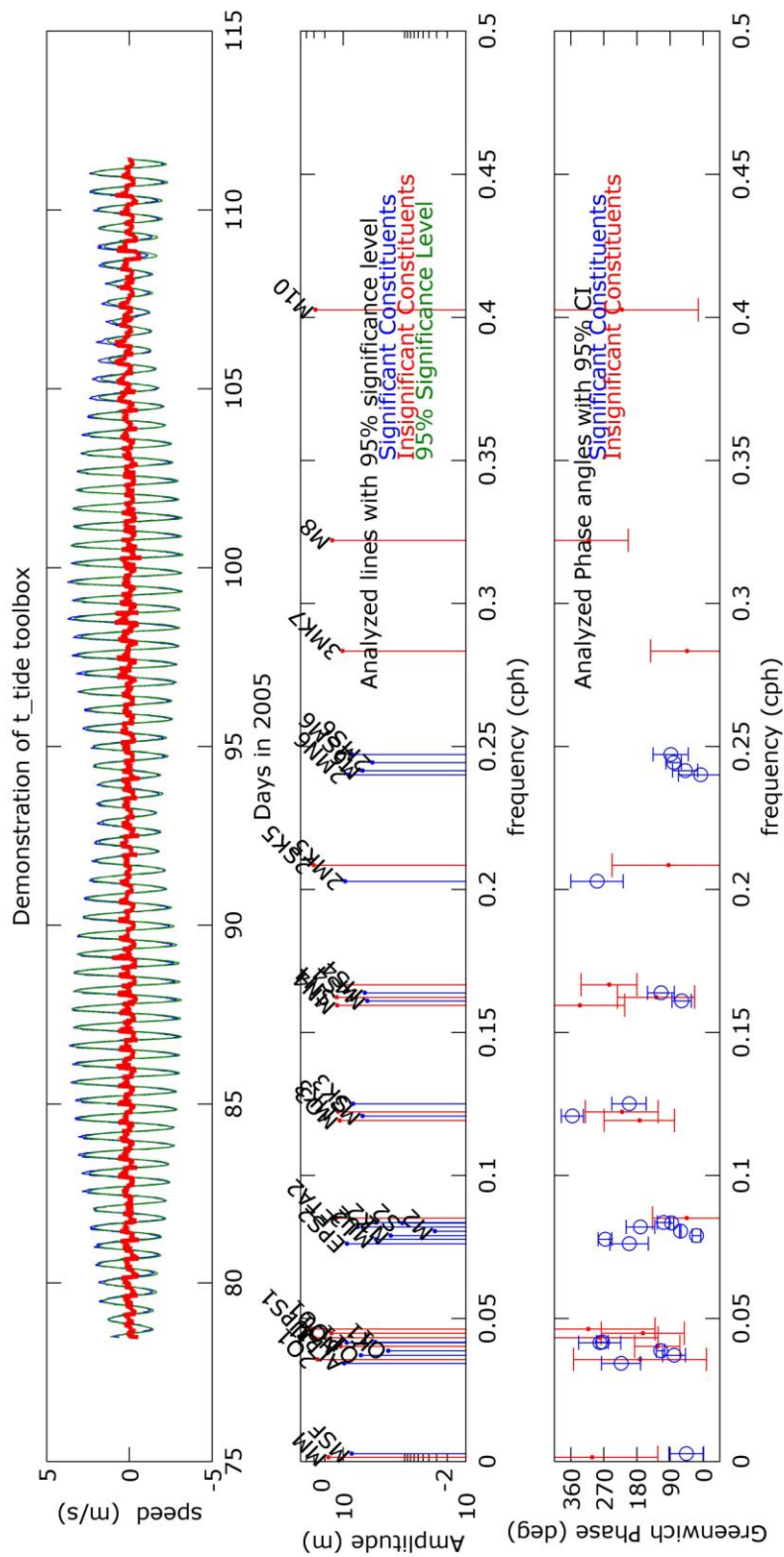
Figure A.7 Confidence interval analysis of LSHM for S7 Warrness
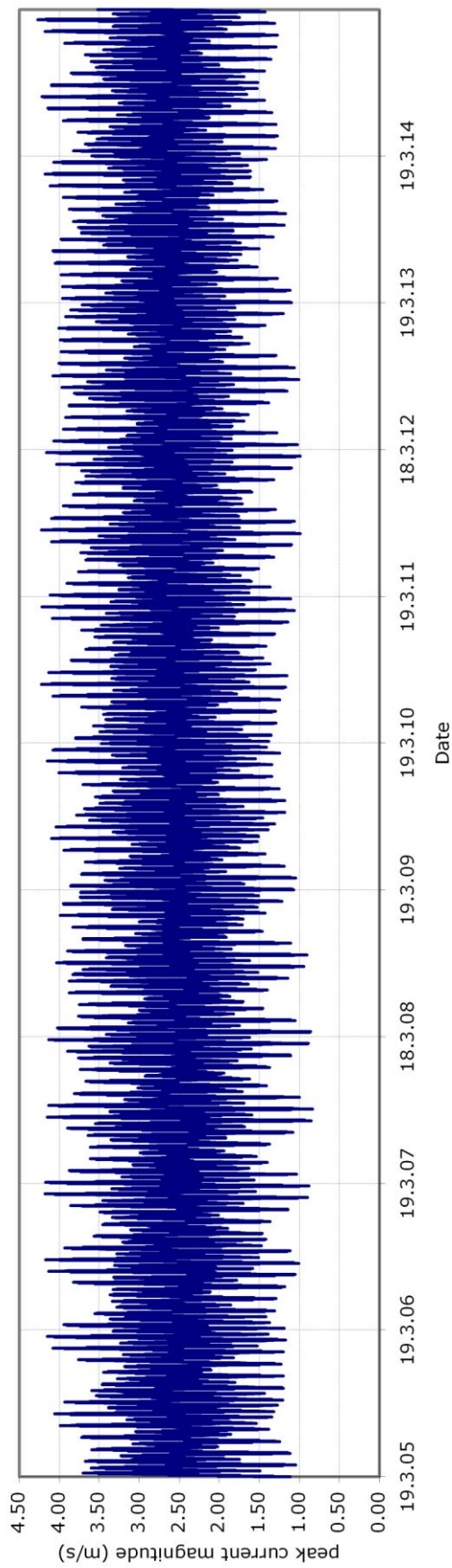
Figure A.8 Peak currenFits prediction for ten years at S7 Warness

APPENDIX B   INPUTS TO ECONOMIC OPTIMISATION MODEL

Table B.1 Inputs to OPTCurrenT Economic Model

	units	Default	used value		units	Default	used value
LocaAtion Filters				**Cable Laying**			
Max. Depth Limit	m	50	50	Cable laying vessel costs	£/day	30000	30000
Min. Depth Limit	m	20	20	Mob/Demob days	day	7	7
Max. Tide Speed	m/s	5	5	Shore approach	day	1	1
Min Average neap Speed	m/s	0.5	0.5	Laying rate	m/day	2000	2000
				Undersea termination	day	1	1
Array Parameters				Grid integration	£	100000	100000
Avg. inter-mill distance	m	90	90				
Lateral spacing factor		3	3	**Mill Construction**			
Axial spacing factor		30	30	Construction support vessel	£/day	30000	30000
Tide Mill Design				**Removal (optional)**			
Maximum Pile Diameter	m	8	8	Support Vessel	£/day	30000	30000
Breakthru Capacity factor		0.2	0.2	Mob/demob	day	7	7
				Removal duration	days/mill	5	5
Costing							
Structure				**Maintenance (low level)**			
Material unit cost	£/t	1000	1000	Grid operations	£/year	30000	30000
minimum Rotor-bed Clearance	m	5	5	Inpection Frequency	times/year	1	1
Elastic Limit	kg/cm^2	2000	2000				
Stress safety factor		3	3	**Maintenance (Overhaul)**			
Buckling safety factor		5	5	Operations vessel	£/day	30000	30000
Elastisity modulus	kg/cm^2	2100000	2100000	Mob/demob	£/day	7	7
Material Density	kg/m^3	7800	7800	Maintenance duration	day/mill	5	5
Seabed shear strength	kg/cm^2		0.75	Overhaul period	year	7	7
seabed internal friction	degrees		45				
seabed bulk density	kg/m^3		1150	**Manpower**	units		
				No. of Engineers		1	1
Cabling				Cost of Engineer	£/year	20000	20000
Manufacture initialisation	£	20000	20000	No. of Technicians		1	1
cost per metre	£/m	70	70	Cost of Technicians	£/year	15000	15000
Surface termination unit.	£	2000	2000				
Undersea termination unit.	£	10000	10000	**General Accounting**	units	Default	used value
Distribution unit	£	50000	50000	Mill Lifetime	years	20	20
				Investor Capital	%	100	100
				Discount Rate	%/yr	12	6
				Subsidy	%	0	0
				Loan	%	0	0
				Loan period	years	10	10
				Interest rate	%/year	8	8
				Breakthru economic efficiency	£/kWh	0.1	0.2